Solid-State NMR Spectroscopy of HIV-1 Vpu and Human CD4 in Lipid Bilayers

Inaugural-Dissertation

zur

Erlangung des Doktorgrades

der Mathematisch-Naturwissenschaftlichen Fakultät

der Heinrich-Heine-Universität Düsseldorf

vorgelegt von

Hoa Quynh Do

aus ***Hanoi***

January, 2012

Aus dem Institut für Physikalische Biologie
der Heinrich-Heine Universität Düsseldorf

Gedruckt mit der Genehmigung
der Mathematisch-Naturwissenschaftlichen Fakultät
der Heinrich-Heine-Universität Düsseldorf

Referent: Prof. Dr. Henrike Heise

Koreferent: Prof. Dr. Karl-Erich Jäger

Tag der mündlichen Prüfung: 23.02.2012

Acknowledgements

Personally, I could not have completed this doctoral work without the help, support and encouragement of many people. Here, I would like to thank all those people who have been with me during my doctoral research.

First of all, I would like to express my deep gratitude to Henrike Heise, my supervisor, for your supervision, support, and trust in me during the last 3 years. Thanks for welcoming me to your group and for introducing me to the exciting world of solid state NMR. Thanks for encouraging me to go further into the interesting theories of NMR. You always asked challenging questions in the work that made my NMR knowledge grow deeply and quickly. You always trained me in such a way that helped me become more and more independent in doing the research. To be honest, it was challenging but there were huge reward. Thanks for sharing your experiences as a researcher and teacher.

I would like to thank Dieter Willbold very much for allowing me to work in your wet lab and especially for your suggestion to choose the full-length Vpu as one of the samples in my doctoral project.

I also would like to thank Bernd W. König for providing me a lab bench, inviting me to your group meetings where I had many interesting discussions and helpful comments. Thanks for supporting me during the time I had worked in the wet lab.

Thanks to other supervisors, Karl-Erich Jäger and Melanie Brocker, for giving me your trust, encouragement, and useful comments on my work. Thanks for sharing with me your ideas how to improve my project.

Many thank to you colleagues, Marc, Julian, Luis, and Sameer for helpful introductions to the expression and purification of VpU and CD4 proteins. Thanks Julian for helping with the preparation of the sample for solid-state NMR measurements.

Special thanks to Pallavi for sharing with me your lab bench and letting me use your pipettes and other solutions in your bench.

Thanks to all of you, wet-lab people, Esther, and Nicole for all precious supports concerning the equipment and the solutions. Thanks to Carsten for helping me with the HPLC system. Thanks all of you for making the warm and supportive atmosphere in the wet lab.

Many thanks Matthias, Rudolf, Vadim, and Mr. Simon for sharing with me your experiences in using VnmrJ software and Varian spectrometers. Special thanks Rudolf for

helping with all difficulties concerning not only the spectrometer, spinning and cooling samples but also the other instruments as my office computer and printer.

Thanks Sven for helping me at the beginning with NMRPipe software and thanks Justin for helping me with my account in the bes and the difficulties in using the Äkta.

Many thanks solid–state colleagues, Santhosh, Sabu, and Henrik for your great humor, for sharing your experiences in using the NMR instruments, for discussing NMR theories, pulse sequences, and for the relaxing lunches we had together.

I would like to thank NRW- Research School BioStruct for the financial support for these three years. Special thanks to Christian, Cordula, and Brigitte for the help in organization works involved.

I am thankful to Nina and Christian for picking me up from Forschungzentrum station and taking me to the warm room in the Guest house on a very cold winter day when I came to Jülich for the first time.

Special thanks to Hà, Pallavi, Nga, Huynh, Raj, Sonia, Silke, Amine, Tobi, Jide, and Chetan for your great friendship, being with me, and cheering me up in difficult times of my doctoral research.

I am very grateful to my parents, Do Manh Suu and Trinh Thi Chien, for the love and constant support you give to me all my life. Thanks for letting me to choose my own way and follow the research.

Many thanks my brother - Thắng and my sister in-law - Nga for cheering me up when I had difficult times in my work. Thanks for taking care of our big family so I could have more time for my doctoral research.

Abstract

In HIV-infected human cells, the viral protein Vpu of HIV-1 directly interacts with the human T-cell surface glycoprotein CD4 and subsequently induces the degradation of this protein in the endoplasmic reticulum. However, the exact mechanism of the interaction is still under debate, and the binding interface between CD4 and Vpu has not yet been determined precisely. In this work, solid-state NMR spectroscopy with magic angle spinning (MAS) was employed to study the behavior of HIV-1 Vpu and human CD4(372-433) in POPC lipid bilayers.

The uniformly labeled ^{13}C, ^{15}N integral membrane proteins, full-length Vpu and CD4(372-433) were reconstituted in POPC bilayers. The resulting proteoliposomes were then lyophilized, packed into sample containers (the rotors), and rehydrated for MAS solid-state NMR measurements. The resonance assignment was performed on data which were acquired using 2D solid-state NMR spectroscopy. Site specific resonance assignments were obtained for 13 residues in CD4, while for Vpu only type-specific assignments could be obtained. The secondary chemical shifts of the identified amino acids report that the transmembrane part of CD4(372-433) in POPC bilayers has an alpha helical structure. The shifts of the amino acids belonging to transmembrane part of full-length Vpu in the POPC bilayers are also indicative of an alpha helical secondary structure, whereas the cytoplasmic part of this protein indicates a conformational disorder.

The mobility of CD4(372-433) and Vpu in POPC bilayers was investigated with the aid of homonuclear 2D solid state NMR techniques at above and below the freezing temperature. Magnetization transfer from mobile protons to the protein utilizing a 3D experiment which is a combination of T_2 filter, ^1H spin diffusion, cross polarization, and proton driven spin diffusion was employed to probe the topology of the membrane proteins in POPC bilayers. Our results are in agreement with a pore-like structure with water accessibility for Vpu. For both proteins Vpu and CD4(372-433), the transmembrane parts were observed in the vicinity of the lipid side-chains. This indicates that the proteins were reconstituted correctly.

Isotope-labeled Vpu was also reconstituted into POPC bilayers in presence of unlabeled CD4(372-433) and investigated using 2D homonuclear C-C correlation spectroscopy. While different mobilities for certain residues of the cytoplasmic domain of

Vpu could be observed, it is not clear whether these effects arise from the interaction or are due to the different hydration levels of these samples.

Zusammenfassung

Bei der HIV-Infektion interagiert das virale HIV-1-Protein VpU mit dem humanen T-Zell-Rezeptorprotein CD4, und induziert dadurch den Abbau dieses Proteins im endoplasmatischen Retikulum. Über den genauen Mechanismus dieser Wechselwirkung wird allerdings noch diskutiert, und die exakten Bindestellen zwischen den Proteinen sind nicht bekannt. Im Rahmen dieser Arbeit haben wir Festkörper-NMR-Spektroskopie unter MAS („Magic-Angle Spinning“, Rotation um den magischen Winkel) angewendet, um die in POPC-Lipiddoppelschichten rekonstituierten Proteine HIV-1 VpU und CD4(372-433) zu untersuchen.

Die vollständig ^{13}C, ^{15}N isotopenmarkierten integralen Membranproteine wurden rekombinant in *E.coli* exprimiert und in POPC Lipiddoppelschichten rekonstituiert. Die Proteoliposomen wurden lyophilisiert, und für MAS-Festkörper-NMR-Spektroskopie in die Probenröhrchen (Rotoren) gepackt und rehydratisiert.

Die Resonanzen wurden anhand zweidimensionaler NMR-Spektren zugeordnet. Sequenzspezifische Zuordnungen wurden für 13 Aminosäuren in CD4 erhalten, während für VpU nur aminosäurespezifische Zuordnungen erhalten wurden.

Die sekundären chemischen Verschiebungen der zugeordneten Aminosäuren zeigen, dass der Transmembranteil von CD4(372-433) in POPC Lipiddoppelschichten –helikale Sekundärstruktur hat. Die Verschiebungen der Aminosäuren, die dem Transmembranteil von VpU zugeordnet werden konnten, deuten ebenfalls auf alpha-helikale Sekundärstruktur hin, während die zytoplasmatische Domäne dieses Proteins konformationell ungeordnet zu sein scheint.

Die Mobilität von CD4(372-433) und VpU in POPC Doppelschichten wurde mit homonuklearen 2D-Festkörper-NMR-Methoden ober- und unterhalb des Gefrierpunktes untersucht. Magnetisierungstransfer von mobile Protonen auf das Protein wurde der Topologie mit Hilfe einer 3D-Pulssequenz, die sich aus T_2-Filter, ^1H Spindiffusion, Kreuzpolarisation und protonengetriebener Spindiffusion zusammensetzt, zur Untersuchung der Topologie der Membranproteine herangezogen. Unsere Ergebnisse stützen die Annahme, dass VpU in Lipiddoppelschichten wasserdurchlässige Poren ausbildet. Für beide Proteine VpU und CD4(372-433) konnte die korrekte Rekonstitution der Transmembrandomänen in die Lipiddoppelschichten durch die räumliche Nachbarschaft zu den Lipidseitenketten bestätigt werden.

Isotopenmarkiertes VpU wurde auch gemeinsam mit unmarkiertem CD4(372-433) in Lipiddoppelschichten co-rekonstituiert und mit Hilfe von homonuklearer 2D C/C-Korrelations- NMR-Spektroskopie untersucht. Mobilitätsunterschiede, die für bestimmte Aminosäurereste der zytoplasmatischen Domäne von VpU beobachtet werden konnte, könnte potenziell auf die Wechselwirkung zwischen den Proteinen, oder auf den unterschiedlichen Wassergehalt der Proben zurückzuführen sein.

Contents

Acknowledgements ..... *iii*

Abstract ..... *v*

Zusammenfassung ..... *vii*

List of Figures ..... *xii*

List of Tables ..... *xiv*

Abbreviation ..... *xv*

Chapter 1. Introduction 1

1.1. Biological functions and Structures of Vpu and CD4 proteins 2

1.1.1. Biological functions and structure of CD4 2

1.1.2. Biological functions and structures of Vpu 4

1.1.3. Structural determinants of Vpu in the interaction between Vpu and CD4 5

1.2. Solid state nuclear magnetic resonance spectroscopy 8

1.2.1. Dipolar-dipolar coupling, chemical shift, and magic angle apinning 8

1.2.2. Cross polarization 14

1.2.3. Heteronuclear spin decoupling 16

1.2.4. Spin recoupling 16

Double quantum SPC-5 18

Rotational resonance condition 18

Proton driven spin diffusion 18

1.2.5. The broadening of the line width 19

1.2.6. J coupling, T_2 filter, and insensitive nuclei enhanced by polarization trasnfer 21

References 23

Chapter 2. Materials and Methods 30
2.1. Sample preparation 30
2.1.1. Protein expression and purification 30
2.1.2. Reconstitution of Protein into POPC lipid bilayer 33
2.2. Solid state NMR spectroscopy 35
2.2.1. Data collection 35
2.2.2. Data processing 35
2.2.3. Assignment strategy 36
References 41
Chapter 3. Experiments and Results 43
3.1. Mobility of the reconstituted protein 43
3.1.1. The changes of protein before and after reconstituted into the POPC bilayers 43
3.1.2. Effects of different reconstitution methods on NMR detection 44
3.1.3. Effects of mobility and temperature on detection of the reconstituted proteins… 47
3.2. Topology of Vpu and CD4(372-433) in POPC lipid bilayers 49
3.2.1. Topology of Vpu in POPC lipid bilayers 49
3.2.2. Topology of CD4(372-433) in POPC lipid bilayers 52
3.3. Resonance assignments of the reconstituted proteins 55
3.3.1. Resonance assignments of Vpu in POPC lipid bilayers 56
3.3.2. Resonance assignments of CD4(372-433) peptide in a POPC bilayers 68
3.4. Interaction of CD4(372-433) and Vpu in POPC bilayers 79
References 83
Chapter 4. Discussion and Conclusions 84
4.1. Mobility of the reconstituted proteins and the effects of reconstitution methods 84

4.2. Vpu in POPC bilayers with and without presence of CD4(372-433) 85
4.3. Topology of Vpu and CD4(372-433) in POPC lipid bilayers..... 86
4.4. Resonance assignments of the reconstituted proteins 88
References 90
Appendix A 92
Appendix B 95

List of Figures

Fig. 1.1 3
Fig. 1.2 4
Fig. 1.3 7
Fig. 1.4 9
Fig. 1.5 10
Fig. 1.6 12
Fig. 1.7 14
Fig. 1.8 16
Fig. 1.9 17
Fig. 1.10 20
Fig. 2.1 31
Fig. 2.2 33
Fig. 2.3 34
Fig. 2.4 38
Fig. 2.5 39
Fig. 2.6 40
Fig. 3.1 44
Fig. 3.2 45
Fig. 3.3 46
Fig. 3.4 48
Fig. 3.5 48
Fig. 3.6 49
Fig. 3.7 50
Fig. 3.8 52
Fig. 3.9 53
Fig. 3.10 55
Fig. 3.11 60
Fig. 3.12 61
Fig. 3.13 64
Fig. 3.14 65
Fig. 3.15 66

Fig. 3.16.. 67
Fig. 3.17. 70
Fig. 3.18.. 71
Fig. 3.19. 72
Fig. 3.20. 72
Fig. 3.21.. 74
Fig. 3.22.. 75
Fig. 3.23.. 76
Fig. 3.24. 76
Fig. 3.25. 81
Fig. 3.26. 82
Fig. A1..... 92
Fig. A2..... 92
Fig. A3..... 93
Fig. A4..... 93
Fig. A5. 94
Fig. A6. 94
Fig. B1..... 95
Fig. B2..... 96
Fig. B3..... 97
Fig. B4..... 98
Fig. B5..... 99
Fig. B6..... 100
Fig. B7..... 101

List of Tables

Table 1..... 57
Table 2..... 62
Table 3..... 62
Table 4..... 69
Table 5..... 77
Table B1 96

Abbreviations

BMRB	**B**iological **m**agnetic **r**esonance **d**ata **b**ank
CD4	**C**lusters of **d**ifferentiation 4
CP	Cross-polarization
CSA	**C**hemical **s**hift **a**nisotropy
DARR	**D**ipolar-**a**ssisted **r**otational **r**esonance
DHPC	1,2-diheptanoyl-*sn*-glycero-3-phosphocholine
DMPC	1,2-**di****m**yristoyl-*sn*-glycero-3-**p**hospho**c**holine
DOPC	1,2-**di****o**leoyl-*sn*-glycero-3-**p**hospho**c**holine
DOPC	1,2-**di****o**leoyl-*sn*-glycero-3-**p**hospho**c**holine
DOPG	1,2-**di****o**leoyl-*sn*-glycero-3-[**p**hospho-*rac*-(1-**g**lycerol)]
DQ	**D**ouble **q**uantum
DTT	**Di****t**hio**t**hreitol
ER	**E**ndoplasmic **r**eticulum
FID	**F**ree **I**nduction **D**ecay
HIV-1	**H**uman **i**mmunodeficiency **v**irus type 1
INEPT	**I**nsensitive **n**uclei **e**nhanced by **p**olarization **t**rasnfer
IPTG	Isopropyl-beta-D-thiogalactopyranoside)
M2TM	**T**rans**m**embrane domain of influenza A **M2** protein
MAS	**M**agic **a**ngle **s**pinning
MHC II	**M**ajor **h**istocompatibility **c**omplex class II
NMR	**N**uclear **m**agnetic **r**esonance
PARIS-xy	**P**hase-**a**lternated **r**ecoupling **i**rradiation **s**cheme using orthogonal radio-frequency phases

PDSD	**P**roton **d**riven **s**pin **d**iffusion
POPC	1-**p**almitoyl-2-**o**leoyl-sn-glycero-3-**p**hospho**c**holine
Rf or rf	**R**adio **f**requency
RR	**R**otational **r**esonance
SPC-5	**S**upercycled **P**OST-**C5**
SPINAL	**S**mall **p**hase **i**ncremental **a**lternation
SQ	**S**ingle **q**uantum
TCA	**T**ri**c**hloroacetic **a**cid
TFE	**T**ri**f**luoro**e**thanol
Vpu	**V**iral **p**rotein **U**

Chapter 1. Introduction

Magic angle spinning (MAS) solid-state nuclear magnetic resonance (NMR) spectroscopy has been demonstrated as a powerful tool for obtaining structure, dynamics, and topology of amyloid, prion and membrane proteins[1-16] for more than a decade. Solid-state NMR spectroscopy has been using to study especially the features of integral membrane proteins in lipid models[17-21] that are not accessible by other methods such as liquid state NMR spectroscopy and diffraction techniques.

Integral membrane proteins are characterized by hydrophobic segments spanning the lipid bilayer, and the structure of these proteins also depends on the hydrophobic thickness of the lipid bilayer. For example, the appearance of a helical kink at Gly34 of the transmembrane domain of influenza A M2 protein (M2TM) is dependent on the thickness of lipid bilayers. The helical kink was found in the drug-bound state of the M2TM but not in the drug-free state of the M2TM when both of the M2TM were reconstituted in DMPC/DMPG bilayers[22,23]. However, the helical kink also appears in the drug-free state of the M2TM when this protein is reconstituted into lipid bilayers that have larger thickness[24]. A similar phenomenon was also observed for HIV-1 Vpu protein[25]. A distinctive kink in the middle of the transmembrane helix of VpU protein was observed in thicker lipid bilayers (18:1-O-PC/DOPG (9:1)) whereas the kink disappears in thinner bilayers such as 14:0-O-PC/DMPG (9:1), 12:0-O-PC/DLPG (9:1), 10:0 PC/10:0 PG (9:1). In addition, a tilt angle of the VpU transmembrane helix is 18° in the thicker lipid bilayers whereas this tilt angle increases to 27°, 35° and 51° in the thinner bilayers, 14:0-O-PC/DMPG (9:1), 12:0-O-PC/DLPG (9:1), 10:0 PC/10:0 PG (9:1), respectively. There, apparently, exists a relationship between the structure of membrane protein and the lipid models, which was taken into account in this study of the membrane proteins.

It has been well known that HIV-1 Vpu directly binds to the human T-cell surface glycoprotein CD4 in the membrane of the endoplasmic reticulum (ER)[26,27]. This causes the degradation of newly synthesized CD4 protein[28,29]. However, binding interfaces (or structural determinants) involved in the interaction have not yet been determined precisely. In case of the Vpu protein, many studies demonstrated that

structural determinants are located somewhere in the cytoplasmic part[26,27,30], whereas other suggested the transmembrane section as the location[31]. The reasons for such contradictions might be associated with differences in Vpu segments, lipid models and methods used during the reported investigations.

To come closer to an agreement on the structural determinants involved in the CD4-Vpu interaction, it is necessary to have Vpu and CD4 reconstituted into lipid bilayers environment which ensures adequate hydrophobic thickness, and the characteristics of these two proteins in the native-like environment concerning topology, mobility and conformation need to be well understood. The interaction between Vpu and CD4 takes place in the ER's membrane whose main lipid component is phosphatidylcholine (PC)[32]. For this reason, it is necessary that 1-**p**almitoyl-2-**o**leoyl-sn-glycero-3-**p**hospho**c**holine (POPC- Fig. B3) is chosen as the lipid model (i.e., phosphatidylcholine with long fatty acid side-chains) in order to ensure the right hydrophobic thickness is achievable. MAS solid-state NMR spectroscopy is then needed to investigate the membrane proteins reconstituted into synthetic lipid bilayers.

In the present thesis, thus, the study employed the full-length sequence of Vpu protein, CD4(372-433) peptide, POPC lipid bilayers as a lipid model and MAS solid-state NMR spectroscopy to explore mobility, topology and structures of the CD4(372-433) peptide and the Vpu protein separately reconstituted into the POPC lipid bilayers as well as to monitor the dynamics of the full-length Vpu reconstituted into the POPC bilayer in presence of CD4(372-433) peptide. To the best of the author's understanding this is the first time the characteristics of the full-length Vpu, the CD4(372-433) peptide and their interaction in the POPC lipid bilayer are reported using MAS solid-state NMR spectroscopy.

1.1. Biological functions and structures of Vpu and CD4 proteins

1.1.1. Biological functions and structure of CD4

The human T-cell surface glycoprotein CD4 is an integral membrane protein which is expressed on the surface of T helper cells, B cells, granulocytes and macrophages. It is also expressed in specific regions of the brain. The mature human CD4 protein (T-cell surface glycoprotein CD4 isoform 1) consists of 433 amino acids that are divided into three segments[33,34] (Fig. 1.1.C). The extracellular segment includes a leading

sequence followed by four domains with total 371 amino acid residues. The second segment, which spans the membrane lipid bilayer, contains 24 amino acid residues. The C-terminal segment, with 38 amino acid residues, resides in the cytosol. Recent studies on the structure of the transmembrane and cytoplasmic segments of CD4(372-433) have indicated the existence of an alpha helical fragment in the transmembrane part (residues 372-395) and a shorter alpha helix in the cytoplasmic region (residue 404-413)[35-37] as shown in Fig. 1.1.B and C.

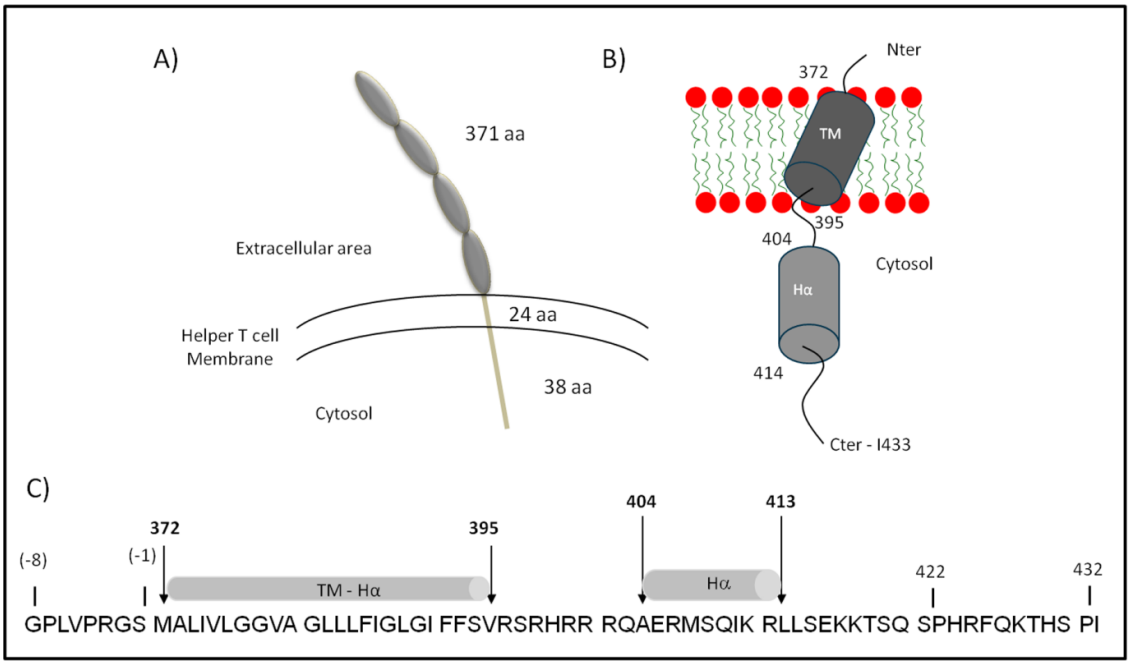

Fig. 1.1. CD4 receptor. A) CD4 receptor with 3 segments. B) Secondary structure of CD4(372-433); TM: transmembrane domain. Hα: alpha helix. C) Primary structure of CD4(372-433) in which (-8) to (-1) are the remaining residues after purification of CD4(372-433) peptide..

CD4 plays an important role in the T-cell receptor signaling pathway and it is also required for the entry of human immunodeficiency virus type 1 (HIV-1). In the signaling pathway, CD4 recognition results in the secretion of cytokines from the T helper cell: (i) CD4 specifically interacts with non-polymorphic regions of the major histocompatibility complex class II (MHC II)[38,39] expressed in the antigen-presenting cells; (ii) the interaction leads to activation of a tyrosine kinase[40] which in turn triggers cytokine secretion by the helper T cell. In HIV-1 infection, CD4 acts as a co-receptor that opens the door for HIV-1 entry into the host cell[41,42]. Paradoxically, after infection HIV-1 strongly down-regulates the expression of the CD4 receptor, which is attributed

to at least two distinct mechanisms: (i) the degradation of newly synthesized CD4 molecules in the endoplasmic reticulum mediated by the HIV-1 Vpu protein[28]; and (i) the degradation of the mature CD4 molecules at the cell surface mediated by HIV-1 Nef protein[43].

1.1.2. Biological functions and structures of Vpu

HIV-1 Vpu protein is a 16 kDa integral membrane protein with 81 amino acids[44-48]. In the virus replication cycle, the Vpu protein has two major biological functions[28,29,49-51] which mediate the degradation of the newly synthesized human CD4 receptor in the endoplasmic reticulum and the enhancement of viral release from infected cells. These two biological activities operate via two distinct structural domains of the Vpu[52]: the transmembrane domain plays a critical role in regulating virus release from infected cells while the cytoplasmic domain severs as a mediator of the CD4 degradation.

Vpu exists in a variety of polymorphic forms on different HIV strains, two of which are commonly utilized for structural studies[46,53]. In the first form, the phosphorylation sites reside at S53 and S57[46] (Fig. 1.2.A) whereas in the second form the phosphorylation sites localize at S52 and S56[53] (Fig. 1.2.B). In both forms, the conserved motifs that are responsible for the phosphorylation function and ion channel activities of Vpu protein are the same.

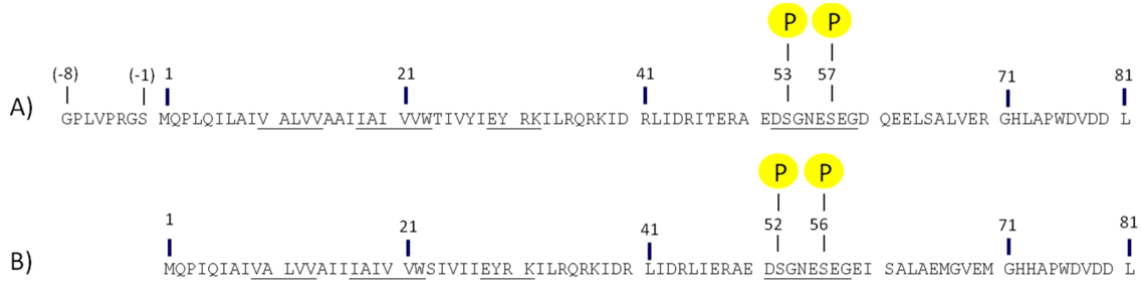

Fig. 1.2. Primary structure of Vpu. A) The phosphorylation sites reside at S53 and S57 in the form used in the current work. This sequence contains a tag at the N-terminus (G(-8) to S(-1)) which is the remaining residues after the purification (Section 2.1). B) The phosphorylation sites reside at S52 and S56. The underlined residues are conserved amino acids.

The structure of the transmembrane (TM) domain of Vpu was determined as alpha helical conformation using both liquid state and solid state NMR spectroscopic methods[54-56]. The structure was investigated in different lipid models such as micelles

(DHPC) and lipid bilayer (made of DMPC and DOPC). It was shown that the alpha helical segment spans from residues 8 to 25 of a 36 residue peptide that contains residues 2-30 of Vpu[54,55]. Recently, another study on a 40 residue segment of Vpu (Vpu(1-40)) employing MAS solid-state NMR spectroscopy reported that the transmembrane alpha helical segment extends beyond the hydrophobic core of the lipid bilayer and that residues 30-40 are part of an amphipathic helix structure[56]. In addition, it was demonstrated that the transmembrane domain formed ion channels in phospholipid bilayers [57,58] . The reported ion channels were formed by the oligomerization of the transmembrane helices and oligomers of various sizes have been found coexisting in the bilayer. The ion channel was shown to possess an activity involved in the regulation of the virus release[59]; this channel activity, however, is insufficient for the complete virus release[60].

The structure of the cytoplasmic domain of Vpu was investigated by liquid state NMR spectroscopy using either non-lipid environment (i.e. Trifluoroethanol solution[61,62] or a mixture of sodium chloride (100mM) and potassium phosphate (20mM), pH 7.0 in H_2O/D_2O (9:1, by volume) or D_2O[63]) or a lipid model (i.e. dodecylphosphatidylcholine micelles[64]). Various fragments of Vpu were employed in order to gain insight into its structure. Investigations performed on three Vpu polypeptides with different sequence lengths, i.e., Vpu(41-58), Vpu(52-74) and Vpu(63-81) in TFE/H_2O solutions, respectively suggested a helical structure for residues 42 - 50, 57 - 69 and 74- 77[62]. Furthermore, investigations conducted on Vpu(39-81) both in aqueous medium[63] and in dodecylphosphatidylcholine (DPC) micelles[64] indicated the presence of two amphipathic alpha helical segments and a short alpha-helix. The first segment is a well-defined alpha helix conformation including residues 39-50. The second segment is a less well-defined alpha helix with residues 60-70. The last segment is short alpha helix residing at the C-terminus of Vpu including residues 75-79.

1.1.3. Structural determinants of Vpu in the interaction between Vpu and CD4

As mentioned earlier, the cytoplasmic domain of Vpu induces degradation of CD4. Before the induction of the CD4 degradation, Vpu first directly interacts with the

cytoplasmic domain of the human CD4 receptor, which then triggers the degradation of CD4[26,27]. In order to obtain insight into the mechanism of interaction between Vpu and CD4, a number of studies employing different investigation techniques, different experimental conditions and various Vpu fragments have been conducted[26,27,30].

The residues of Vpu involved in the interaction were mapped on a Vpu construct with residues from 28 to 81[27]. This study using multiple deletions, point mutants and the two-hybrid assay method reported residues 28-47 and 76-81 as being required for the interaction with CD4. Furthermore, the double mutant of the casein kinase II phosphorylation sites (S52N-S56N) was shown to effectively prevent the Vpu-CD4 interaction while the single mutant (either S52N or S56G) was observed to retain the capacity of Vpu for binding to the cytoplasmic domain of the CD4 receptor. This result is in contrast with a previous study[26] using the coimmunoprecipitation method, which indicated that the binding capacity was conserved even for the double mutant (S52N-S56N). Another study[30], which employed coimmunoprecipitation, mutational analysis, and cytoplasmic domain of CD4 and full-length Vpu, showed that Vpu proteins containing mutations in either or both of the phosphorylation sites (Ser52G or/and Ser56G) retained the capacity to interact with the cytoplasmic domain of CD4. Furthermore, in an effort to delineate the structural determinant involved in the interaction between Vpu and CD4, the study found that the primary binding site for CD4 in the cytoplasmic domain of Vpu is the amphipatic alpha helix I (residues 30-50). Taken together, it is likely that these binding determinants are located in the cytoplasmic domain of Vpu but have not yet been accurately defined.

It has been postulated from recent investigations on the interaction between Vpu and CD4 (including both of their TM and cytosolic domains) that the retention of CD4 on the ER membrane in presence of Vpu relies on the interaction between the TM domains of both peptides but not their cytoplasmic domains[31].

Thus, more studies are necessary to fully understand the mechanism by which Vpu interacts with CD4.

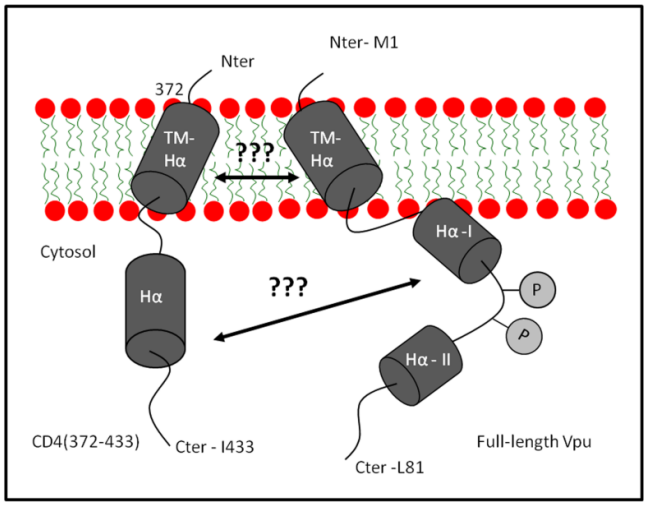

Fig. 1.3. The contradiction of the structural determinants in interaction between Vpu and CD4(372-433). The scheme is depicted without consideration of orientation of proteins. TM – transmembrane. Hα –alpha helix. P – Phosphorylation sites.

1.2. Solid state nuclear magnetic resonance spectroscopy

1.2.1. Dipolar-dipolar coupling, chemical shift, and magic angle spinning

Dipolar-dipolar coupling[65]

The dipolar – dipolar coupling[65] is an interaction between nuclear spin magnetic moments (Fig. 1.4 and Fig. 1.7.B). This interaction is described as homonuclear dipolar-dipolar coupling when the concerned isotopes are of the same type (e.g. ^{1}H-^{1}H or ^{13}C-^{13}C interactions), and as heteronuclear dipolar coupling for different types of isotopes (e.g. ^{1}H-^{15}N, ^{1}H-^{13}C, or ^{13}C-^{15}N interactions). The Hamiltonian operator of the dipolar-dipolar interactions is given by:

$$\mathcal{H}_{dd} = -\left(\frac{\mu_0}{4\pi}\right)\frac{\gamma_I\gamma_S\hbar}{r^3}[A+B+C+D+E+F] \quad (1)$$

where:

$$A = I_zS_z(3cos^2\theta - 1)$$

$$B = -\frac{1}{4}[I_+S_- + I_-S_+](3cos^2 - 1)$$

$$C = \frac{3}{2}[I_zS_+ + I_+S_z]sin\theta cos\theta e^{-i\phi}$$

$$D = \frac{3}{2}[I_zS_- + I_-S_z]sin\theta cos\theta e^{+i\phi}$$

$$E = \frac{3}{4}[I_+S_+]sin^2\theta e^{-2i\phi}$$

$$F = \frac{3}{4}[I_-S_-]sin^2\theta e^{+2i\phi}$$

The angles θ and ϕ are defined in Fig. 1.7.B. γ_I and γ_S are gyromagnetic ratios of spin *I* and *S*. *r* is internuclear distance between I and S. I_+, S_+ and I_-, S_- are raising and lowering operators, respectively acting on spins I and S, in which:

$$I_+ \equiv I_x + \mathrm{i}I_y \qquad I_- \equiv I_x - \mathrm{i}I_y$$

$$S_+ \equiv S_x + \mathrm{i}S_y \qquad S_- \equiv S_x - \mathrm{i}S_y$$

where i is the imaginary unit; I_z, S_z, I_x, S_x *and* I_y, S_y are spin operators which respectively represent the z, x and y-components of the magnetization of spin I and S.

In a coordinate system that rotates about the laboratory z-axis at or near the Larmor frequency (the rotating frame), only the terms A and B in equation (1) are unaffected provided the spin system is homonuclear, while only term A is unaffected provided the spin system is heteronuclear; the terms *C-F* are canceled out by the rotating frame transformation.

The term A acts on a spin system in such a way that it shifts the energy of Zeeman states while term B causes the degenerate Zeeman states in a homonuclear system to exchange, resulting in zero quantum transitions (flip-flop transitions). Thus, without the molecular orientation dependence of the transition frequencies, very broad NMR lines are still observed in the NMR spectrum (Fig. 1.5).

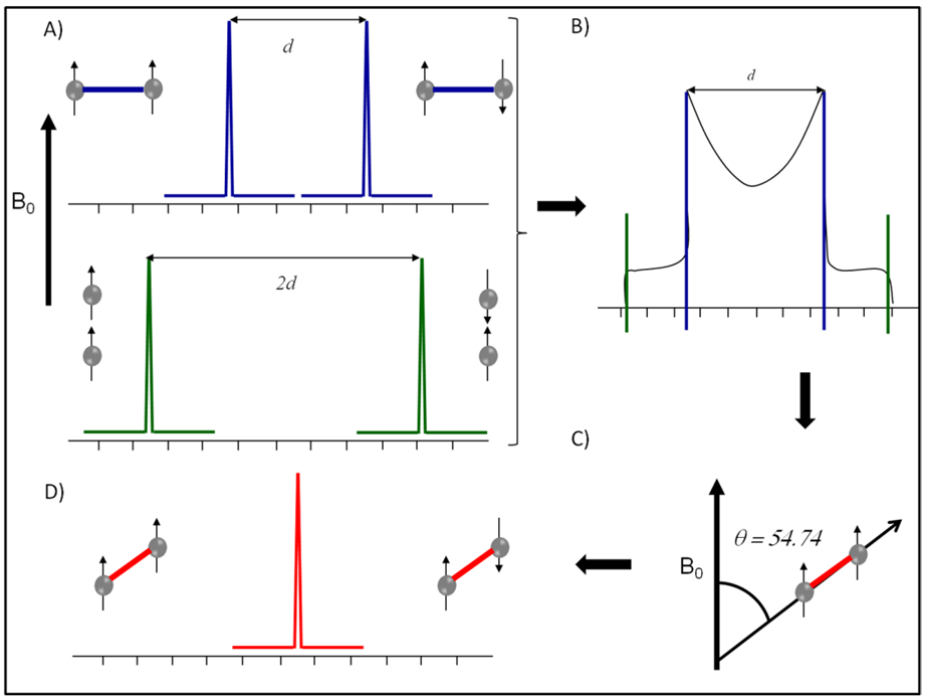

Fig. 1.4. Orientation dependence of the dipolar-dipolar interaction of an isolated spin pair. A) The position of NMR lines depends on the orientation of inter-nuclear vector between 2 spins with respect to the B_0 field. B) Dipolar power pattern of the isolated spin pair. C) The inter-nuclear vector is parallel to the spin axis when $\theta = 54.74°$ and therefore the line gets narrowed in D).

In the rotating frame, if the dipolar-dipolar coupling is heteronuclear, only term A will affect the spin system. And the Hamiltonian operator (in angular frequency units of rad s^{-1}) is represented in equation (2). If the dipolar-dipolar coupling is

homonuclear, both terms A and B will affect the spin system. And the Hamiltonian is given in equation (3).

$$\mathcal{H}_{dd}^{hetero} = -d(3cos^2\theta - 1)I_z S_z \qquad (2)$$

where d is the dipolar coupling constant (in units of rad s^{-1}) and given by:

$$d = \hbar\left(\frac{\mu_0}{4\pi}\right)\frac{1}{r^3}\gamma_I\gamma_S$$

The Hamiltonian of the homonuclear dipolar-dipolar coupling:

$$\mathcal{H}_{dd}^{homo} = -d \cdot \tfrac{1}{2}(3cos^2\theta - 1)[3I_zS_z - \mathbf{I}\cdot\mathbf{S}] \qquad (3)$$

where:

$$\mathbf{I}\cdot\mathbf{S} = I_x S_x + I_y S_y + I_z S_z$$

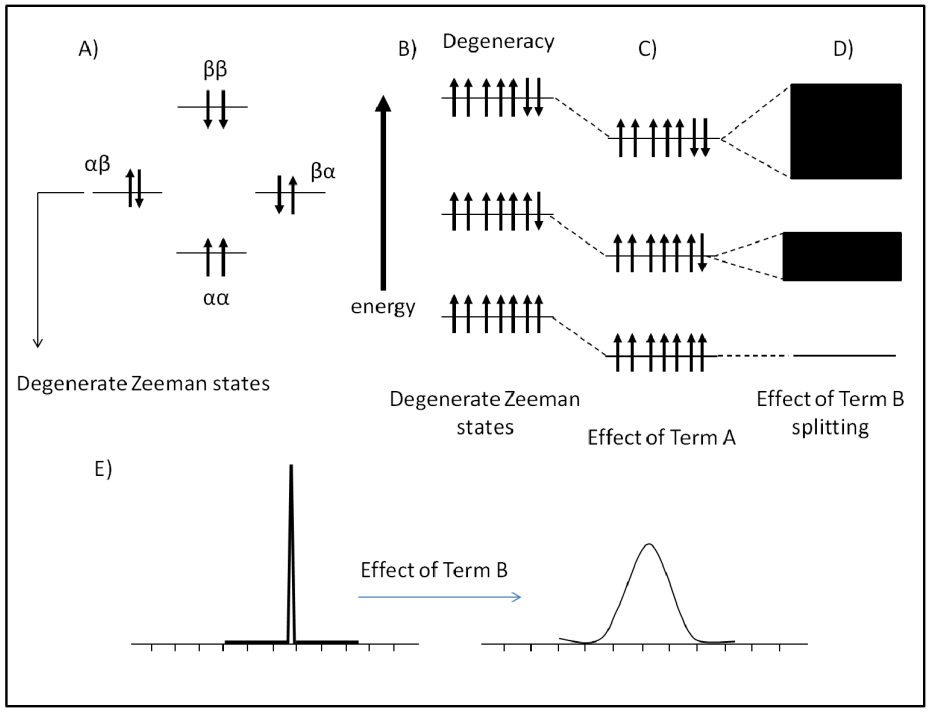

Fig. 1.5. A) Zeeman states of a homonuclear two spin-$\frac{1}{2}$ system without effects of the dipolar coupling. B) Degenerate Zeeman states of multiple homonuclear spin system in absence of dipolar coupling. C) and D) Effect of dipolar coupling leads to the mixing the degenerate Zeeman states and splitting their energy. E) Homonuclear dipolar coupling in multispin system causes very broad lines in NMR spectra.

Chemical shift [65,66]

When a strong external magnetic field B_0 is applied, the electrons that circulate around a particular nucleus induce a local field which "shields" the nucleus with the effect that the nucleus experiences a sum of both the externally applied and the induced local fields: this leads to the shift of the nucleus Larmor frequency. The frequency shift is observed in NMR spectrum and is termed the chemical shift.

For a semi-solid sample lacking the typical molecular tumbling motion, the chemical shift includes two components – isotropic (orientation-independent) and anisotropic (orientation-dependent). The sum of isotropic and anisotropic chemical shifts is presented in equation (4) as the observed chemical shift in a NMR spectrum.

$$\delta_{obs} = \delta_{iso} + \frac{1}{3}\sum_{k=1}^{3}(3cos^2\theta_k - 1).\delta_{kk} \qquad (4)$$

$$\delta_{iso} = \frac{1}{3}(\delta_{11} + \delta_{22} + \delta_{33})$$

where δ_{obs} is the observed chemical shift. δ_{iso} is the isotropic chemical shift, and the second term of the equation (4) is the anisotropic chemical shift. δ_{11}, δ_{22}, δ_{33} are orientation-dependent chemical shifts which are the three principal values of the chemical shielding tensor (Fig. 1.7). The principal values specify the size of the tensor. The orientation of the tensor with respect to the applied field and the size of the tensor are used to define the size and the direction of the local field at a particular nucleus. In other words, the tensor is a measure of the electron distribution around the nucleus. The orientation of the tensor is fixed within the molecule. Thus, the chemical shift depends on the orientation of the molecule with respect to the external magnetic field.

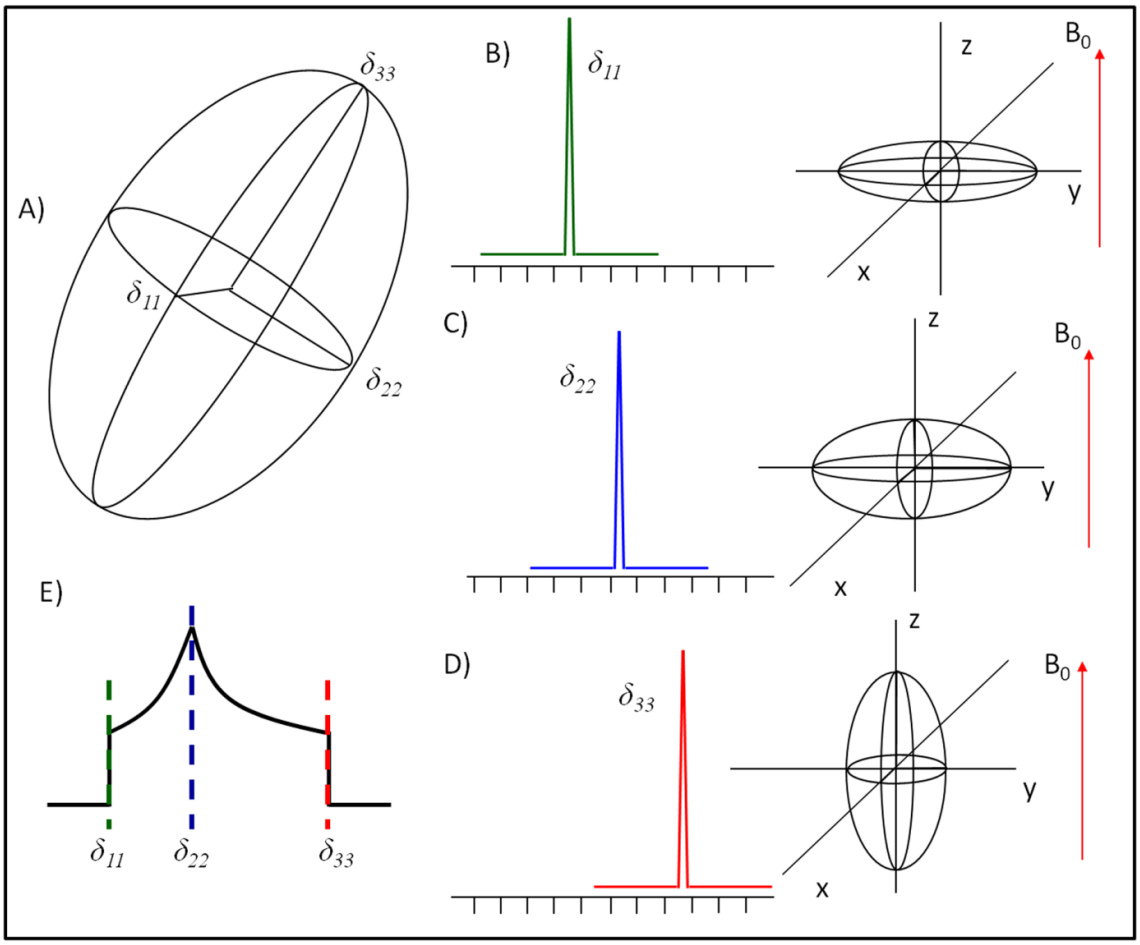

Fig. 1.6. Chemical shielding tensor and chemical shift anisotropy A) Asymmetric chemical shielding tensor. The principal axis frame has 3 axes and the sizes of the axes (the principal values of the chemical shielding tensor) are δ_{11}, δ_{22} and δ_{33} (in unit of ppm). B) One orientation in which the smallest principle axis frame δ_{11} is parallel to the z axis of the laboratory frame and the longest principle axis frame δ_{33} is perpendicular to the B_0 field direction. Thus the chemical shift of the nuclear has the value δ_{11}. C) The principle axis δ_{22} is parallel to the z axis of the laboratory frame and the principle axis δ_{33} is perpendicular to the B_0 field direction, so the chemical shift of the nuclear has the value of δ_{22}. D) The principle axis δ_{33} is parallel to the z axis of the laboratory frame or parallel to the B_0 field direction, the chemical shift of the nuclear gets value of δ_{33}. E) The chemical shift powder pattern.

Magic angle spinning

The samples in this work are proteoliposomes that are composed of POPC lipid bilayers and membrane proteins. The overall tumbling rate of these proteoliposomes is slow in comparison with the NMR time-scale. Therefore, the anisotropic chemical shift and the dipolar-dipolar coupling of atoms in the proteoliposomes cannot be averaged out. This gives rise to the powder patterns, which are observed in a NMR spectrum (Fig. 1.4.A&C). The powder patterns deriving from multiple unique nuclear sites that are chemically nonequivalent may overlap. This overlap and the powder patterns can adversely affect the NMR spectral resolution. Crucial information from the sample might therefore become obscured. To overcome this problem, magic angle spinning[67,68] (MAS) was applied to our sample. MAS technique removes the orientation-dependence of the chemical shift and the orientation dependence of nuclear dipolar couplings (^{1}H-^{13}C, ^{1}H-^{15}N, ^{13}C-^{13}C).

The removal is performed by rotating the sample in a cylindrical rotor around a spinning axis that is orientated at the magic angle of 54.74° with respect to the applied magnetic field B_0 (Fig. 1.7.D). When setting the magic angle θ = 54.74°, the term (1-3cos$^2\theta$) of the chemical shift anisotropy in the equation (4) and the term (3cos$^2\theta$ -1) of dipolar coupling Hamiltonian in the equation (2) and (3) vanish, provided the rate of spinning is faster than the dipolar-coupling line-width. Narrow lines are thus obtained (Fig. 1.4 and Fig. 1.7E&F). If the spinning speed is not sufficiently fast in comparison to the anisotropy of the interaction being spun out, a set of spinning sidebands will appear next to the line at the isotropic chemical shift. These spinning sidebands appear at the distance ±n·νrot from the isotropic signal (n is an integral number and νrot is spinning rate in unit Hz).

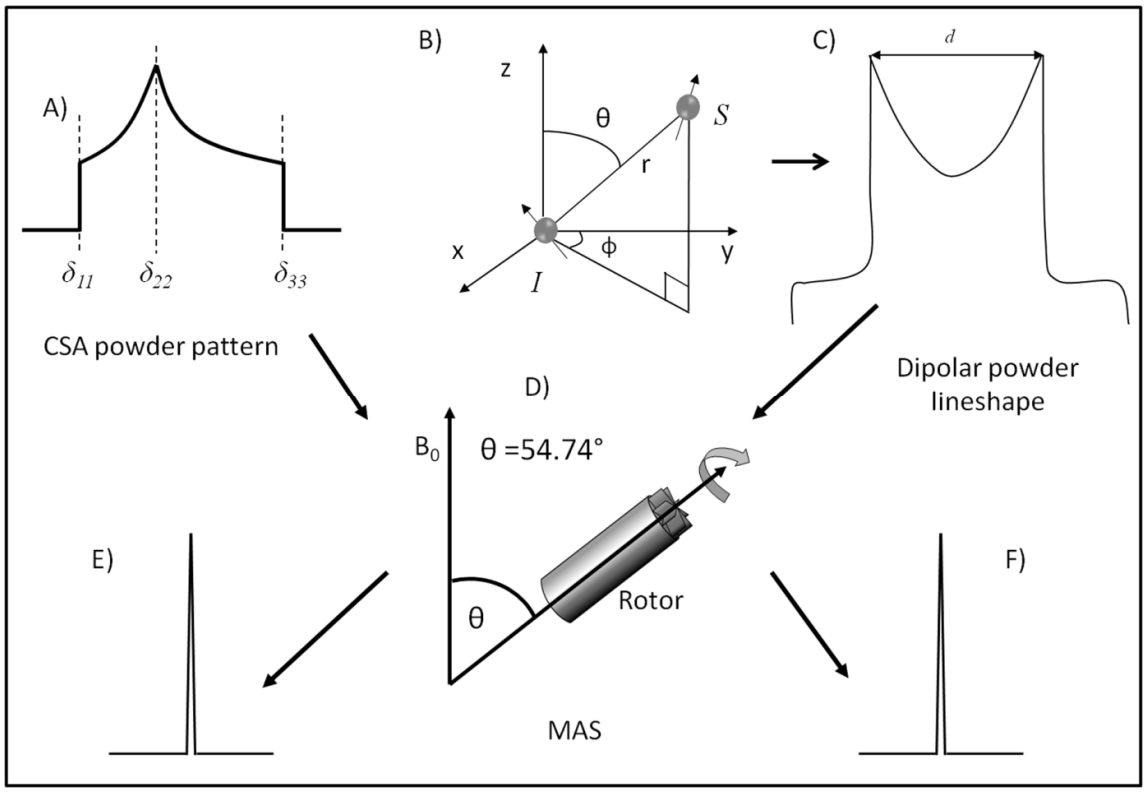

Fig. 1.7. The lines in an NMR spectrum get narrowed by MAS. A) Chemical shift anisotropy powder pattern. δ_{11}, δ_{22} δ_{33} are the principal values of the shielding tensor. B) Nuclear spin dipolar-dipolar interaction between 2 spins *I* and *S* apart each other by an internuclear distance *r*. C) Dipolar powder pattern for *I* spin in heteronuclear two-spin system with dipolar constant *d*. The horns of the powder pattern are created by spins in which the *I*-*S* internuclear vector is perpendicular to the applied field B_0(Fig. 1.5). D) Experimental set-up of MAS technique, the sample is packed into the rotor. E and F) Sharp line obtained in a NMR spectrum after the CSA and the dipolar coupling are eliminated MAS.

1.2.2. Cross polarization

The membrane proteins used in this work were labeled with ^{13}C and ^{15}N spins which have low gyromagnetic ratios. The low gyromagnetic ratio causes the small magnetization (Fig. 1.10) as shown here $(M_z = \frac{1}{2}\hbar\gamma(n_\alpha - n_\beta))$[69], where M_z is the magnetization, γ is gyromagnetic ratio, and n_α and n_β are the populations of the α and β energy states. When a pulse rotates this magnetization towards the xy plane, this transverse (or xy) magnetization starts to precess around the external magnetic field at or near the Larmor frequency. This precession induces an oscillating electric current in a wire coil, wound around the sample. The oscillating electric current is then detected by an r.f detector. This time-dependent current is called free induction decay, FID. The larger the transverse magnetization, the stronger current or the stronger NMR signal is

induced. In other words, the lower gyromagnetic ratio gives rise to lower signal to noise ratio. Moreover, the rather long T_1 relaxation times for ^{13}C and ^{15}N give rise to long delays between scans. This eventually prolongs time for data collection, provided several thousand scans are required to enhance the NMR signal to a level of interest.

To overcome these issues, the magnetization from a nearby network of spins with higher gyromagnetic ratio (^{1}H) is used to enhance the intensity of the NMR signals that are given by spins with lower gyromagnetic ratio (^{13}C, ^{15}N). The time that is needed for data collection is thereby shortened. This approach is implemented by the aid of cross polarization technique[70-72].

The main task of the technique is to transfer the polarization from the highly abundant ^{1}H spins in the sample to the low abundance X spins. This work is performed in a doubly rotating frame (^{1}H rotating frame and X rotating frame) that rotates about B_0 with the frequencies of rf irradiations that are applied on ^{1}H and X channels during the contact pulse (Fig. 1.9). X can be either ^{13}C or ^{15}N. The magnetization transfer is mediated via the heteronuclear dipolar coupling between ^{1}H and X spins in presence of the Hartmann-Hahn matching condition[70].

During the contact pulse, the rf irradiation that is applied on ^{1}H channel is called $B_1{}^{1H}$ while the rf irradiation that is applied on X channel is called $B_1{}^{X}$. These rf fields are applied on the rf channels in such a way that it leads to Hartmann-Hahn matching condition (Fig. 1.10):

$$\omega_1{}^{1H} = \gamma_H * B_1{}^{1H} = \gamma_X * B_1{}^{X} = \omega_1{}^{X} \quad (5)$$

where there is no MAS condition and γ is the gyromagnetic ratio of the respective nucleus. $\omega^1{}_{1H}$ is the nutation frequency of ^{1}H spins and $\omega_1{}^{X}$ is the nutation frequency of X spins.

Under MAS, the Hartmann-Hahn matching condition is given as follows:

$$\frac{\omega_1^{1H}}{2\pi} = \frac{\omega_1^{X}}{2\pi} \pm n\frac{\omega_r}{2\pi} \quad (6)$$

where: $\frac{\omega_r}{2\pi}$ is the spinning frequency in Hz, n is an integral number, n = 1, 2.

1.2.3. Heteronuclear spin decoupling

In biological sample such as proteoliposomes, the heteronuclear dipolar couplings (^{1}H-^{15}N and ^{1}H -^{13}C) are of the order of 20-50 kHz and cannot be removed completely by moderate MAS speeds (8 kHz - 25 kHz). To remove the effects of such heteronulear dipolar couplings, a simple way is to apply radiofrequence (rf) irradiation on the proton channel during evolution time and acquisition of NMR experiments. The application of the rf irradiation is conducted in such a way that the ^{1}H spin states are rapidly altered and therefore the diluted spins (^{13}C or ^{15}N) experience only the average spin state of ^{1}H. As a result, the heteronuclear dipolar couplings are eliminated. This reduces significantly the contribution of the energy transitions to line width of the NMR signals. The spectral resolution is thereby improved.

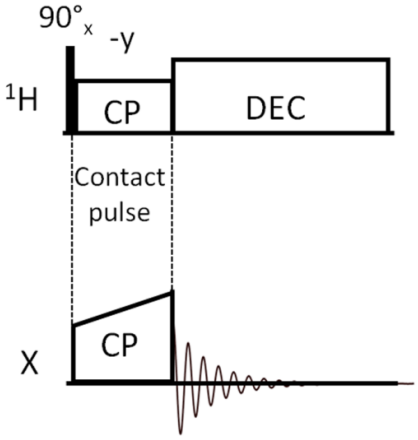

Fig. 1.8. Experimental set-up of cross-polarization (CP). The black bar indicates the 90° pulse. The transfer of polarization from ^{1}H to X happens during the contact pulse. The subscript x in "90°$_x$" means the initial pulse applied on ^{1}H channel has the phase +x. The –y is the phase of the spin lock field applied on ^{1}H channel during the contact pulse. DEC means decoupling (see Section 1.2.3).

1.2.4. Spin recoupling

As mentioned above, MAS is used to obtain the high resolution that separates NMR signals from different chemical shift sites. However, MAS also removes the effect of the dipolar coupling from which crucial geometry and structure of the sample is derived. To recover the information of interest, the dipolar coupling is reintroduced for selected periods of NMR experiment using specific recoupling pulse sequences.

For the work in this thesis, the dipolar coupling between the spins of interest is reintroduced by different recoupling mechanisms such as the double quantum SPC-5[73], the rotational resonance[74], and the proton driven spin diffusion[75-77].

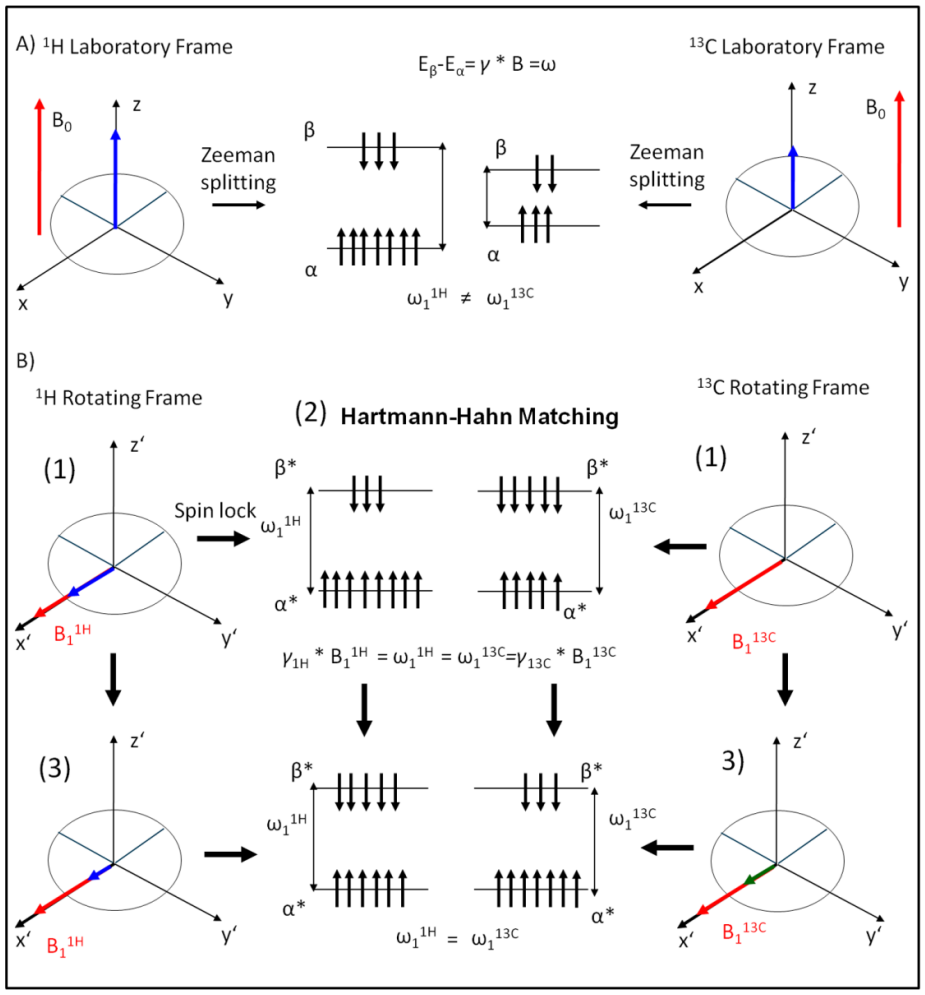

Fig. 1.9. Zeeman splitting and Cross Polarization in presence of Hartmann-Hahn Matching without MAS. Blue and green arrows represent the magnetizations. Red arrow in B) shows the rf pulses. A) Under effect of the field B_0 (red arrow) in the laboratory frame, the energy gap of ^{1}H spin states (β and α) ($\omega_0{}^{1H}$) is different from the energy gap of ^{13}C spin states ($\omega_0{}^{13C}$) due to the fixed strength of the external field B_0 and the difference of the gyromagnetic ratios ($\gamma_{1H} \neq \gamma_{13C}$). B) Similar to the effect of the field B_0 which gives rise to the nuclear Zeeman splitting (spin up ↑ (α), spin down ↓ (β)), the ^{1}H spin lock field in the doubly rotating frame lead to a splitting of ^{1}H spin states in the rotating frame (spin up ↑ (α*), spin down ↓ (β*) (1). The spin lock fields during the contact pulse ($B_1{}^{1H}$ and $B_1{}^{13C}$) are set in such a way the energy gap of the ^{1}H spin states ($\omega^1{}_{1H}$) equals the energy gap of ^{13}C spin states ($\omega^1{}_{13C}$), thus the Hartmann-Hahn matching condition is met (2). In such a situation, the magnetization can be transferred from a ^{1}H spin to a ^{13}C spin via ^{1}H -^{13}C dipolar-dipolar interaction (3).

Double quantum SPC-5

Double Quantum SPC5 recoupling[73] allows recoupling of the ^{13}C-^{13}C dipolar interaction and exciting double quantum coherence between dipolar coupled ^{13}C spins by application of rotor-synchronized rf pulses. The recoupling pulse sequence is applied on the ^{13}C spins synchronously with the sample spinning. This removes the averaging effect of MAS on the ^{13}C -^{13}C dipolar interaction. The rf irradiation on the ^{13}C is set 5 times higher than MAS frequency for exciting the double quantum state, whereas the ^{1}H -^{13}C dipolar interaction is suppressed by rf irradiation on ^{1}H spins. After t_1 evolution, the double quantum coherence is converted into single quantum coherence by another SPC-5 block and a 90° pulse and measured during the acquisition (Fig. A7).

Rotational resonance condition[74]

At MAS frequencies from 8 kHz to 13 kHz, the ^{13}C -^{13}C dipolar coupling is effectively removed. This situation can however be altered if two ^{13}C spins have an isotropic chemical shift difference ($\Delta\omega=\omega_1^{13C}- \omega_2^{13C}$) that equals to MAS frequency, $n\omega_R = \Delta\omega$ where $n = \pm1, \pm2$. In such a case, the effect of the term B in ^{13}C-^{13}C dipolar coupling (see Fig. 1.6 and equation (1) for the details of term B) is reintroduced. Thus, the degenerate Zeeman levels of the spin system are split and therefore the longitudinal magnetization between the spins is exchanged. Finally, the dipolar-dipolar coupling between the two ^{13}C spin is reintroduced.

Proton driven spin diffusion[75-77]

At moderate spinning frequencies (from 8 kHz to 13 kHz) and external magnetic fields B_0 with ^{1}H Larmor frequencies from 600 MHz to 800 MHz, ^{1}H –^{13}C dipolar interactions in the sample cannot be averaged to zero. As mentioned in section 1.2.1, term A of heteronuclear dipolar coupling shifts Zeemann energy levels. This leads to different energy transitions and hence different transition frequencies for each chemically unique ^{13}C spin across the sample. Thus, every chemically unique ^{13}C spin of the sample has a slightly different resonance frequency. This gives rise to broadened lines. The broadening of ^{13}C lines in an NMR spectrum leads to spectral overlap. Within the spectral overlap, ^{13}C spins that have the same energy states (i.e. the flip-

flop states) spontaneously exchange their energy resulting in the flip-flop transitions. The ^{13}C-^{13}C dipolar interactions are therefore reintroduced.

The proton driven spin diffusion (PDSD) is used in this work as presented in the pulse sequence in Fig. A4. The pulse sequence is implemented at spinning frequency of 9375 Hz and 12500 Hz under the external magnetic fields of 600 MHz and 800 MHz ^{1}H Larmor frequencies, respectively. These spinning frequencies correspond to the n = 2 rotational resonance between Cα and CO and thus facilitate interresidual magnetization transfer between neighboring residues.

In the pulse sequence, after CP, during t_1, an rf irradiation is applied on ^{1}H spins (decoupling) to remove the heteronuclear dipolar between ^{1}H and ^{13}C while the ^{13}C isotropic chemical shifts evolve and are recorded. In the end of t_1, the transverse magnetization of ^{13}C spins is rotated toward the z-axis. Here, the rf irradiation on ^{1}H spins is turned off thus leading to the recovery of the ^{1}H –^{13}C dipolar interactions. The PDSD is therefore activated by giving rise to recoupling of ^{13}C-^{13}C interactions. This period in the pulse sequence is also called ^{13}C mixing time. At the end of the ^{13}C mixing time, the ^{13}C magnetization along to the z-axis is rotated back to the transverse plane. The decoupling is turned on again when ^{13}C signals are detected in t_2. Fourier transformation of time domain data collected during t_1 and t_2 will give rise to spectra with cross peaks that provide the information of ^{13}C-^{13}C correlations.

1.2.5. The broadening of the line width

The more the NMR lines in a NMR spectrum are clearly separated from one another, the more information of the sample is obtained. The separation of the NMR lines or the resolution of a NMR spectrum is determined by the line width of the NMR line (peak). The line width of a peak is specified by the width measured at half the peak height[69]. The size or the broadening of this width is dependent not only on the relaxation rate of the transverse magnetization but also on the conformational disorder caused by anisotropic environment of sample (i.e. lipid models in case of membrane proteins) or the non-homogeneity of the applied magnetic field across the sample.

The bulk magnetization of the sample is created by adding together the magnetic moments from each spin in presence of an applied magnetic field B_0 (Fig.1.10). At

equilibrium state, x and y-components of this magnetization (the transverse magnetization) are equal to zero and the z-component (the longitudinal magnetization) is given by the Boltzmann distribution. When an rf pulse is applied to the equilibrium magnetization, the z-magnetization is rotated towards the transverse plane (xy plane) and thus a transverse magnetization is created. The transverse magnetization then precesses about the field direction (z axis). This precession is detected in the form of the FID that is described by the function[69]

$$S(t) = A\exp(i\Omega t)\exp(-Rt)$$

where i is the imaginary unit, Ω is the precession frequency, and $R = 1/T_2$, T_2 is the decay constant of the transverse magnetization and R is the rate constant the transverse relaxation.

Fourier transformation of this function gives a line width of R/π Hz. Thus, the faster the relaxation goes, the greater R, the broader the NMR line is. The relaxation rate of the transverse magnetization in the proteoliposome sample of this work can be slowed down by attenuating the dipolar interactions with the aid of MAS and radio frequency pulses as shown in Section 1.2.1 and 1.2.3.

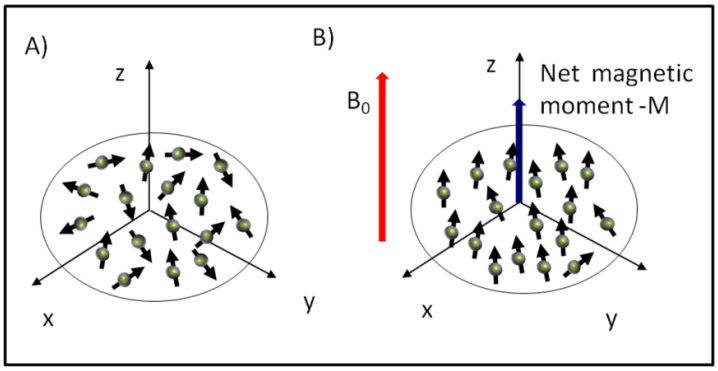

Fig. 1.10. Net magnetic moment – Longitudinal magnetization. A) Nuclear magnetic moments without the external magnetic field B_0 (red arrow). B) Net magnetic moment (blue arrow) is built up in presence of the field.

The conformational disorder in the sample gives rise to different Larmor frequencies for each chemically unique nuclear spin in the same manner that chemically nonequivalent spins cause different Larmor frequencies. This leads to different line widths existing for the chemically unique nuclear spin across the sample. As a result, the sum of these line widths from the whole sample results in a broad line.

The line broadening caused by an inhomogeneous external field can be eliminated by well-adjusted shimming when performing NMR experiments. However, line broadening caused by conformational disorder [78] may still limit the resolution of solid-state NMR spectra of membrane proteins.

1.2.6. J coupling, T_2 filter, and insensitive nuclei enhanced by polarization transfer

As mentioned in section 1.2.1, the dipolar coupling between two spins occurs when the magnetic moment of one spin interacts with the magnetic moment of another spin through space. Thus, the distance between spins is encoded in their dipolar coupling. However, if the molecules in the sample rotate significantly faster than the frequency associated with the coupling (i.e. the molecules are tumbling in solution), the dipolar interaction would be averaged to zero and no structural information of the sample can be observed via the dipolar coupling. In such a case, the indirect (*J* coupling)[79] interaction between nuclear magnetic moments which is mediated by the electrons may be employed. The information on the chemical connectivity between atoms can therefore be obtained.

In a heteronuclear spin system as ^{1}H-^{13}C, the transverse magnetization of ^{1}H during a spin echo (delay -180° - delay) will dephase under the effect of strong dipolar couplings, which are averaged out for mobile regions. This allows for selecting the mobile ^{1}H magnetizations by adjusting the delay duration without any effect on the mobile magnetization. This technique is known as T_2 filter[80] which together with the ^{1}H spin-diffusion[2] and the CP technique is incorporated into the water-edited solid-state NMR[2,80,81] used in the current work to probe the topology of the membrane proteins in the lipid bilayer (the pulse sequence is presented in Fig. A3). In the pulse sequence, T_2 filter (τ -180°C - τ) is employed to select mobile water and lipid ^{1}H magnetizations which then evolve and are recorded during time t_1. In the end of t_1, after the ^{1}H magnetizations of water and lipid are rotated towards the z-axis, these ^{1}H magnetizations spin-diffuses to the rigid protons of the protein during the period of t(HH). After the magnetizations transfer from ^{1}H spins to ^{13}C spins via CP, ^{13}C signals are detected during time t_2.

However, the evolution of the transverse magnetization of ^{1}H and ^{13}C in the heteronuclear spin system will be affected by *J* coupling if the spin echo is applied on both ^{1}H and ^{13}C spins as in case of INEPT[69,82,83] (Insensitive Nuclei Enhanced by Polarization Trasnfer, the pulse sequence is shown in Fig. A1 and A2). In this situation, the effect of *J* coupling on ^{1}H spins makes the in-phase magnetization of ^{1}H spins evolve into the anti-phase magnetization that is then transferred to ^{13}C spins to enhance the signals observed from ^{13}C spins. After the polarization transfer, under the effect of *J* coupling, the anti-phase magnetization of ^{13}C spins will evolve into the in-phase magnetization which is observable magnetization and will be detected during the acquisition. In current work, the INEPT technique was also used to detect the mobile part of the sample.

References

1. Huster, D., Yao, Y.L., Jakes, K. & Hong, M. Conformational changes of colicin Ia channel-forming domain upon membrane binding: a solid-state NMR study. *Biochimica Et Biophysica Acta-Biomembranes* **1561**, 159-170 (2002).
2. Huster, D., Yao, X.L. & Hong, M. Membrane protein topology probed by H-1 spin diffusion from lipids using solid-state NMR spectroscopy. *Journal of the American Chemical Society* **124**, 874-883 (2002).
3. Huster, D. Investigations of the structure and dynamics of membrane-associated peptides by magic angle spinning NMR. *Progress in Nuclear Magnetic Resonance Spectroscopy* **46**, 79-107 (2005).
4. Etzkorn, M., Martell, S., Andronesi, O.C., Seidel, K., Engelhard, M. & Baldus, M. Secondary structure, dynamics, and topology of a seven-helix receptor in native membranes, studied by solid-state NMR spectroscopy. *Angewandte Chemie-International Edition* **46**, 459-462 (2007).
5. Lange, A., Giller, K., Hornig, S., Martin-Eauclaire, M.F., Pongs, O., Becker, S. & Baldus, M. Toxin-induced conformational changes in a potassium channel revealed by solid-state NMR. *Nature* **440**, 959-962 (2006).
6. Li, C., Qin, H., Gao, F.P. & Cross, T.A. Solid-state NMR characterization of conformational plasticity within the transmembrane domain of the influenza A M2 proton channel. *Biochimica Et Biophysica Acta-Biomembranes* **1768**, 3162-3170 (2007).
7. Li, Y., Berthold, D.A., Gennis, R.B. & Rienstra, C.M. Chemical shift assignment of the transmembrane helices of DsbB, a 20-kDa integral membrane enzyme, by 3D magic-angle spinning NMR spectroscopy. *Protein Science* **17**, 199-204 (2008).
8. Andronesi, O.C., Becker, S., Seidel, K., Heise, H., Young, H.S. & Baldus, M. Determination of membrane protein structure and dynamics by magic-angle-spinning solid-state NMR spectroscopy. *Journal of the American Chemical Society* **127**, 12965-12974 (2005).
9. Heise, H., Hoyer, W., Becker, S., Andronesi, O.C., Riedel, D. & Baldus, M. Molecular-level secondary structure, polymorphism, and dynamics of full-length alpha-synuclein fibrils studied by solid-state NMR. *Proceedings of the National Academy of Sciences of the United States of America* **102**, 15871-15876 (2005).
10. Wasmer, C., Lange, A., Van Melckebeke, H., Siemer, A.B., Riek, R. & Meier, B.H. Amyloid fibrils of the HET-s(218-289) prion form a beta solenoid with a triangular hydrophobic core. *Science* **319**, 1523-1526 (2008).
11. Van Melckebeke, H., Wasmer, C., Lange, A., Eiso, A.B., Loquet, A., Bockmann, A. & Meier, B.H. Atomic-Resolution Three-Dimensional Structure of HET-s(218-289) Amyloid Fibrils by Solid-State NMR Spectroscopy. *Journal of the American Chemical Society* **132**, 13765-13775 (2010).
12. Schuetz, A., Wasmer, C., Habenstein, B., Verel, R., Greenwald, J., Riek, R., Boeckmann, A. & Meier, B.H. Protocols for the Sequential Solid-State NMR Spectroscopic Assignment of a Uniformly Labeled 25 kDa Protein: HET-s(1-227). *Chembiochem* **11**, 1543-1551 (2010).

13. Cady, S.D., Schmidt-Rohr, K., Wang, J., Soto, C.S., Degrado, W.F. & Hong, M. Structure of the amantadine binding site of influenza M2 proton channels in lipid bilayers. *Nature* **463**, 689-92 (2010).
14. Cady, S., Wang, T. & Hong, M. Membrane-Dependent Effects of a Cytoplasmic Helix on the Structure and Drug Binding of the Influenza Virus M2 Protein. *Journal of the American Chemical Society* **133**, 11572-11579 (2011).
15. Maslennikov, I., Klammt, C., Hwang, E., Kefala, G., Okamura, M., Esquivies, L., Moers, K., Glaubitz, C., Kwiatkowski, W., Jeon, Y.H. & Choe, S. Membrane domain structures of three classes of histidine kinase receptors by cell-free expression and rapid NMR analysis. *Proceedings of the National Academy of Sciences of the United States of America* **107**, 10902-10907 (2010).
16. Kumar, J., Sreeramulu, S., Schmidt, T.L., Richter, C., Vonck, J., Heckel, A., Glaubitz, C. & Schwalbe, H. Prion Protein Amyloid Formation Involves Structural Rearrangements in the C-Terminal Domain. *Chembiochem* **11**, 1208-1213 (2010).
17. Zhong, L., Bamm, V.V., Ahmed, M.A.M., Harauz, G. & Ladizhansky, V. Solid-state NMR spectroscopy of 18.5 kDa myelin basic protein reconstituted with lipid vesicles: Spectroscopic characterisation and spectral assignments of solvent-exposed protein fragments. *Biochimica Et Biophysica Acta-Biomembranes* **1768**, 3193-3205 (2007).
18. Shi, L., Ahmed, M.A.M., Zhang, W., Whited, G., Brown, L.S. & Ladizhansky, V. Three-Dimensional Solid-State NMR Study of a Seven-Helical Integral Membrane Proton Pump-Structural Insights. *Journal of Molecular Biology* **386**, 1078-1093 (2009).
19. Hiller, M., Krabben, L., Vinothkumar, K.R., Castellani, F., van Rossum, B.J., Kuhlbrandt, W. & Oschkinat, H. Solid-state magic-angle spinning NMR of outer-membrane protein G from Escherichia coli. *Chembiochem* **6**, 1679-84 (2005).
20. Mani, R., Cady, S.D., Tang, M., Waring, A.J., Lehrert, R.I. & Hong, M. Membrane-dependent oligomeric structure and pore formation of beta-hairpin antimicrobial peptide in lipid bilayers from solid-state NMR. *Proceedings of the National Academy of Sciences of the United States of America* **103**, 16242-16247 (2006).
21. Yang, J., Aslimovska, L. & Glaubitz, C. Molecular Dynamics of Proteorhodopsin in Lipid Bilayers by Solid-State NMR. *Journal of the American Chemical Society* **133**, 4874-4881 (2011).
22. Hu, J., Asbury, T., Achuthan, S., Li, C., Bertram, R., Quine, J.R., Fu, R. & Cross, T.A. Backbone structure of the amantadine-blocked trans-membrane domain M2 proton channel from influenza A virus. *Biophysical Journal* **92**, 4335-4343 (2007).
23. Yi, M., Cross, T.A. & Zhou, H.-X. Conformational heterogeneity of the M2 proton channel and a structural model for channel activation. *Proceedings of the National Academy of Sciences of the United States of America* **106**, 13311-13316 (2009).

24. Hu, F., Luo, W., Cady, S.D. & Hong, M. Conformational plasticity of the influenza A M2 transmembrane helix in lipid bilayers under varying pH, drug binding, and membrane thickness. *Biochimica Et Biophysica Acta-Biomembranes* **1808**, 415-423 (2011).
25. Park, S.H. & Opella, S.J. Tilt angle of a trans-membrane helix is determined by hydrophobic mismatch. *Journal of Molecular Biology* **350**, 310-318 (2005).
26. Bour, S., Schubert, U. & Strebel, K. The human-immunodeficiency-virus type-1 Vpu protein specifically binds to the cytoplasmic domain of CD4 - implications for the mechanism of degradation. *Journal of Virology* **69**, 1510-1520 (1995).
27. Margottin, F., Benichou, S., Durand, H., Richard, V., Liu, L.X., Gomas, E. & Benarous, R. Interaction between the cytoplasmic domains of HIV-1 Vpu and CD4: Role of Vpu residues involved in CD4 interaction and in vitro CD4 degradation. *Virology* **223**, 381-386 (1996).
28. Willey, R.L., Maldarelli, F., Martin, M.A. & Strebel, K. Human-immunodeficiency-virus type-1 vpu protein induces rapid degradation of CD4. *Journal of Virology* **66**, 7193-7200 (1992).
29. Chen, M.Y., Maldarelli, F., Karczewski, M.K., Willey, R.L. & Strebel, K. Human-immunodeficiency-virus type-1 Vpu protein induces degradation of CD4 invitro - the cytoplasmic domain of CD4 contributes to Vpu sensitivity. *Journal of Virology* **67**, 3877-3884 (1993).
30. Tiganos, E., Yao, X.J., Friborg, J., Daniel, N. & Cohen, E.A. Putative alpha-helical structures in the human immunodeficiency virus type 1 Vpu protein and CD4 are involved in binding and degradation of the CD4 molecule. *Journal of Virology* **71**, 4452-4460 (1997).
31. Magadan, J.G., Perez-Victoria, F.J., Sougrat, R., Ye, Y., Strebel, K. & Bonifacino, J.S. Multilayered mechanism of CD4 downregulation by HIV-1 Vpu involving distinct ER retention and ERAD targeting steps. *PLoS Pathog* **6**, e1000869 (2010).
32. Alberts, B., Johnson, A., Lewis, J., M., R., Roberts, K. & Walter, P. *Molecular Biology of The Cell*, (Garland Science, the United Stated of America, 2008).
33. Maddon, P.J., Littman, D.R., Godfrey, M., Maddon, D.E., Chess, L. & Axel, R. The isolation and nucleotide-sequence of a cDNA-encoding the T-cell surface protein-T4 - a new member of the immunoglobulin gene family. *Cell* **42**, 93-104 (1985).
34. Maddon, P.J., Molineaux, S.M., Maddon, D.E., Zimmerman, K.A., Godfrey, M., Alt, F.W., Chess, L. & Axel, R. Structure and expression of the human and mouse T4 genes. *Proceedings of the National Academy of Sciences of the United States of America* **84**, 9155-9159 (1987).
35. Willbold, D. & Roesch, P. Solution structure of the human CD4 (403-419) receptor peptide. *Journal of Biomedical Science* **3**, 435-441 (1996).
36. Wittlich, M., Koenig, B.W., Hoffinann, S. & Willbold, D. Structural characterization of the transmembrane and cytoplasmic domains of human CD4. *Biochimica Et Biophysica Acta-Biomembranes* **1768**, 2949-2960 (2007).

37. Wittlich, M., Thiagarajan, P., Koenig, B.W., Hartmann, R. & Willbold, D. NMR structure of the transmembrane and cytoplasmic domains of human CD4 in micelles. *Biochim Biophys Acta* **1798**, 122-7 (2010).
38. Meuer, S.C., Schlossman, S.F. & Reinherz, E.L. Clonal analysis of human cytotoxic lymphocytes-T - T4+ and T8+ effector T-cells recognize products of different major histocompatibility complex regions. *Proceedings of the National Academy of Sciences of the United States of America-Biological Sciences* **79**, 4395-4399 (1982).
39. Biddison, W.E., Rao, P.E., Talle, M.A., Goldstein, G. & Shaw, S. Possible involvement of the T4-molecule in T-cell recognition of class-II HLA antigens - evidence from studies of CTL-target cell binding. *Journal of Experimental Medicine* **159**, 783-797 (1984).
40. Veillette, A., Bookman, M.A., Horak, E.M. & Bolen, J.B. The CD4 and CD8 T-cell surface-antigens are associated with the internal membrane tyrosine-protein kinase p56lck. *Cell* **55**, 301-308 (1988).
41. Dalgleish, A.G., Beverley, P.C.L., Clapham, P.R., Crawford, D.H., Greaves, M.F. & Weiss, R.A. The CD4 (T4) antigen is an essential component of the receptor for the aids retrovirus. *Nature* **312**, 763-767 (1984).
42. Lasky, L.A., Nakamura, G., Smith, D.H., Fennie, C., Shimasaki, C., Patzer, E., Berman, P., Gregory, T. & Capon, D.J. Delineation of a region of the human immunodeficiency virus type 1 gp120 glycoprotein critical for interaction with the CD4 receptor. *Cell* **50**, 975-85 (1987).
43. Aiken, C., Konner, J., Landau, N.R., Lenburg, M.E. & Trono, D. Nef induces CD4 endocytosis: requirement for a critical dileucine motif in the membrane-proximal CD4 cytoplasmic domain. *Cell* **76**, 853-64 (1994).
44. Strebel, K., Klimkait, T. & Martin, M.A. A novel gene of HIV-1, vpu, and its 16-kilodalton product. *Science* **241**, 1221-1223 (1988).
45. Cohen, E.A., Terwilliger, E.F., Sodroski, J.G. & Haseltine, W.A. Identification of a protein encoded by the vpu gene of HIV-1. *Nature* **334**, 532-534 (1988).
46. Chengmayer, C., Quiroga, M., Tung, J.W., Dina, D. & Levy, J.A. Viral determinants of human-immunodeficiency-virus type-1 T-cell or macrophage tropism, cytopathogenicity, and CD4 antigen modulation. *Journal of Virology* **64**, 4390-4398 (1990).
47. Strebel, K., Klimkait, T., Maldarelli, F. & Martin, M.A. Molecular and biochemical analyses of human immunodeficiency virus type-1 *vpu* protein. *Journal of Virology* **63**, 3784-3791 (1989).
48. Maldarelli, F., Chen, M.Y., Willey, R.L. & Strebel, K. Human-immunodeficiency-virus type-1 Vpu protein is an oligomeric type-I integral membrane-protein. *Journal of Virology* **67**, 5056-5061 (1993).
49. Klimkait, T., Strebel, K., Hoggan, M.D., Martin, M.A. & Orenstein, J.M. The human immunodeficiency virus type 1-specific protein vpu is required for efficient virus maturation and release. *Journal of Virology* **64**, 621-629 (1990).
50. Willey, R.L., Maldarelli, F., Martin, M.A. & Strebel, K. Human immunodeficiency virus type-1 Vpu protein regulates the formation of intracellular gp160-CD4 complexes. *Journal of Virology* **66**, 226-234 (1992).

51. Terwilliger, E.F., Cohen, E.A., Lu, Y.C., Sodroski, J.G. & Haseltine, W.A. Functional role of human immunodeficiency virus type 1 vpu. *Proc Natl Acad Sci U S A* **86**, 5163-7 (1989).
52. Schubert, U., Bour, S., FerrerMontiel, A.V., Montal, M., Maldarelli, F. & Strebel, K. The two biological activities of human immunodeficiency virus type 1 Vpu protein involve two separable structural domains. *Journal of Virology* **70**, 809-819 (1996).
53. Reitz, M.S., Jr., Hall, L., Robert-Guroff, M., Lautenberger, J., Hahn, B.M., Shaw, G.M., Kong, L.I., Weiss, S.H., Waters, D., Gallo, R.C. & et al. Viral variability and serum antibody response in a laboratory worker infected with HIV type 1 (HTLV type IIIB). *AIDS Res Hum Retroviruses* **10**, 1143-55 (1994).
54. Park, S.H., Mrse, A.A., Nevzorov, A.A., Mesleh, M.F., Oblatt-Montal, M., Montal, M. & Opella, S.J. Three-dimensional structure of the channel-forming trans-membrane domain of virus protein "u" (Vpu) from HIV-1. *Journal of Molecular Biology* **333**, 409-424 (2003).
55. Park, S.H., De Angelis, A.A., Nevzorov, A.A., Wu, C.H. & Opella, S.J. Three-dimensional structure of the transmembrane domain of Vpu from HIV-1 in aligned phospholipid bicelles. *Biophysical Journal* **91**, 3032-3042 (2006).
56. Sharpe, S., Yau, W.M. & Tycko, R. Structure and dynamics of the HIV-1 Vpu transmembrane domain revealed by solid-state NMR with magic-angle spinning. *Biochemistry* **45**, 918-933 (2006).
57. Lu, J.X., Sharpe, S., Ghirlando, R., Yau, W.M. & Tycko, R. Oligomerization state and supramolecular structure of the HIV-1 Vpu protein transmembrane segment in phospholipid bilayers. *Protein Sci* **19**, 1877-96 (2010).
58. Ewart, G.D., Sutherland, T., Gage, P.W. & Cox, G.B. The Vpu protein of human immunodeficiency virus type 1 forms cation-selective ion channels. *Journal of Virology* **70**, 7108-7115 (1996).
59. Schubert, U., FerrerMontiel, A.V., OblattMontal, M., Henklein, P., Strebel, K. & Montal, M. Identification of an ion channel activity of the Vpu transmembrane domain and its involvement in the regulation of virus release from HIV-1-infected cells. *Febs Letters* **398**, 12-18 (1996).
60. Bolduan, S., Votteler, J., Lodermeyer, V., Greiner, T., Koppensteiner, H., Schindler, M., Thiel, G. & Schubert, U. Ion channel activity of HIV-1 Vpu is dispensable for counteraction of CD317. *Virology* **416**, 75-85 (2011).
61. Federau, T., Schubert, U., Flossdorf, J., Henklein, P., Schomburg, D. & Wray, V. Solution structure of the cytoplasmic domain of the human immunodeficiency virus type 1 encoded virus protein U (Vpu). *Int J Pept Protein Res* **47**, 297-310 (1996).
62. Wray, V., Federau, T., Henklein, P., Klabunde, S., Kunert, O., Schomburg, D. & Schubert, U. Solution Structure of the Hydrophilic Region of Hiv-1 Encoded Virus Protein-U (Vpu) by Cd and H-1-Nmr Spectroscopy. *International Journal of Peptide and Protein Research* **45**, 35-43 (1995).
63. Willbold, D., Hoffmann, S. & Rosch, P. Secondary structure and tertiary fold of the human immunodeficiency virus protein U (Vpu) cytoplasmic domain in solution. *European Journal of Biochemistry* **245**, 581-588 (1997).

64. Wittlich, M., Koenig, B.W., Stoldt, M., Schmidt, H. & Willbold, D. NMR structural characterization of HIV-1 virus protein U cytoplasmic domain in the presence of dodecylphosphatidylcholine micelles. *Febs Journal* **276**, 6560-6575 (2009).
65. Duer, M.J. *Introduction to Solid-State NMR Spectroscopy*, 349 (Blackwell Publishing Ltd, 2004).
66. Harris, R.K. *Nuclear Magnetic Resonance Spectroscopy*, 260 (Longman, 2005).
67. Lowe, I.J. Free Induction Decays of Rotating Solids. *Physical Review Letters* **2**, 285-287 (1959).
68. Andrew, E.R., Bradbury, A. & Eades, R.G. Nuclear Magnetic Resonance Spectra from a Crystal Rotated at High Speed. *Nature* **182**, 1659-1659 (1958).
69. Keeler, J. *Understanding NMR Spectroscopy*, (Wiley, 2011).
70. Hartmann, S.R. & Hahn, E.L. Nuclear Double Resonance in Rotating Frame. *Physical Review* **128**, 2042-& (1962).
71. Pines, A., Gibby, M.G. & Waugh, J.S. Proton-Enhanced Nmr of Dilute Spins in Solids. *Journal of Chemical Physics* **59**, 569-590 (1973).
72. Stejskal, E.O., Schaefer, J. & Waugh, J.S. Magic-Angle Spinning and Polarization Transfer in Proton-Enhanced Nmr. *Journal of Magnetic Resonance* **28**, 105-112 (1977).
73. Hohwy, M., Rienstra, C.M., Jaroniec, C.P. & Griffin, R.G. Fivefold symmetric homonuclear dipolar recoupling in rotating solids: Application to double quantum spectroscopy. *Journal of Chemical Physics* **110**, 7983-7992 (1999).
74. Raleigh, D.P., Levitt, M.H. & Griffin, R.G. Rotational Resonance in Solid-State Nmr. *Chemical Physics Letters* **146**, 71-76 (1988).
75. Suter, D. & Ernst, R.R. Spectral Spin Diffusion in the Presence of an Extraneous Dipolar Reservoir. *Physical Review B* **25**, 6038-6041 (1982).
76. Meier, B.H. *Polarization transfer and spin diffusion in solid-state NMR*, (Academic Press, New York, 1994).
77. Bloembergen, N. On the Interaction of Nuclear Spins in a Crystalline Lattice. *Physica* **15**, 386-426 (1949).
78. Su, Y. & Hong, M. Conformational Disorder of Membrane Peptides Investigated from Solid-State NMR Line Widths and Line Shapes. *Journal of Physical Chemistry B* **115**, 10758-10767 (2011).
79. Gordon, R.S. & Hitchens, K.T. *Fundamentals of Protein NMR Spectroscopy*, (Springer, Netherlands, 2006).
80. Kumashiro, K.K., Schmidt-Rohr, K., Murphy, O.J., Ouellette, K.L., Cramer, W.A. & Thompson, L.K. A novel tool for probing membrane protein structure: Solid-state NMR with proton spin diffusion and X-nucleus detection. *Journal of the American Chemical Society* **120**, 5043-5051 (1998).
81. Kijac, A., Shih, A.Y., Nieuwkoop, A.J., Schulten, K., Sligar, S.G. & Rienstra, C.M. Lipid-Protein Correlations in Nanoscale Phospholipid Bilayers Determined by Solid-State Nuclear Magnetic Resonance. *Biochemistry* **49**, 9190-9198 (2010).
82. Morris, G.A. & Freeman, R. Enhancement of Nuclear Magnetic-Resonance Signals by Polarization Transfer. *Journal of the American Chemical Society* **101**, 760-762 (1979).

83. Burum, D.P. & Ernst, R.R. Net Polarization Transfer Via a J-Ordered State for Signal Enhancement of Low-Sensitivity Nuclei. *Journal of Magnetic Resonance* **39**, 163-168 (1980).

Chapter 2. Materials and Methods

2.1. Sample preparation

2.1.1. Protein expression and purification[1]

Expression of CD4(372-433) peptide and full-length Vpu protein

The plasmids pTKK19_CD4tmcyt[1] and pTKK19_Vpu were transformed into *Escherichia coli* C43(DE3) competent cells to express fusion ubiquitine/CD4 peptide and ubiquitine/full-length Vpu protein, respectively. The expression was then conducted either in LB medium or in M9 medium. In M9 medium, which contains 2 g of ^{13}C-glucose and 1 g of ^{15}N-ammonium chloride per litter, the fusion ubiquitine/CD4 peptide and the ubiquitine/full-length Vpu protein were labeled with isotopes ^{13}C and ^{15}N, which gives rise to NMR signals. When the absorbance of the cells in the media reaches around 7 at the wave length of 600 nm, the expression was induced using IPTG concentration of 1 mM. The expression was performed at 37°C with shaking of the expression media at the speed of 160 rotations per minute. Five and eight hours after the IPTG induction, the CD4 and VpU containing cells in the LB culture were harvested, respectively, whereas 12 hours after the IPTG induction, the cells in the M9 expression culture were harvested. After harvesting, the cell mass was frozen and stored at -20°C.

Extraction of CD4(372-433) peptide and full-length Vpu protein

The fusion protein/peptide was extracted using sonication and the detergent based cell lysis. The harvested cells were resuspended in Resuspension buffer (pH 8.0, 50 mM Tris–HCl, 25% (w/v) sucrose, 0.1% (w/v) NaN_3) that was then supplemented with the protease inhibitor mix Complete (Boehringer Mannheim). The resulting mixture was subsequently sonicated on ice using a Branson 250® equipped with a microtip for 3 cycles. Each cycle has 30 seconds of sonication and 60 seconds without sonication. During the period of 60 seconds, the mixture stands inside the ice to avoid heating up the protein of interest. The duty cycle and the output control parameters were set to 50% and 6, repsepectively. In the following step, the detergent-based cell lysis, a lysis buffer (pH 8.0, 50 mM Tris–HCl, 1% (v/v) Triton X-100, 1% (w/v) cholic acid, 600 mM NaCl, 0.1% (w/v) NaN_3 and 8mM $MgCl_2$) was added to the mixture.

The mixture was then incubated at 4°C for 14 hours on a roller shaker. The soluble protein was afterward separated from other parts of the cells by centrifugation at a 48000 g, 10°C for 20 minutes.

Purification of CD4(372-433) peptide and full-length Vpu protein

The purification workflow was summarized in the Fig. 2.1.

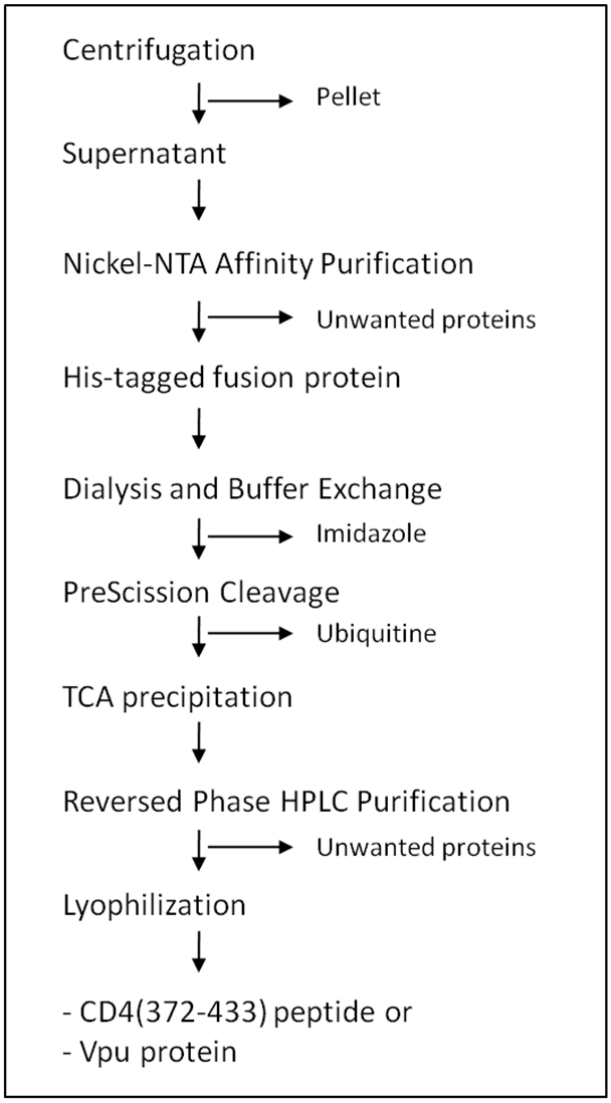

Fig. 2.1. Summary of purification strategy for the CD4(372-433) peptide and full-length Vpu

As shown Fig. 2.1, the supernatant that is collected after the centrifugation was loaded onto a gravity column (bed volume 4 mL) previously packed with nickel–NTA agarose (Qiagen) and already equilibrated with the binding buffer (pH 8.0, 50 mM Tris–HCl, 12.5% (w/v) sucrose, 0.5% (v/v) Triton X-100, 0.5% (w/v) cholic acid, 300

mM NaCl, 0.1% (w/v) NaN_3, Protease cocktail tablet inhibitor EDTA free (by Roche)).

To remove non-specifically bound proteins, the column was washed with the washing buffer that contains the binding buffer and imidazole at different concentrations (20 and 50 mM imidazole). Each washing step was performed with 10 bed column volumes. The purified protein was eluted with 5 bed column volumes of the eluting buffer that contains the binding buffer and imidazole of 300 mM.

In the following step, the dialysis was performed to remove the imidazole from the purified protein using a dialysis buffer (50 mM Tris–HCl, 150 mM NaCl, 0.5% (v/v) Triton X-100, 1 mM DTT, pH 7.0). This lasts for 32 - 48 hours. The fusion protein/peptide was then cleaved by PreScision protease (GE Healthcare) to get the CD4(372-433) peptide or the full-length Vpu protein. The reaction was conducted in the dialysis buffer with 3 mM of DTT for 12 hours at 4°C or room temperature with gentle agitation.

TCA (10%) precipitation was then conducted at 4°C, 1 hour with gentle agitation to separate the cleaved protein/peptide of interest from other contaminants. The precipitate, CD4(372-433) peptide and Vpu protein, were thereafter collected by centrifugation at 4°C, 15000 rpm, for 20 minutes and washed two times using pure and cold acetone (minus 20°C). The residual acetone was removed by evaporation on the lab bench for 10 to 20 minutes. At this step, the precipitates were kept on ice. The samples were then dissolved in the buffer containing 40% of Acetonitrile and 0.09% of Trichloroacetic acid and used for the reversed phase chromatography.

Purification of the cleaved proteins using the reversed phase chromatography

The protein solution was loaded onto an equilibrated RESOURCE RPC 3 ml column (GE Healthcare) mounted on the HPLC system (Agilent). The column was previously equilibrated using buffer A (0.1% TCA in water). The column was operated at room temperature at a flow rate of 1 ml/min. The absorbance was monitored at 214 nm and the proteins were eluted using a buffer gradient from 100% buffer A to 100% buffer B (80% Acetonitrile and 0.08% TCA) as shown Fig. 2.2. All proteins were eluted between minutes 18 and 27, which corresponds to a concentration of buffer B in the range from 60% to 80% as presented in Fig. 2.2.

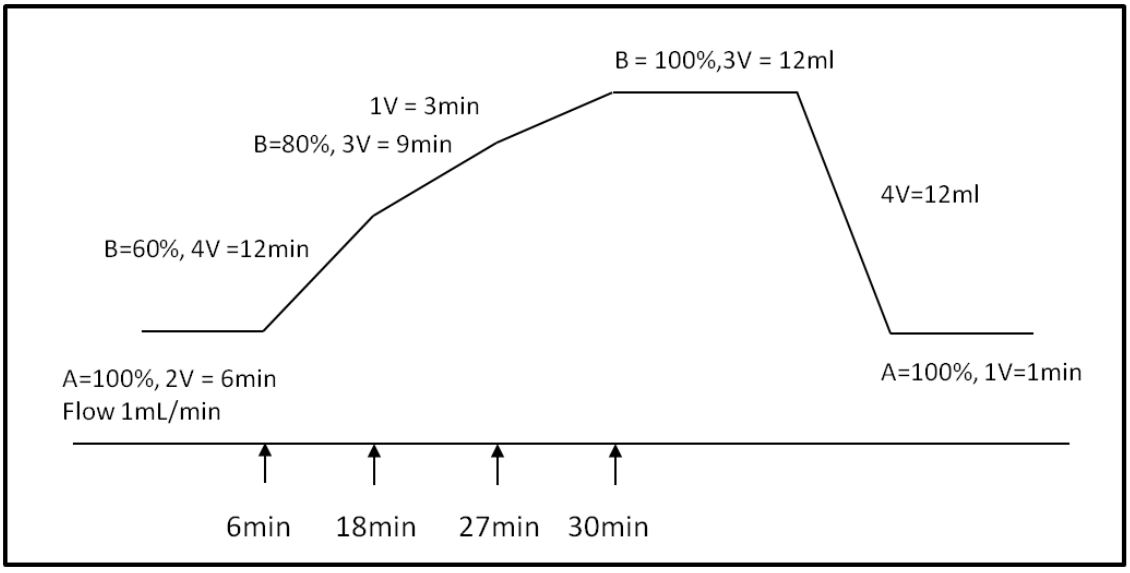

Fig. 2.2. The gradient of the protein elution from the reverse phase column.

The protein fractions obtained after the reversed phase chromatography were subsequently transferred into 2 ml Eppendorf tubes with 750µL soluble protein per tube. The soluble protein was then lyophilized to dryness. Electrospray ionization mass spectrometry was performed to confirm the purification and the mass of the lyophilized sample.

2.1.2. Reconstitution of protein into POPC lipid bilayers

Proteoliposomes were made of the POPC lipid with the uniformly ^{13}C and ^{15}N labeled CD4(372-433) peptide or full-length Vpu protein using organic solvent mediated reconstitution method[2]. The summary of the protocol is presented in Fig. 2.3.

First, the lyophylized protein was combined with the POPC lipid in an organic solvent mixture containing 30% methanol and 70% chloroform. The lipid to protein molar ratio is in the range of 70:1 to 140:1. The organic solvent was later removed by passing a stream of nitrogen gas leaving a dried lipid film that contains the protein. Second, the mixture was re-suspended in cyclohexane. Cyclohexane was then evaporated by a vacuum pump at low temperature for 6-8 hours to overnight to remove the residual organic solvent.

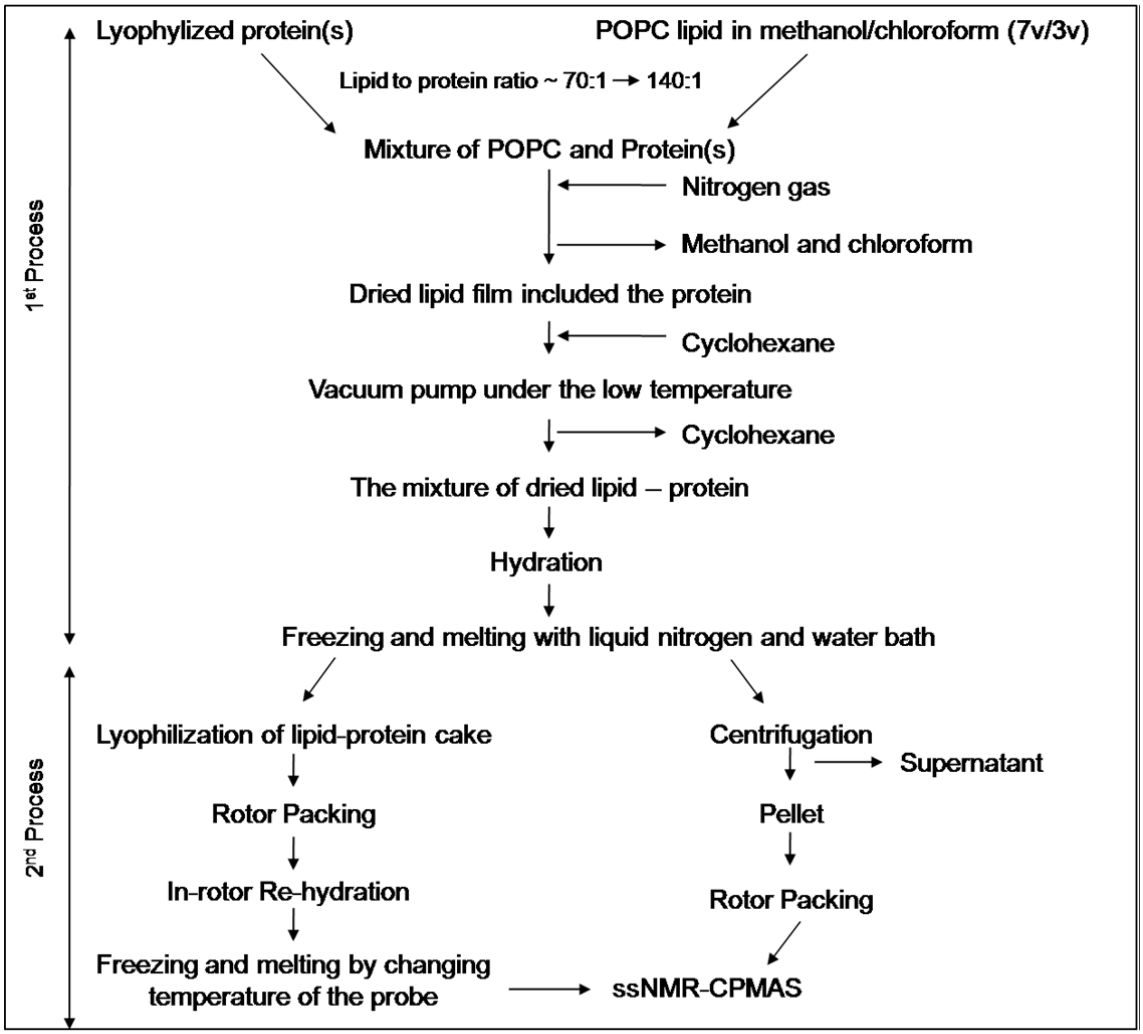

Fig. 2.3. Summary of the reconstitution procedure of the proteins into the POPC lipid bilayer

In the third step, the proteoliposome was prepared by hydrating the mixture of the dried lipid -protein in 10 µL phosphate buffer (pH 7.4, 20 mM (Na_2HPO_4 and NaH_2PO_4), 70 mM NaCl, 0.02% NaN_3) and 490 µL of H_2O. Five freezing and melting cycles were performed using liquid nitrogen and a water bath with the room temperature to make the sample to be more homogeneous. Finally, the sample was treated using two different methods, lyophilization and centrifugation. In the lyophilization method, the solvents in the hydrated lipid-protein cake were removed overnight at very low temperature. The proteoliposome was subsequently packed into a 3.2 mm rotor and rehydrated with pure water. In the centrifugation method, the solvents were separated from proteoliposome via 1-hour centrifugation at 4°C, 15000 rounds per minute. The collected pellet was then packed into the 3.2 mm rotor.

Before CP-MAS solid-state NMR measurements, all in-rotor rehydrated samples went through five cycles of freezing and melting performed inside the probe under spinning condition in order to get the sample homogeneous.

Three sets of proteoliposomes were prepared and studied in this work: (i) the uniformly labeled ^{13}C-, ^{15}N- full-length Vpu protein in POPC lipid bilayers, (ii) uniformly labeled ^{13}C, ^{15}N CD4(372-433) in POPC lipid bilayers, (iii) the uniformly labeled ^{13}C-, ^{15}N- full-length Vpu protein in POPC lipid bilayers in presence of the unlabeled CD4(372-433) peptide.

2.2. Solid state NMR spectroscopy

2.2.1. Data collection

All experiments in the present work were carried out on 2 types of Varian narrow bore spectrometers. The first type of spectrometer operates at a ^{1}H Larmor frequency of 600 MHz and the second type of spectrometer operates at ^{1}H Larmor frequency of 800 MHz. Triple resonance probes that were tuned to either $^{1}H/^{13}C$ or $^{1}H/^{13}C/^{15}N$ were used. Sample temperatures were referenced externally using Nickelocene as demonstrated[3]. All experiments utilized CP-MAS[4-8] with SPINAL[9] decoupling of the protons. The decoupling was in range of 80 kHz to 83 kHz during the acquisition and the evolution periods. Water Edited Solid State NMR Spectroscopy[10-12], Insensitive Nuclei Enhanced by Polarization Transfer (INEPT)[13-15] and CPMAS techniques were employed to get insights into topology and dynamics of the proteins in POPC lipid bilayers. Proton Driven Spin Diffusion (PDSD)[16,17], Double Quantum Filter SPC5[18] (DQ-SPC5) polarization were used to obtain information of spin systems. Sequential link NCOCX[19,20] and the PDSD in combination with Rotational Resonance (PDSD-RR)[21] techniques were utilized to obtain information of linking spin systems.

2.2.2. Data processing

After the acquisition, the time domain data were processed and converted into frequency domain with the aid of the NMRPipe[22] software using either Lorentzian-to-Gaussian or Sine-bell apodization. ^{13}C chemical shifts were referenced externally to the upfield signal of Adamantane that resonances at 31.4 ppm on the DSS scale. ^{1}H chemical shifts and ^{15}N chemical shifts were referenced according to the shift of ^{13}C.

Additional details of experiments and data processing are provided in the figure captions of Chapter 3.

Lorentzian-to-Gaussian function apodization function

Lorentzian-to-Gaussian apodization function applies a Lorentz-to-Gauss window to the time domain. The formula of Lorentizian-to-Gauss window is given by:

$$W_{LG}(t) = \exp(\pi * 100 * t)\exp(-\alpha t^2)$$

where: $\alpha = (0.6 * \pi * 200)^2$ and t is time and t_{max} = 1.1 ms

Sine-bell apodization function **(SP)**

Sine-bell apodization function applies a sine-bell window to the time domain. The formula of sine -bell window is given by:

$$W_S[t] = \sin\left(\frac{(\pi - \pi * \text{off})t}{t_{acq}} + \pi * \text{off}\right)^2$$

where:

- off: The offset specifies the starting point of the sine-bell in units of $\boldsymbol{\pi}$ radians. In current work the offset value of 0.5 is used to process the direct dimensions. The offset values of 0.33 and 0.45 are used to process indirect dimensions.
- t_{acq}: the acquisition time.

2.2.3. Assignment strategy

To gain insight into the conformation of the Vpu and CD4, the resonance assignment was performed for the spectra that are obtained after the data processing (Section 2.2.2) using Sparky assignment software[23]. The assignment work comprises identifying amino acid types and sequential links.

Identifying amino acid types

Amino acid type-assignment was performed using a combination of the random coil chemical shifts from BMRB, ^{13}C shifts in the ^{13}C -^{13}C correlation spectra of the current work, and the ^{13}C shifts from previous work obtained for CD4(372-433) and Vpu(39-81) using liquid state NMR spectroscopy[24-26]. The random coil chemical shifts were represented under the form of an intra-molecular correlation map (Fig. 2.4) in order to simplify the comparison between the random coil chemical shift patterns of

amino acids and the ^{13}C shifts of this work. This comparison predicts the positions of intra-residue cross peaks in ^{13}C-^{13}C 2D spectra acquired at short mixing times (from 10 ms to 50 ms of homonulear ^{13}C-^{13}C PDSD mixing).

The side-chain carbon patterns of amino acid types Val, Ala, Leu, Ile, Thr, Pro were then identified using the intra-residue cross peaks in the ^{13}C-^{13}C 2D PDSD spectra. The chemical shift patterns of the identified residues were affirmed using ^{13}C-^{13}C 2D double quantum-SPC5 spectra. Glu residues were determined via Cδ shifts with specific value of chemical shift (~ 182 ppm) in the ^{13}C-^{13}C 2D PDSD spectra and the correlation between Cδ and Cγ in the ^{13}C-^{13}C 2D double quantum-SPC5 spectrum acquired above the freezing point. Residue types Ser, Gly, Asp were assigned using ^{13}C-^{13}C 2D double quantum-SPC5 spectra.

The ^{13}C shifts are represented in the form of ^{13}C -^{13}C 2D DQ-SPC5 spectra as shown in Fig. 2.5 and Fig. 2.6. These spectra are called the DQ/SQ map. These maps were utilized to identify the ^{13}C NMR signals that could not be assigned using the random coils chemical shift patterns due to the lack of specific ^{13}C shifts.

Identifying sequential links

The sequential links were identified using a combination of the pairs of consecutive amino acids on the primary sequence, inter-residue cross-peaks in the ^{13}C-^{13}C 2D PDSD-RR spectra acquired at long mixing times (from 70 ms to 300 ms) and the ^{15}N-^{13}C 2D spectra (in case of CD4(372-433)). The possible intermolecular correlations of the consecutive amino acids in the primary sequence were compared with the inter-residue cross peaks in the ^{13}C-^{13}C 2D PDSD-RR spectra and the ^{15}N-^{13}C 2D spectra. The site-specific assignments are then reported if the pair is unique in the primary sequence.

Secondary Chemical Shifts[27,28]

After the cross peaks are assigned to amino acid types, the secondary chemical shifts (scs) of identified amino acids were calculated using the following formula:

$$scs = \Delta\delta C\alpha - \Delta\delta C\beta$$

where: ΔδCα is subtraction of the experimental Cα chemical shift random coil Cα shift from BMRB. ΔδCβ is subtraction of the experimental Cβ shift random coil Cβ shift from BMRB.

Conformations of amino acids were then determined based on the values of the secondary shifts. If the secondary chemical shift is greater than +1.5 then the respective amino acid has α helical structure. If the secondary chemical shift is smaller than -1.5 then the respective amino acid presents β-strand element.

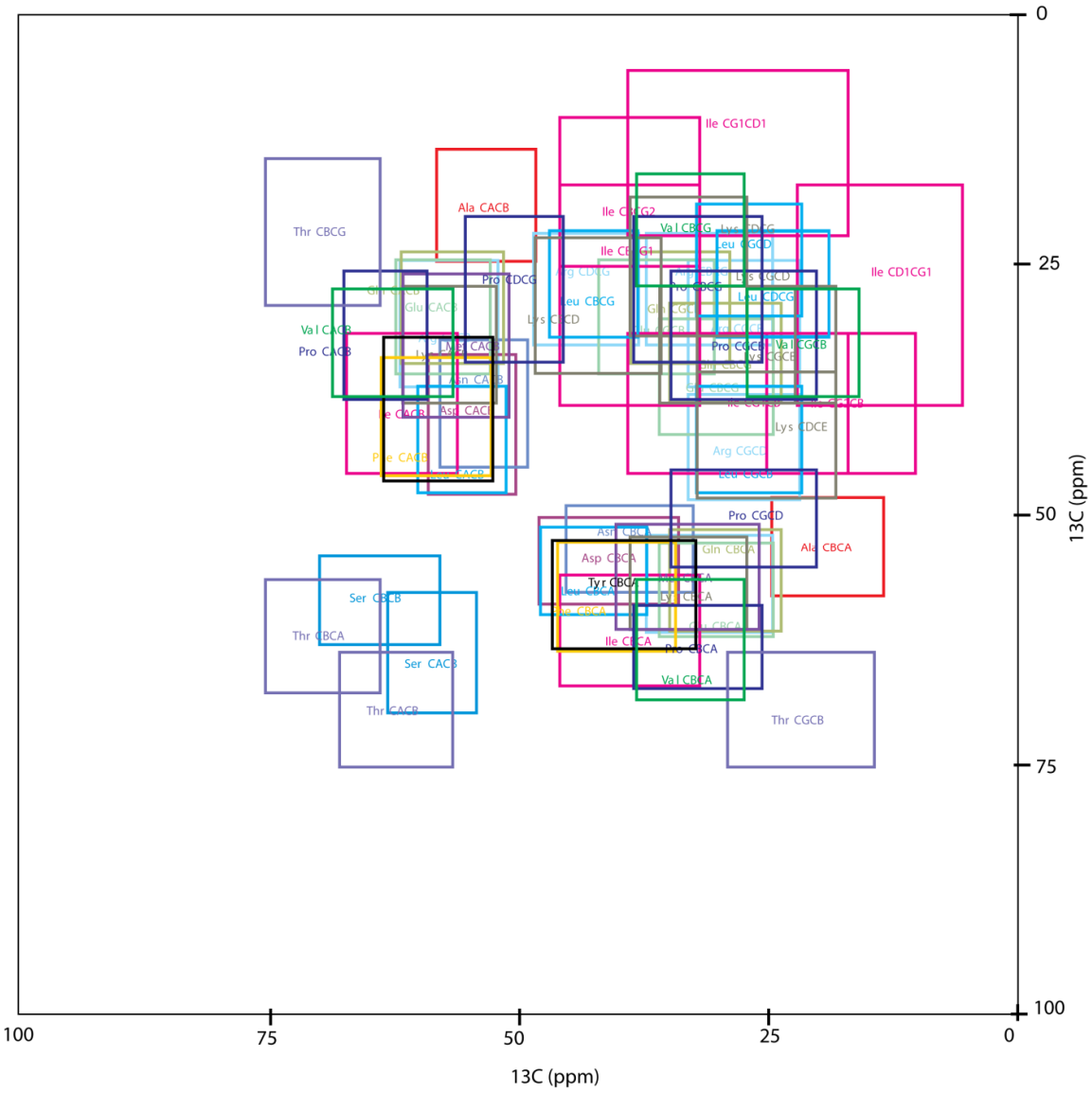

Fig. 2.4. Map of possible intermolecular correlations. Each rectangle in the map represents an ^{13}C-^{13}C correlation of side-chain carbons in an amino acid. The center of each rectangle represents the average shifts of the respective ^{13}C atoms from BMRB. For example, a red rectangle named Ala CACB contains the average chemical shifts of alpha and beta carbons of amino acid alanine (ACα = 53.14 ppm and ACβ =19.01 ppm) at the center of the rectangle. The distances from the center to the edges of each rectangle represent the standard deviations of the chemical shifts.

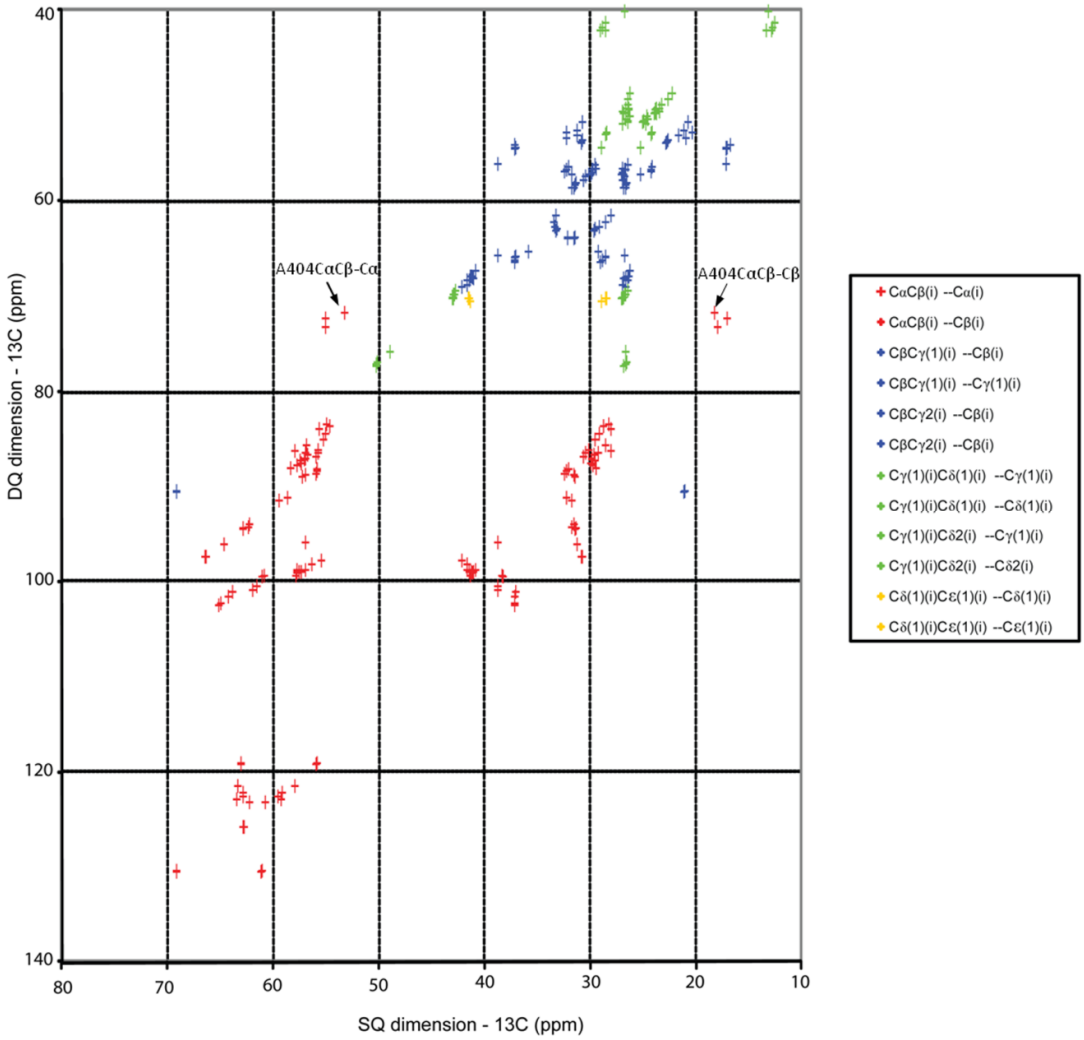

Fig. 2.5. The DQ/SQ map of CD4(372-433). The ^{13}C shifts obtained from previous studies[24,25] using liquid state NMR spectroscopy is represented in the form of DQ-SPC5 spectrum in which the horizontal axis represents SQ dimension while the vertical axis represents DQ dimension. The ^{13}C shifts in the SQ dimension are the ^{13}C shifts of the CD4(372-433). A ^{13}C shift in the DQ dimension is a sum of two ^{13}C shifts in the SQ dimension provided the two respective ^{13}C atoms has one bond correlation. An example is given for the case of A404. A404Cα and A404Cβ have one bond correlation. The DQ shift, A404CαCβ (71.6 ppm), is sum of the SQ shifts, A404Cα (53.3 ppm) and A404Cβ (18.3 ppm). This DQ/SQ map was build using the excel program. Every plus symbol represents a cross peak.

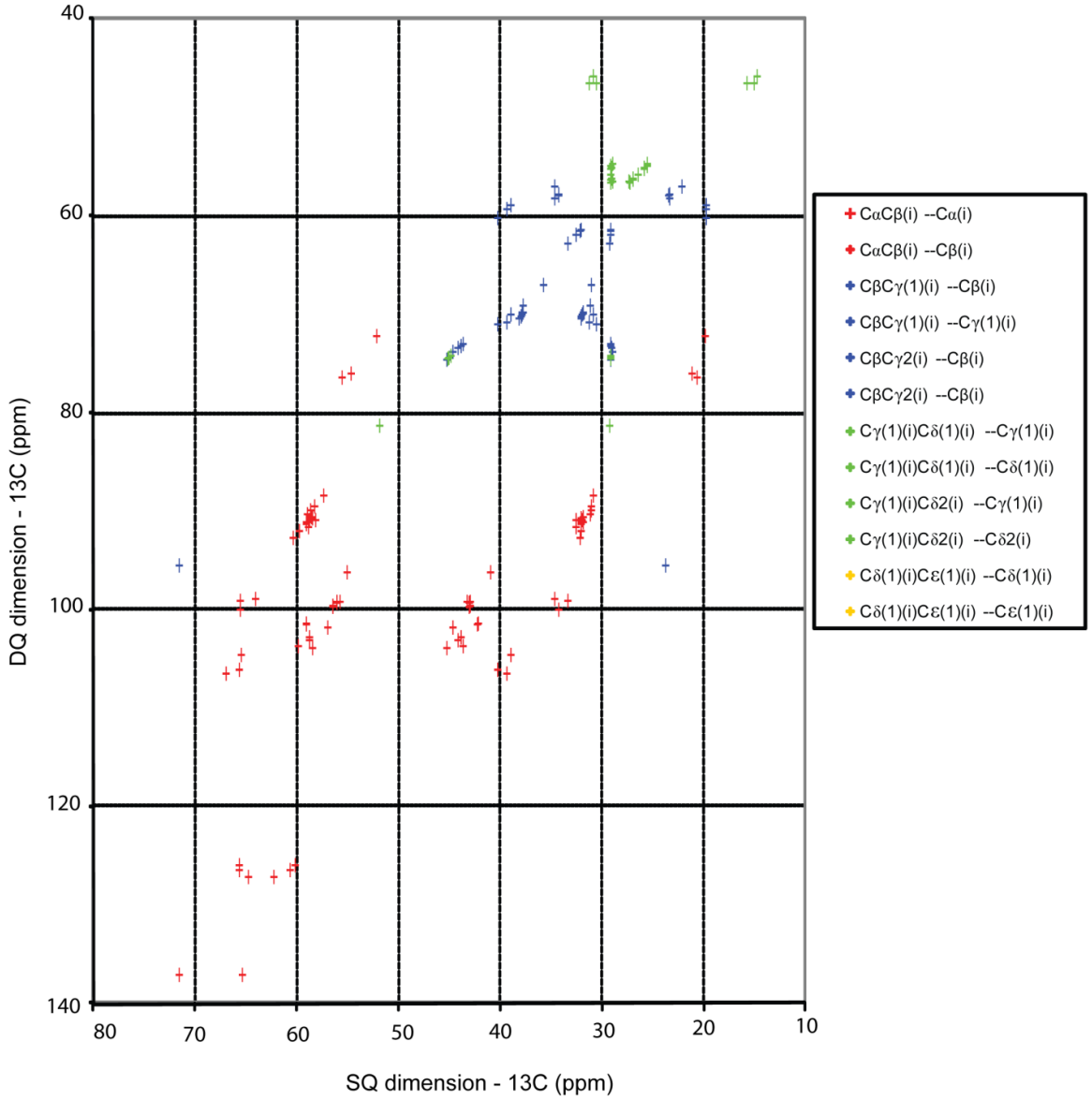

Fig. 2.6. The DQ/SQ map of Vpu(39-81). The ^{13}C shifts of Vpu(39-81) obtained from a previous studies[26] using liquid state NMR spectroscopy is represented in the form of DQ-SPC5 spectrum in which the horizontal axis represents SQ dimension while the vertical axis represents DQ dimension. The ^{13}C shifts in the SQ dimension are the ^{13}C shifts of the Vpu(39-81). The ^{13}C shifts of in the DQ is the sum of two ^{13}C shifts in the SQ dimension provided the two respective ^{13}C atoms has one bond correlation. This DQ/SQ map was build using the excel program. Every plus symbol represents a cross peak.

References

1. Wittlich, M., Wiesehan, K., Koenig, B.W. & Willbold, D. Expression, purification, and membrane reconstitution of a CD4 fragment comprising the transmembrane and cytoplasmic domains of the receptor. *Protein Expression and Purification* **55**, 198-207 (2007).
2. Page, R.C., Li, C., Hu, J., Gao, F.P. & Cross, T.A. Lipid bilayers: an essential environment for the understanding of membrane proteins. *Magn Reson Chem* **45**, S2-S11 (2007).
3. Heise, H., Kohler, F.H. & Xie, X.L. Solid-state NMR spectroscopy of paramagnetic metallocenes. *Journal of Magnetic Resonance* **150**, 198-206 (2001).
4. Andrew, E.R., Bradbury, A. & Eades, R.G. Nuclear Magnetic Resonance Spectra from a Crystal Rotated at High Speed. *Nature* **182**, 1659-1659 (1958).
5. Lowe, I.J. Free Induction Decays of Rotating Solids. *Physical Review Letters* **2**, 285-287 (1959).
6. Duer, M.J. *Introduction to Solid-State NMR Spectroscopy*, 349 (Blackwell Publishing Ltd, 2004).
7. Pines, A., Gibby, M.G. & Waugh, J.S. Proton-Enhanced Nmr of Dilute Spins in Solids. *Journal of Chemical Physics* **59**, 569-590 (1973).
8. Hartmann, S.R. & Hahn, E.L. Nuclear Double Resonance in Rotating Frame. *Physical Review* **128**, 2042-& (1962).
9. Fung, B.M., Khitrin, A.K. & Ermolaev, K. An improved broadband decoupling sequence for liquid crystals and solids. *Journal of Magnetic Resonance* **142**, 97-101 (2000).
10. Huster, D., Yao, X.L. & Hong, M. Membrane protein topology probed by H-1 spin diffusion from lipids using solid-state NMR spectroscopy. *Journal of the American Chemical Society* **124**, 874-883 (2002).
11. Kumashiro, K.K., Schmidt-Rohr, K., Murphy, O.J., Ouellette, K.L., Cramer, W.A. & Thompson, L.K. A novel tool for probing membrane protein structure: Solid-state NMR with proton spin diffusion and X-nucleus detection. *Journal of the American Chemical Society* **120**, 5043-5051 (1998).
12. Kijac, A., Shih, A.Y., Nieuwkoop, A.J., Schulten, K., Sligar, S.G. & Rienstra, C.M. Lipid-Protein Correlations in Nanoscale Phospholipid Bilayers Determined by Solid-State Nuclear Magnetic Resonance. *Biochemistry* **49**, 9190-9198 (2010).
13. Morris, G.A. & Freeman, R. Enhancement of Nuclear Magnetic-Resonance Signals by Polarization Transfer. *Journal of the American Chemical Society* **101**, 760-762 (1979).
14. Keeler, J. *Understanding NMR Spectroscopy*, (Wiley, 2011).
15. Burum, D.P. & Ernst, R.R. Net Polarization Transfer Via a J-Ordered State for Signal Enhancement of Low-Sensitivity Nuclei. *Journal of Magnetic Resonance* **39**, 163-168 (1980).
16. Bloembergen, N. On the Interaction of Nuclear Spins in a Crystalline Lattice. *Physica* **15**, 386-426 (1949).

17. Szeverenyi, N.M., Sullivan, M.J. & Maciel, G.E. Observation of Spin Exchange by Two-Dimensional Fourier-Transform C-13 Cross Polarization-Magic-Angle Spinning. *Journal of Magnetic Resonance* **47**, 462-475 (1982).
18. Hohwy, M., Rienstra, C.M., Jaroniec, C.P. & Griffin, R.G. Fivefold symmetric homonuclear dipolar recoupling in rotating solids: Application to double quantum spectroscopy. *Journal of Chemical Physics* **110**, 7983-7992 (1999).
19. Baldus, M., Petkova, A.T., Herzfeld, J. & Griffin, R.G. Cross polarization in the tilted frame: assignment and spectral simplification in heteronuclear spin systems. *Molecular Physics* **95**, 1197-1207 (1998).
20. vanRossum, B.J., Forster, H. & deGroot, H.J.M. High-field and high-speed CP-MAS C-13 NMR heteronuclear dipolar-correlation spectroscopy of solids with frequency-switched Lee-Goldburg homonuclear decoupling. *Journal of Magnetic Resonance* **124**, 516-519 (1997).
21. Seidel, K., Lange, A., Becker, S., Hughes, C.E., Heise, H. & Baldus, M. Protein solid-state NMR resonance assignments from (C-13, C-13) correlation spectroscopy. *Physical Chemistry Chemical Physics* **6**, 5090-5093 (2004).
22. Delaglio, F., Grzesiek, S., Vuister, G.W., Zhu, G., Pfeifer, J. & Bax, A. NMRPipe: a multidimensional spectral processing system based on UNIX pipes. *J Biomol NMR* **6**, 277-93 (1995).
23. Goddard, T.D., KnellerD. G. & Sparky 3. *University of California, San Francisco*.
24. Wittlich, M., Koenig, B.W., Hoffinann, S. & Willbold, D. Structural characterization of the transmembrane and cytoplasmic domains of human CD4. *Biochimica Et Biophysica Acta-Biomembranes* **1768**, 2949-2960 (2007).
25. Wittlich, M., Thiagarajan, P., Koenig, B.W., Hartmann, R. & Willbold, D. NMR structure of the transmembrane and cytoplasmic domains of human CD4 in micelles. *Biochim Biophys Acta* **1798**, 122-7 (2010).
26. Wittlich, M., Koenig, B.W., Stoldt, M., Schmidt, H. & Willbold, D. NMR structural characterization of HIV-1 virus protein U cytoplasmic domain in the presence of dodecylphosphatidylcholine micelles. *Febs Journal* **276**, 6560-6575 (2009).
27. Spera, S. & Bax, A. Empirical Correlation between Protein Backbone Conformation and C-Alpha and C-Beta C-13 Nuclear-Magnetic-Resonance Chemical-Shifts. *Journal of the American Chemical Society* **113**, 5490-5492 (1991).
28. Wishart, D.S. & Sykes, B.D. The C-13 Chemical-Shift Index - a Simple Method for the Identification of Protein Secondary Structure Using C-13 Chemical-Shift Data. *Journal of Biomolecular Nmr* **4**, 171-180 (1994).

Chapter 3. Experiments and Results

3.1. Mobility of the reconstituted protein

3.1.1. The changes of protein before and after reconstituted into the POPC bilayers

Before going to probe any characteristics of membrane protein reconstituted into the POPC lipid bilayers, it is necessary to know if the reconstituted protein adopts a well-folded conformation. Therefore, the ^{13}C and ^{15}N labeled full-length Vpu protein either reconstituted or not (lyophilized protein) into POPC bilayers was measured using the PDSD-RR method (pulse sequence scheme is shown in Fig. A4.B). The results are presented in Fig. 3.1.

As shown in Fig. 3.1, the signals of the lipid-reconstituted Vpu (Fig. 3.1.B and D) have better resolution and more constructive line-shape than those of the none-reconstituted Vpu (Fig. 3.1.A). Furthermore, within a spectral area that is limited by chemical shifts between 50 ppm – 65 ppm and 20 ppm - 45 ppm (the ovals 1 and 2), multiple NMR signals are only visible in the non-reconstituted Vpu (Fig. 3.1.C). The similar phenomenon was found within the oval 3 at the carbonyl region. Thus, the employed native-like lipid environment induces a rearrangement in Vpu's structure.

When overlaying the signals in the Fig. 3.1.C with the map of inter-residue cross-peaks (Fig. 2.4.), the missing signals due to the reconstitution were found belonging to residue types Thr, Ser, Asp, Lys, Glu, and Gln (Fig. 3.2). These residues are the main types of amino acids that reside at the cytoplasmic domain in the primary structure of full-length Vpu (Fig. 1.2.A).

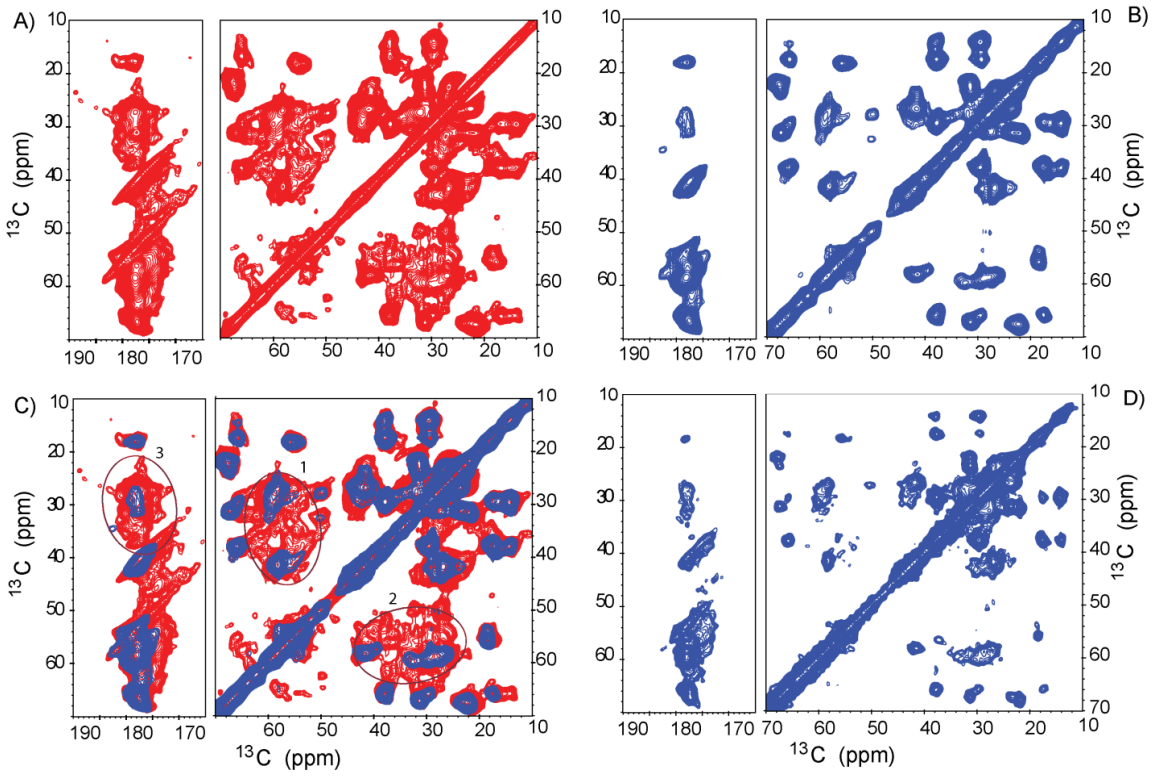

Fig. 3.1. Changes in appearance of NMR signals of uniformly labeled ^{13}C, ^{15}Nfull-length Vpu protein due to the reconstitution into POPC lipid bilayers. Spectra in A, B were recorded on a Varian spectrometer operating at a ^{1}H Larmor frequency of 600 MHz using the PDSD-RR technique with 160 scans and 10 ms of ^{13}C mixing time. A) The Vpu *protein in the lyophilized form* was acquired with the evolution period of 3.6ms. B) The Vpu protein *reconstituted into POPC lipid bilayers with the rehydrated level of ~18%* was acquired with the evolution period of 6.5ms. C) The overlay of the spectra at A) and B). D) The Vpu protein *reconstituted into POPC lipid bilayers without the in-rotor rehydration* was acquired on a Varian spectrometer operating at a ^{1}H Larmor frequency of 800 MHz with 160 scans and the evolution period is 3.6ms. The temperature of the samples in all experiments was around 0°C. Data were processed using Lorentzian-to-Gaussian apodization function with 100 Hz of Lorentzian line sharpening, 200 Hz of Gaussian line broadening prior to Fourier transform.

3.1.2. Effects of different reconstitution methods on NMR detection

NMR lines of the reconstituted Vpu (Fig. 3.1.B and C) have an average line width in the order of 0.8 ppm to 3 ppm and this large line width was also observed for the reconstituted CD4. This might obscure the site-specific assignment that is necessary for determination of the protein structure. Therefore, another reconstitution method, the centrifugation, was tested as described in Fig. 2.3 (the second process) to see if the line width is improved. Thus, instead of using the lyophilization method in which the proteoliposome was lyophilized and then rehydrated inside the rotor, the centrifugation

was applied to remove excess solvents from the proteoliposome before packing it into a rotor. The samples resulting from both reconstitution methods were measured by using the same technique and the results are shown in Fig. 3.3.

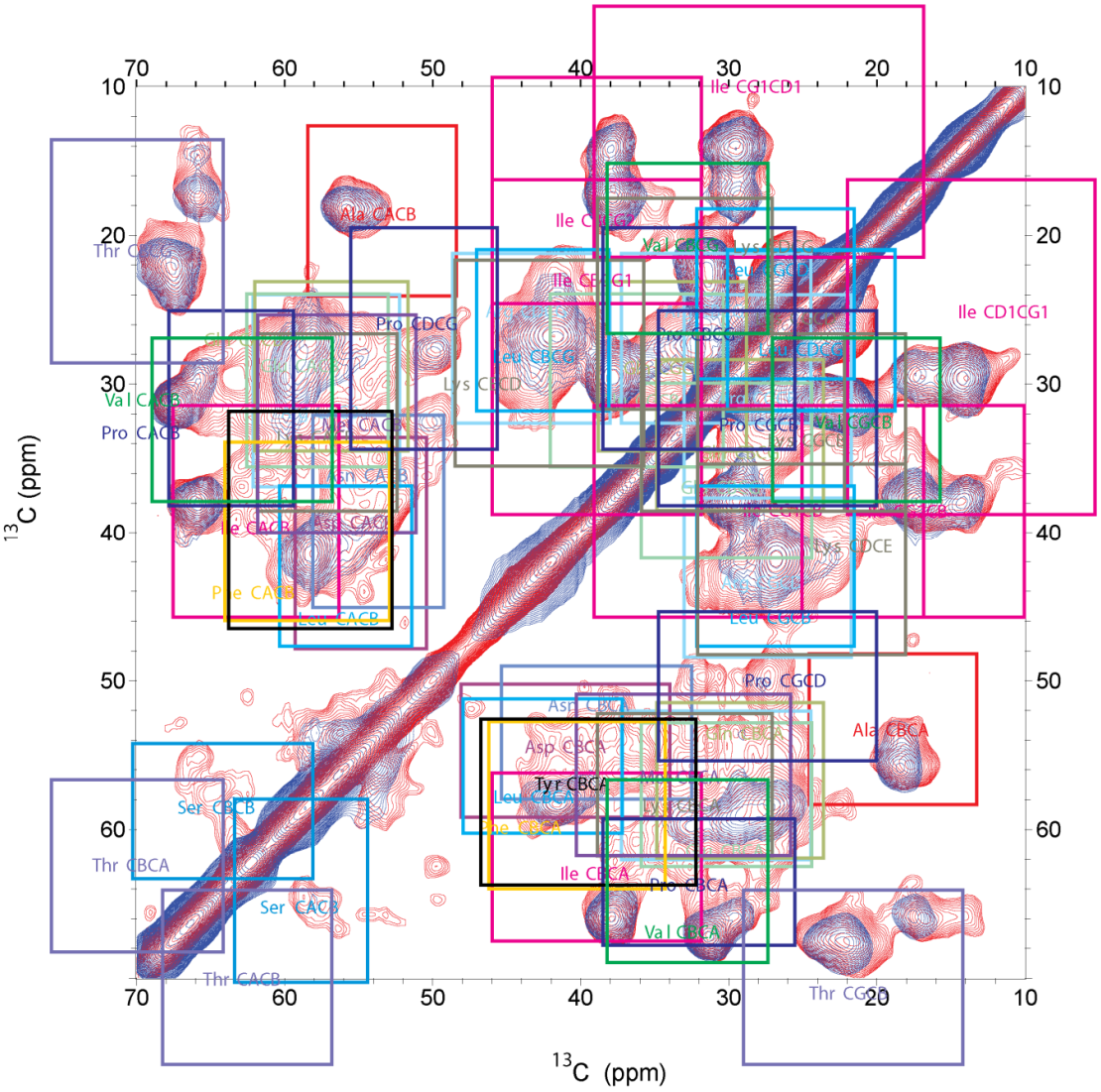

Fig. 3.2. Overlay between the intra-molecular correlation map and the signals in Fig. 3.1.C.

In Fig. 3.3, the blue spectrum was obtained from the CD4(372-433) proteoliposome that was prepared using the lyophilization method, while the red spectrum was from another CD4(372-433) proteoliposome that was prepared using the centrifugation method. Observation of the red cross-peaks indicates that there is no significant improvement in the line widths of the peaks. Moreover, in the red spectrum, many signals that are visible in the blue spectrum are missing. These

missing signals may be due to an increased mobility of the protein at the interface between the hydrophobic and hydrophilic regions of in the lipid bilayers

Naturally, the lipid bilayers prepared using the centrifugation method have a higher amount of residual water in the interface of the hydrophobic and hydrophilic regions than the lipid bilayers prepared using the lyophilization method. The higher amount of the residual water might lead to an increase of mobility of the reconstituted protein at the interface of the lipid bilayers and therefore causes the missing of signals in the red spectrum. The missing signals indicate that the residual water in the interface of the lipid bilayers exists with large amount that could not be frozen completely even when the sample temperature was reduced to -20°C.

Thus, if using the centrifugation method to prepare the proteoliposomes, not only the line width will not be improved but also the major information of the reconstituted proteins is missing. The lyophilization method was thereby used for preparing the proteoliposomes in the current work.

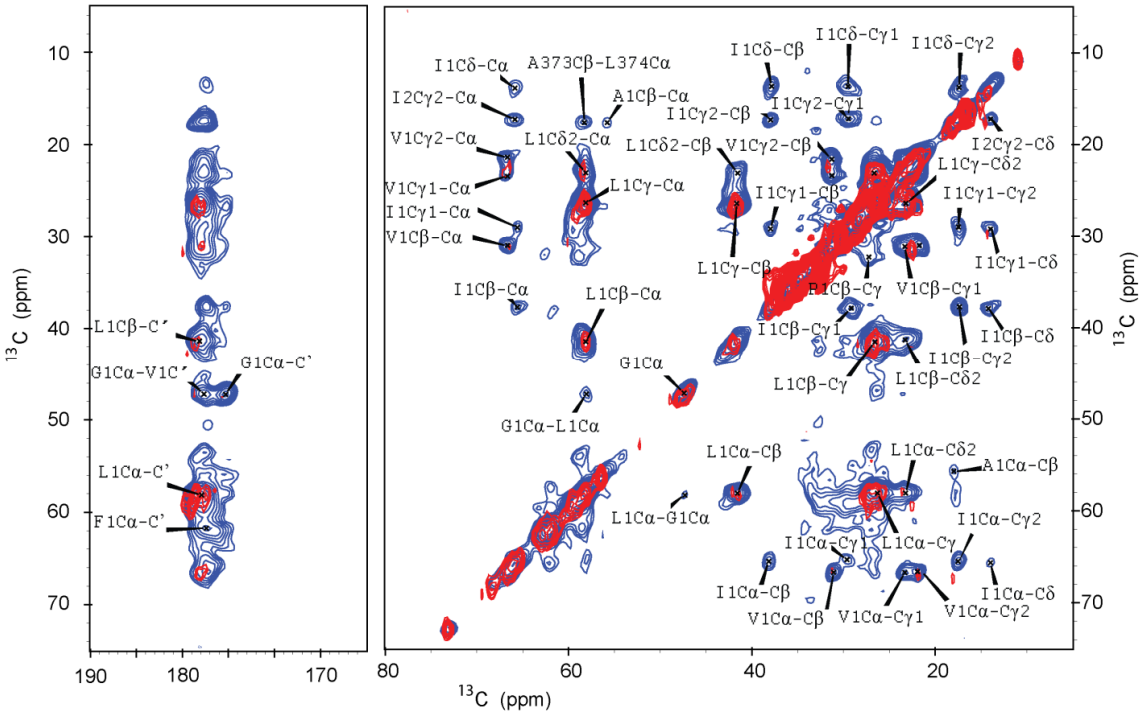

Fig. 3.3. Effect of various reconstitution methods on the detection of the NMR signals. The sample utilized in the NMR experiment is the uniformly labeled ^{13}C, ^{15}N CD4(372-433) peptide in POPC bilayers. The spectra were acquired on a Varian spectrometer operating at a ^{1}H Larmor frequency of 600 MHz with an MAS speed of 9375 Hz using the PDSD-RR method with a carbon – carbon mixing

time of 70 ms. The blue spectrum (64 scans, 3 mg of protein) was collected from the proteoliposome prepared by lyophilization followed by rehydration. The temperature of the sample during data collection was around 0°C. The red spectrum (224 scans, 1.3 mg of protein) was collected from the proteoliposome prepared using the centrifugation method. The temperature of the sample during data collection was around around -20°C. Data were processed using Lorentzian-to-Gaussian apodization function with 100 Hz of Lorentzian line sharpening, 200 Hz of Gaussian line broadening prior to Fourier transform.

3.1.3. Effects of mobility and temperature on detection of the reconstituted proteins

The results in Fig. 3.1 and 3.3 were collected using the CP technique[1,2] that allows the detection of the immobile part of the sample. The missing Vpu and CD4 signals resulting from either the reconstitution into the lipid bilayers (Fig. 3.1.C) or the different ways of the reconstitution (Fig. 3.3) are indicative of the presence of mobile parts in addition to the immobile parts of the reconstituted proteins. To obtain further insight into the dynamic properties, the INEPT technique[3,4] that allows the detection of mobile regions in samples was employed.

The results from INEPT and CP experiments (Fig. 3.4) were collected from uniformly labeled ^{13}C-, ^{15}N-full-length Vpu protein in POPC bilayers. At 14 °C, the 1D- CP ^{13}C spectrum (blue) shows the protein signals deriving from the rigid part of the reconstituted Vpu, whereas the 1D- INEPT ^{13}C spectrum (red) only shows lipid signals. The absence of NMR signals deriving from the protein indicates that the protein was not mobile enough at 14 °C to yield signals in an INEPT ^{13}C spectrum. The intensity of the NMR signals of the Vpu sample is significantly increased with a 14 °C-decrease in temperature (Fig. 3.6). Similar experiments were performed on the CD4(372-433) in POPC bilayers at 0 °C (Fig. 3.5). The increase of the protein signals indicates that at 0 °C the proteins were sufficiently immobile to yield CP ^{13}C spectra.

It is likely that the mobile part of the proteins appears in the NMR spectra at temperatures either higher than 14 °C if using the INEPT technique or lower 0 °C if using the CP technique. Increasing the sample temperature used in the MAS solid state NMR carbon-detected experiments above 14°C can potentially render the sample unstable during spectroscopy over the long measurement period (7-10 days). In addition, given the typically low expression and purification yield of labeled recombinant membrane proteins, the preparation of the Vpu and CD4(372-433)

proteoliposomes is a costly and time consuming process in order to have sufficient amount of sample required for suitable intensity of NMR signals. In the further studies of both Vpu and CD4(372-433) in POPC bilayers, the temperature of the experiments in the current work was therefore reduced to about 0°C and below the freezing point.

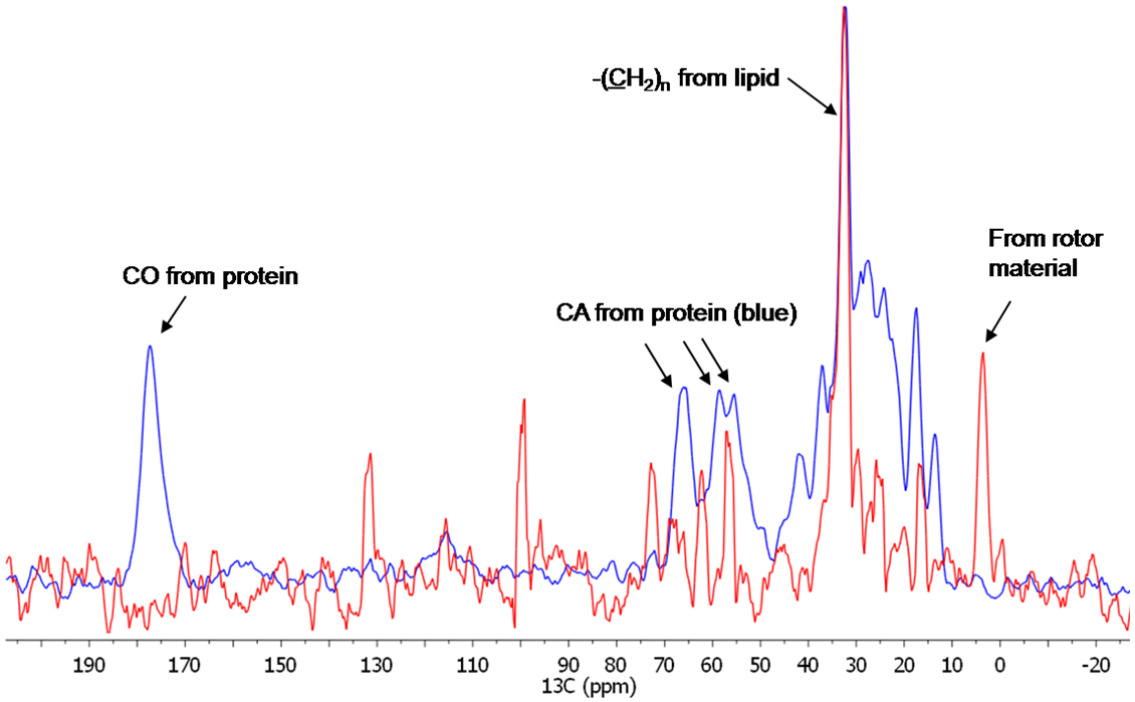

Fig. 3.4. The NMR signals of uniformly labeled ^{13}C, ^{15}N full-length Vpu protein in POPC bilayers under various polarization transfer mechanisms, INEPT (red carbon spectrum) and CP (blue carbon spectrum). The spectra were collected at 14°C and at ^{1}H Larmor frequencies of 600 MHz with 128 scans for each spectrum. Both spectra were processed with exponential function apodization of 20 Hz.

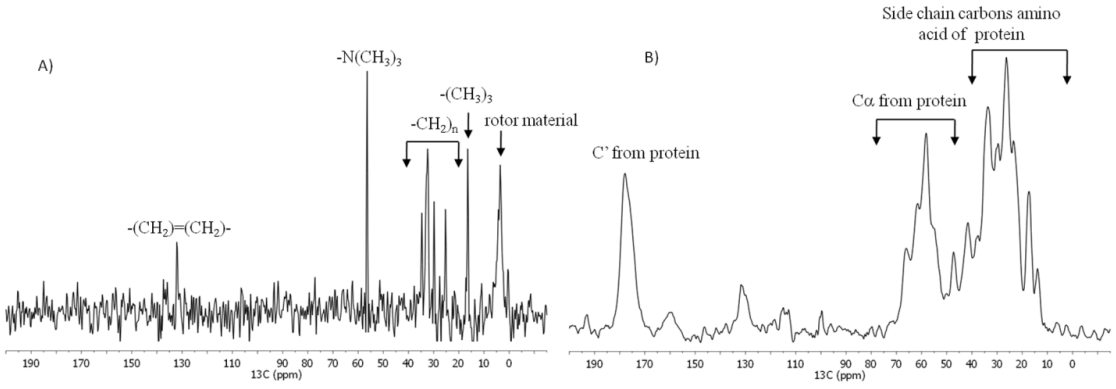

Fig. 3.5. The NMR signals of uniformly labeled ^{13}C, ^{15}N CD4(372-433) in POPC bilayers under different polarization transfer mechanisms. A) INEPT carbon spectrum was acquired at 14 °C. -(CH_2)=(CH_2)- re-presents the carbon of POPC at the unsaturated bond located in side-chain (see Fig. B2A for POPC structure).–N–$(CH_2)_3$ shows shifts of carbon atoms in the methyl group at the head of

POPC. –(CH_2)n– presents shifts of carbons which reside in the side-chain of POPC.–$(CH_2)_3$ shows the peak of methyl carbon in the end of POPC side-chain. B) CP carbon spectrum was recorded at 0°C. CO indicates the carbonyl groups of amino acids. CA indicates the alpha carbons of amino acids. The spectra were acquired at ^{1}H Larmor frequency of 600 MHz with 128 scans for each spectrum. Both spectra were processed with an exponential line broadening of 20 Hz.

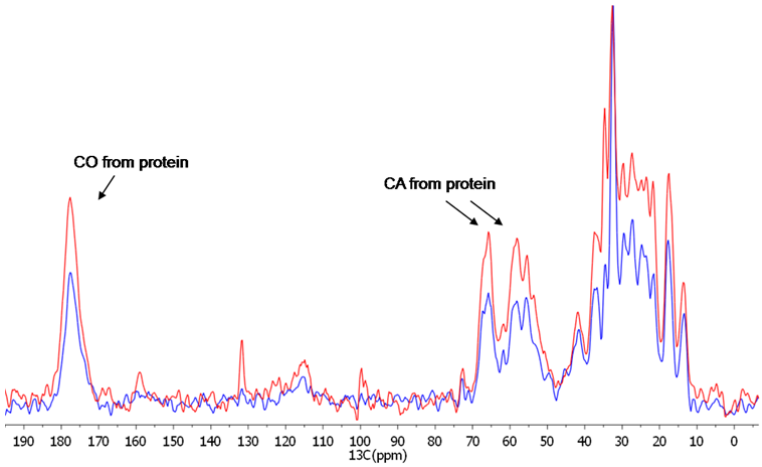

Fig. 3.6. A comparison of 1D- CP ^{13}C spectra of uniformly labeled ^{13}C, ^{15}N full-length Vpu protein in POPC bilayers at various temperatures. The red spectrum was obtained at the sample temperature of ~ 0°C. The blue spectrum was obtained at a sample temperature of 14°C. The data were acquired on a Varian spectrometer operating at a ^{1}H Larmor frequency of 600 MHz with the same acquisition parameters: the spinning frequency (9375Hz), the CP condition, the number of scans (128 scans) and the power of proton decoupling for each spectrum. Both spectra were processed with exponential line broadening of 20 Hz and the intensities of the peaks were normalized by largest peak in each spectrum.

3.2. Topology of Vpu and CD4(372-433) in POPC lipid bilayers

In order to probe the topology of the membrane protein in POPC lipid bilayers, the water-edited solid state NMR method was utilized. The method includes the T_2 filter, the ^{1}H spin-diffusion, and CP techniques as introduced in section 1.2.6. The pulse sequence of the technique is presented in Fig. A3 while the results are shown in Fig. 3.7 – Fig 3.10.

3.2.1. Topology of Vpu in POPC lipid bilayers

Fig. 3.7 shows an overlay of two 2D ^{1}H – ^{13}C correlation spectra recorded from the lipid-reconstituted Vpu (blue) and the unlabeled POPC lipid (red). The majority of ^{13}C signals on the blue spectrum were not superimposed with the ^{13}C signals in the red spectrum. This indicates that these blue ^{13}C signals stem from the Vpu protein. Through the chemical shifts of ^{13}C and ^{1}H in the blue spectrum, it becomes clear that

the protein ^{13}C spins receive the ^{1}H magnetization from various proton sources: (i) POPC lipid acyl-chains; (ii) the methyl group of the lipid head, $-N(CH_3)_3$; and (iii) water, H_2O. The protein ^{13}C shifts were assigned to amino acid types Val, Leu, Ileu, Arg and Ala. This assignment is based on the assignment strategy in section 2.2.3 and the assignment of the Vpu in section 3.3.1. The signals deriving from V1Cα were found to receive ^{1}H magnetization from more than one proton source (i.e. from the lipid head and water proton sources). This raises a question on whether these signals arise from the same valine in the protein or from different valines located in different parts of the protein. Similar phenomenon was found for L1Cα, A1Cα, I1Cβ I1Cδ, and I1Cγ2. To overcome this issue, a three-dimensional (3D) version of the water-edited solid state NMR spectrum (the pulse sequence in Fig. A3.B) was employed. The ^{1}H dimension was retained and an indirect ^{13}C dimension was added. The results are presented in Fig. 3.8.

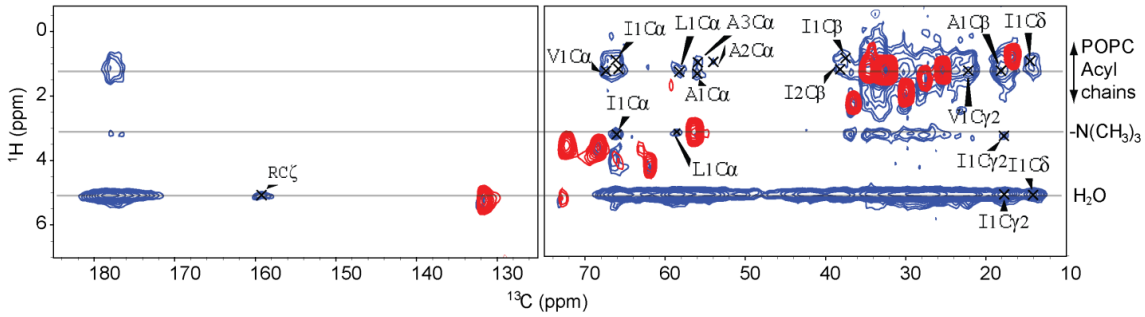

Fig. 3.7. Overlay of 2D ^{13}C - ^{1}H correlation spectra of the uniformly labeled ^{13}C, ^{15}N full-length Vpu protein in POPC bilayers (blue) and the unlabeled POPC lipid (red). The blue spectrum was recorded using the water edited solid state NMR method with 128 scans (pulse sequence in Fig. A3.A). 240 µs of the T_2 filter time and 3ms of proton spin diffusion were used. The red spectrum was recorded using the INEPT technique with 10ms mixing time for proton spin diffusion and 128 scans (pulse sequence in Fig. A2). The experiments were conducted around 0°C (the sample temperature), at a ^{1}H Larmor frequency of 600 MHz with a spinning speed of 9375 Hz. Data were processed using a sine-bell apodization function prior to the Fourier transform. Signals aligned with $-N(CH_3)_3$, POPC acyl chains, and H_2O lines are derived from the head of POPC lipid, side-chains of POPC lipid and water, respectively.

Fig. 3.8 shows ^{13}C - ^{13}C planes of the 3D ^{1}H- ^{13}C- ^{13}C spectrum at the chemical shifts of water protons (^{1}H of 5.0 ppm), the methyl protons of the lipid head group (^{1}H of 3.2 ppm), the methyl protons of the lipid side-chain (^{1}H of 0.88 ppm), and the lipid side-chain protons (^{1}H of 1.15 ppm).

While no intra-residue cross-peak of the Vpu protein was found in the lipid head plane (Fig. 3.9.B), multiple intra-residue cross-peaks were found in the water plane (Fig. 3.8.A) as well as in the lipid chain planes (Fig. 3.8.C&D). The intra-residue cross-peaks of the amino acids Val, Ile and Ala appear both in the lipid chain planes (i.e. VCα-Cβ,VCα-Cγ1, VCα-Cγ2, VCβ-Cγ1, VCβ-Cγ2, ICα-Cγ2, ICβ-Cγ1, ICβ-Cγ2, ICβ-Cδ, ICγ1-Cδ, ICγ1- Cγ2, ACα-Cβ) and in the water plane (i.e. VCα-Cγ2, ICα-Cγ2, ACβ-Cα). This suggests two possibilities. The first one is that Val, Ile, and Ala residues are located both in the protein part in proximity to the water and in the part near the lipid side-chain. However, the ^{13}C chemical shifts of these Val, Ile, and Ala residues in the lipid planes are not significantly different from those in the water plane. Therefore, another possibility would be that Val, Ile, and Ala residues are located in the same part of the protein in which some side-chain carbons in these Val, Ile, and Ala residues face to lipid bilayers and the other side-chain carbons face to the water interface. This may indicate the formation of a channel that has a pore-like structure where water is accessible[5,6].

Furthermore, the number of intra-residue cross-peaks of Val and Ile was found to be greater in the lipid chain planes (i.e 7 peaks for Val, 12 peaks for Ileu; this counts both symmetric cross-peaks) than in the water plane (i.e. 1 peak for Val, 1 peak for Ile). This indicates that the magnetization transfer between ^{13}C spins in the protein part close to the lipid side-chain is more effective than that in the protein part close to the water interface.

In addition, results from amino acid-type assignment (see section 2.2.3 for the assignment strategy and section 3.3.2 for more details of the assignment of Vpu.) suggest that the signals within the oval regions which are visible in the water plane but invisible in the lipid planes belong to the amino acid types of Glu, Gln, Lys, Val, Leu where the shift of LCα is characteristics of the alpha helical structure. The finding of Glu, Gln, Lys, Val, Leu residues in the water planes is consistent with the hypothesis premised on the fact that the number of Leu residues is larger in the cytoplasmic domain (6/10) than in the transmembrane domain (2/10) of the Vpu primary structure[7] in this work (Fig.1.2.A). And there are no Glu, Gln and Lys residues in the transmembrane part of the Vpu primary structure.

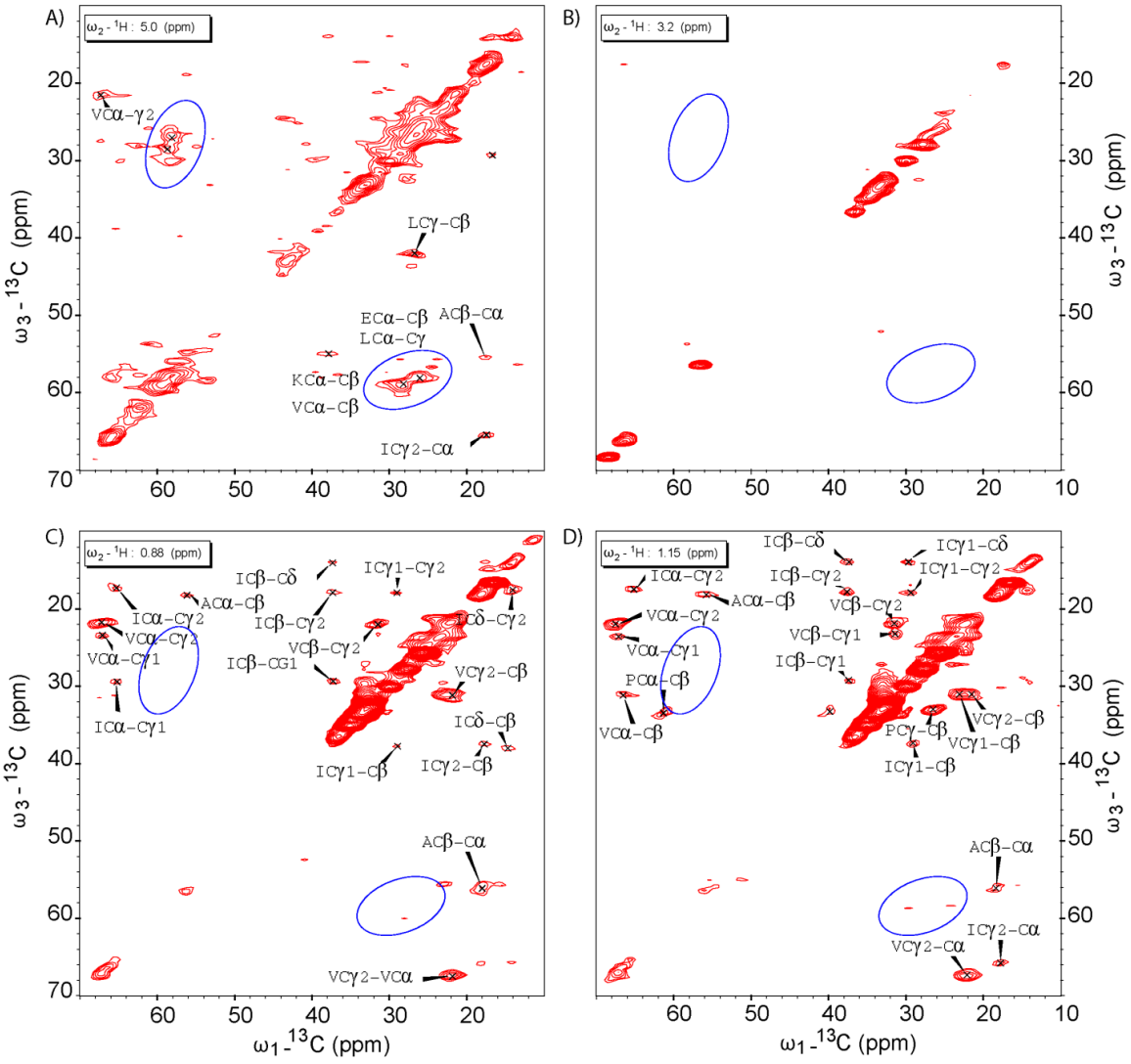

Fig. 3.8. 2D ^{13}C-^{13}C planes of 3D ^{1}H - ^{3}C - ^{13}C spectrum of uniformly labeled ^{13}C, ^{15}N full-length Vpu protein in POPC bilayers. T_2 filter time is 240 μs, the ^{1}H spin diffusion is 1.5 ms, the ^{13}C mixing time is 50 ms. The experiment was conducted around 0°C (the sample temperature). The spectrum was acquired at a ^{1}H Larmor frequency of 600 MHz with a spinning speed of 9375 Hz and 128scans. The evolution times of ^{1}H and ^{13}C are 1.7 ms and 3.2 ms, respectively. The data were processed with forward linear prediction (only for ^{1}H dimension) and sine-bell apodization function prior to the Fourier transform. A) ^{13}C-^{13}C plane at chemical shift of water proton. B) ^{13}C-^{13}C plane at chemical shift of methyl proton of the lipid head. C) ^{13}C-^{13}C plane at chemical shifts of lipid side-chain proton. D) ^{13}C-^{13}C plane at chemical shift of methyl proton of lipid side-chain.

3.2.2. Topology of CD4(372-433) in POPC lipid bilayers

Similarly, the topology of CD4(372-433) in POPC bilayers was monitored using the water-edited solid state NMR and the results are shown in Fig. 3.9. The spectral overlay demonstrates the existence of CD4(372-433) signals in the blue spectrum. The

protein signals appear in three different areas of the spectrum along the ^{1}H chemical shift scale. This implies that the ^{13}C spins of CD4(372-433) also received ^{1}H magnetization from three various sources i.e. POPC lipid acyl-chains, the methyl proton of the lipid head (-$N(CH_3)$, and water (H_2O). Of the ^{13}C signals of CD4(372-433), GCα receives ^{1}H magnetization only from the methyl proton of the lipid head while Cα of amino acids Val, Ile and Leu get the ^{1}H magnetization from all three sources. To separate the water and lipid signals, 3D version of the water edited experiment was performed on the reconstituted CD4(372-433) and results are shown in Fig. 3.10.

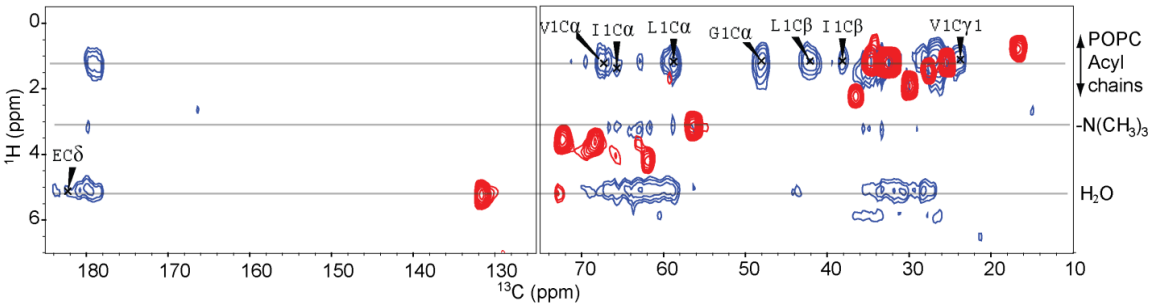

Fig. 3.9. Overlay of 2D ^{13}C - ^{1}H correlation spectra of the uniformly labeled ^{13}C, ^{15}N CD4(372-433) in POPC bilayers (blue) and of the unlabeled POPC lipid (red). The blue spectrum was recorded using the water edited solid state NMR method with 512 scans. 100 µs of the T_2 filter time and 2 ms of the proton spin diffusion were used. The red spectrum was recorded using the INEPT technique with 10ms of proton spin diffusion and 128 scans. The experiments were conducted around 0°C (the sample temperature) at a ^{1}H Larmor frequency of 600 MHz with a spinning speed of 9375 Hz. Data were processed using sine-bell apodization function prior to Fourier transform. Signals aligned with –$N(CH_3)_3$, POPC acyl chains, and H_2O lines are derived from the head of POPC lipid, side-chains of POPC lipid and water, respectively.

Fig. 3.10 presents 2D ^{13}C - ^{13}C planes of 3D ^{1}H- ^{13}C- ^{13}C spectrum at the different chemical shifts of ^{1}H: water proton (^{1}H of 5.0 ppm) in Fig. 3.8.A, the methyl proton of the lipid head group (^{1}H of 3.2 ppm) in Fig. 3.9.B, the methyl proton of the lipid side-chain (^{1}H of 0.88 ppm) in Fig. 3.8.C and the lipid side-chain proton (^{1}H of 1.15 ppm) in Fig. 3.8.D.

In case of CD4(372-433), the cross-peaks between ^{13}C spins were found in all the planes. These cross-peaks were also assigned according to the assignment strategy in section 2.2.1 (see section 3.3.2 for more details of CD4(372-433) assignment). Among assigned peaks, the peaks from Val and Ile residues were found only in the lipid chain

planes (3/4 valines and 3/5 isoleucines are located in the transmembrane domain of the primary sequence of CD4(372-433) (Fig. 1.1.C)). The number of peaks from Leu residue is fewer in either the water (i.e. LCγ-Cβ, LCγ-Cα) or the lipid head planes (i.e. LCα-Cγ, LCγ-Cβ) in comparison to that in each of the lipid chain planes (LCα-Cγ, LCβ –Cγ, LCγ-Cβ, LCγ-Cα). This observation is consistent with the fact that the number of Leu residues (6/9, where 9 is total number of Leu residues) in the transmembrane part of the primary sequence of CD4(372-433) is greater than that in the cytoplasmic part (2/9). In addition, the intensity of GCα in the lipid chain planes (signal to noise equals 11 and 14) is more pronounced than either of the one in the water plane or in the lipid head plane (signal to noise equals 9 or 7). Taken together, the appearance of the cross-peaks suggests that the magnetization transfer between ^{13}C spins in the protein segment close to the lipid side chain is more effective than that in the protein segment in the proximity of either the lipid head or the water regions.

The chemical shifts (of the same kind of ^{13}C atoms) of the Leu residues found in either the water plane or the lipid head plane are not significantly different from those found in the lipid chain planes and indicate alpha helical structure. This result agrees with the previous studies of CD4(372-433) in aqueous solution and micelles[8,9] reported that two Leu residues in the cytoplasmic part have the similar alpha helical structure to the Leu residues in the transmembrane part.

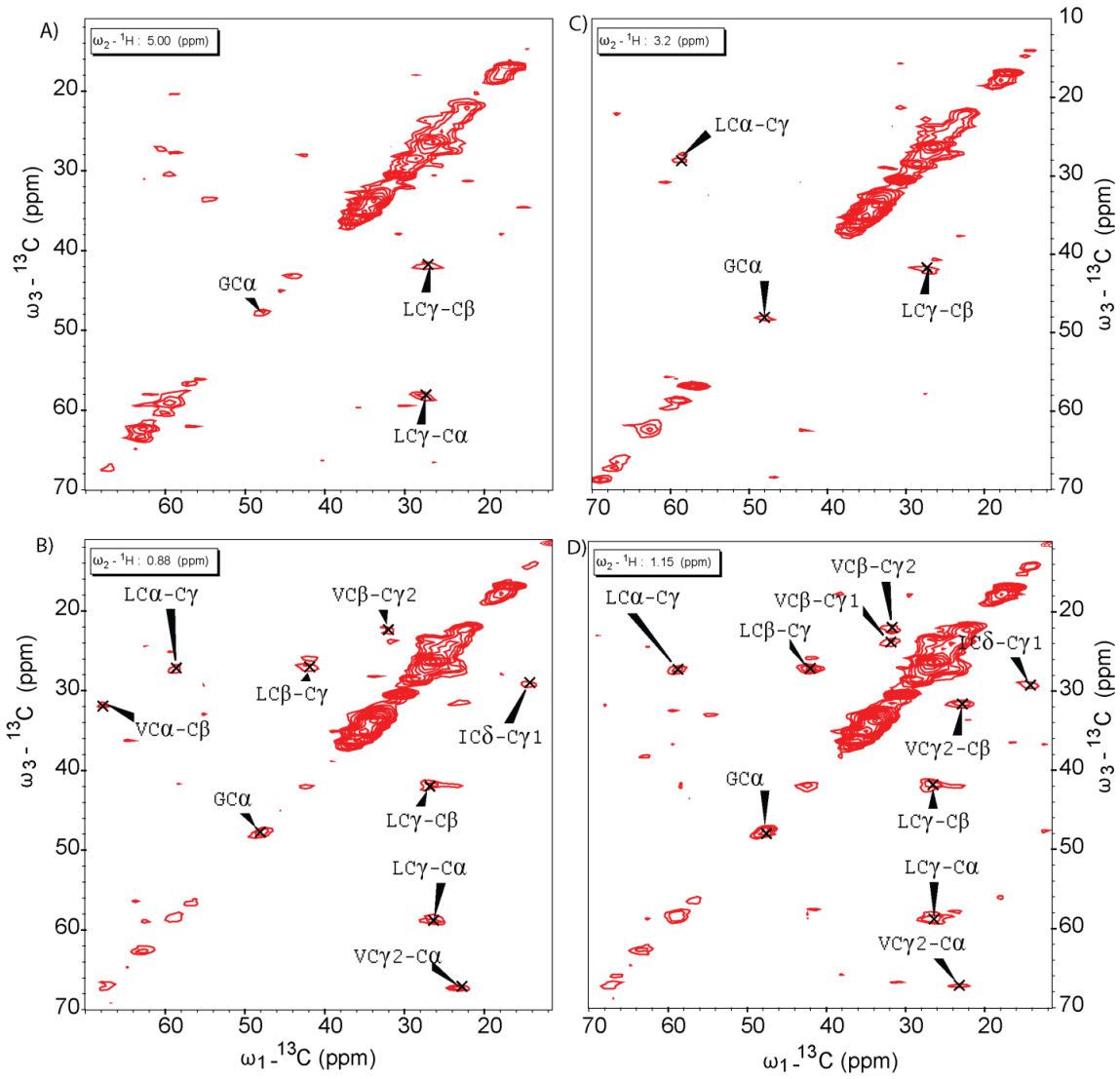

Fig. 3.10. 2D ^{13}C-^{13}C planes of 3D ^{1}H - ^{3}C - ^{13}C spectrum of uniformly labeled ^{13}C, ^{15}N CD4(372-433) in POPC bilayers. T_2 filter time is 100μs, the ^{1}H spin diffusion is 1.5 ms, ^{13}C mixing time is 30 ms. The experiment was conducted around -3°C (the sample temperature). The spectrum was acquired at a ^{1}H Larmor frequency of 600 MHz with a spinning speed of 9375 Hz and 122 scans. The evolution times of ^{1}H and ^{13}C are 1.28 ms and 3.1 ms, respectively. The data were processed with forward linear prediction (only for ^{1}H dimension) and sine-bell apodization function prior to the Fourier transform. A) ^{13}C-^{13}C plane at chemical shift of water proton. B) ^{13}C-^{13}C plane at chemical shift of methyl proton of the lipid head. C) ^{13}C-^{13}C plane at chemical shifts of lipid side-chain proton. D) ^{13}C-^{13}C plane at chemical shift of methyl proton of lipid side-chain. The assignment was based on the assignment in Section 3.3.2.

3.3. Resonance assignments of the reconstituted proteins

In order to gain insight into the conformation of the rigid parts discovered in the previous sections and to look for the missing mobile part, the resonance assignment

was performed for the lipid-reconstituted proteins at different temperatures using the assignment software Sparky and the assignment strategy as described in Section 2.2.3. The results are presented in the following part.

3.3.1. Resonance assignments of Vpu in POPC lipid bilayers

Figures from Fig. 3.11 to 3.15 present the representatives of the assignment of the reconstituted Vpu. The spectra in Fig. 3.11 and 3.12 present the PDSD-RR spectra and the spectrum in Fig. 3.13 to 3.15 displays the aliphatic region of 2D ^{13}C-^{13}C correlation DQ/SQ-SPC5 spectrum.

At short mixing times for proton-driven spin diffusion in the range of 10 ms -70 ms, intra-residue cross peaks deriving from amino acid types Ala, Val, Ile, Leu, Pro, Glu, and Arg were found as shown Fig. 3.11. Of the identified spin systems, the amino acid types Ala, Val, and Ile provide the most dominant signals in the spectra. The line width of the peaks is in the order of 1 ppm -3 ppm and there is a limited chemical shift dispersion. This gives rise to poor resolution of ^{13}C shifts, which leads to the identification of one Val, one Ile, one Leu, and two Ala residues. Another Ala residue was found in DQ/SQ spectrum (Fig. 3.13 and 3.16). Other amino acid types such as Pro, Glu, Ser, and Arg were confirmed at longer the ^{13}C mixing times. Two Pro residues, five Glu residues, one Ser residue, and two Arg residues were detected in the spectrum recorded with a spin diffusion mixing time of 300 ms (Fig. 3.12). Furthermore, an additional Ser residue and other residues as one Thr (via correlation of TCβ and TCγ), one Gly (via correlation of GCα and GC'), and there Asp (via correlation of DCβ and DCγ) are affirmed in DQ/SQ-SPC5 spectra (Fig. 3.13-3.14). The resonance list of the detected residues and their ^{13}C chemical shifts are shown in Table 1 and their secondary chemical shifts are presented in Fig. 3.15.

Among the identified residues, Ala3 is indicative of slightly beta strand structure whereas Pro1, Asp2, Asp3, Glu2, Glu4, Gly1, Pro2 and Ser2 possess random coil conformation and the remainder present alpha helical conformation. Thus, amino acid types Asp, Glu, Ser, Arg, which represent the majority of the residues in the cytoplasmic part of the Vpu, have larger chemical shift dispersion. This indicates different secondary structure elements within the cytoplasmic domain.

Table 1. Resonance list of the identified amino acids of Vpu in POPC bilayers

Number of Resonance	Group	Atom	Nucleus	Shift (ppm)	Assignments	Standard Deviation
1	A1	Cα	13C	55.795	154	0.174
2	A1	Cβ	13C	18.186	96	0.166
3	A1	C’	13C	178.014	35	0.38
4	D1	Cα	13C	56.018	32	0.256
5	D1	Cβ	13C	37.387	33	0.316
6	D1	Cγ	13C	177.625	1	0
7	E1	Cα	13C	55.271	1	0
8	E1	Cβ	13C	28.941	3	0.076
9	E1	Cδ	13C	182.709	5	0.204
10	E1	Cγ	13C	34.929	2	0.008
11	G1	Cα	13C	44.804	10	0.208
12	G1	C’	13C	173.476	8	0.273
13	I1	Cα	13C	65.886	183	0.239
14	I1	Cβ	13C	37.779	172	0.123
15	I1	Cδ	13C	14.109	149	0.176
16	I1	Cγ1	13C	29.516	129	0.125
17	I1	Cγ2	13C	17.561	116	0.132
18	I1	C’	13C	177.562	38	0.338
19	L1	Cα	13C	58.232	162	0.173
20	L1	Cβ	13C	41.657	126	0.258
21	L1	Cδ12	13C	23.467	43	0.0313
22	L1	Cγ	13C	26.858	100	0.405
23	L1	C’	13C	177.86	19	0.443
24	P1	Cα	13C	62.309	18	0.297
25	P1	Cβ	13C	32.223	44	0.308
26	P1	Cδ	13C	50.231	38	0.267
27	P1	Cγ	13C	27.573	53	0.203
28	R1	Cα	13C	59.874	15	0.459
29	R1	Cβ	13C	29.506	20	0.29
30	R1	Cδ	13C	42.543	15	0.415

31	R1	Cγ	13C	26.713	1	0
32	R1	C’	13C	178.327	1	0
33	R1	Cζ	13C	159.98	8	0.226
34	S1	Cα	13C	69.911	9	0.075
35	S1	Cβ	13C	62.432	9	0.089
36	V1	Cα	13C	67.317	175	0.169
37	V1	Cβ	13C	31.287	126	0.136
38	V1	Cγ1	13C	23.619	126	0.13
39	V1	Cγ2	13C	21.949	135	0.176
40	V1	C’	13C	177.536	39	0.302
41	Y1	Cα	13C	62.579	15	0.236
42	Y1	Cβ	13C	38.333	26	0.236
43	Y1	Cδ	13C	133.25	4	0.216
44	Y1	Cε	13C	117.939	6	0.396
45	Y1	Cγ	13C	130.022	6	0.243
46	A2	Cα	13C	53.827	78	0.180
47	A2	Cβ	13C	18.238	37	0.173
48	A2	C’	13C	179.644	6	0.854
49	D2	Cα	13C	52.328	2	0
50	D2	Cβ	13C	39.386	7	0.285
51	D2	Cγ	13C	179.201	3	0.135
52	E2	Cα	13C	56.691	2	0.148
53	E2	Cβ	13C	26.96	3	0.057
54	E2	Cδ	13C	182.345	6	0.21
55	E2	Cγ	13C	34.214	4	0.228
56	P2	Cα	13C	64.298	1	0
57	P2	Cβ	13C	32.588	1	0
58	P2	Cδ	13C	50.615	6	0.285
59	P2	Cγ	13C	27.346	7	0.14
60	R2	Cα	13C	59.511	9	0.336
61	R2	Cβ	13C	29.467	20	0.363
62	R2	Cδ	13C	43.136	14	0.196
63	R2	Cγ	13C	27.546	1	0

64	R2	Cζ	13C	159.474	6	0.069
65	S2	Cα	13C	58.409	7	0.265
66	S2	Cβ	13C	63.969	7	0.622
67	T2	Cα	13C	62.47	3	0.149
68	T2	Cβ	13C	67.473	16	0.33
69	T2	Cγ	13C	22.244	9	0.169
70	A3	Cα	13C	50.048	4	0.453
71	A3	Cβ	13C	18.305	5	0.203
72	D3	Cα	13C	52.49	2	0.073
73	D3	Cβ	13C	37.789	4	0.453
74	D3	Cγ	13C	179.114	2	0
75	E3	Cα	13C	57.178	2	0.296
76	E3	Cβ	13C	29.109	1	0
77	E3	Cδ	13C	181.739	5	0.358
78	E3	Cγ	13C	34.476	4	0.289
79	E4	Cα	13C	58.727	4	0.127
80	E4	Cβ	13C	26.888	1	0
81	E4	Cδ	13C	182.408	5	0.164
82	I28	Cα	13C	65.494	2	0.053
83	I28	Cβ	13C	37.751	2	0.141
84	I28	Cγ2	13C	17.297	2	0.159
85	E29	Cα	13C	59.45	8	0.366
86	E29	Cβ	13C	28.44	17	0.181
87	E29	Cδ	13C	182.293	9	0.326
88	E29	Cγ	13C	34.666	11	0.287

The inter-residue cross peaks between residue pairs Ala-Val and Leu-Ile are already detected in spectra recorded with a mixing time of 70 ms. These cross peaks are reproduced at longer mixing times up to 300 ms (Fig. 3.12). Furthermore, additional inter-residue cross peaks deriving from residue pairs as Ala-Ala, Ala-Ile, Leu-Val, Ile-Leu, and Ile-Val were found at the long mixing time of 300 ms. Such inter-residue cross peaks are predominantly visible at the 300 ms mixing time, whereas

no inter-residue cross peak deriving from other detected amino acid types as Ser, Pro, and Asp was found. For amino acid type Glu, only one pair of inter-residue cross peaks was found as shown in Table 3.

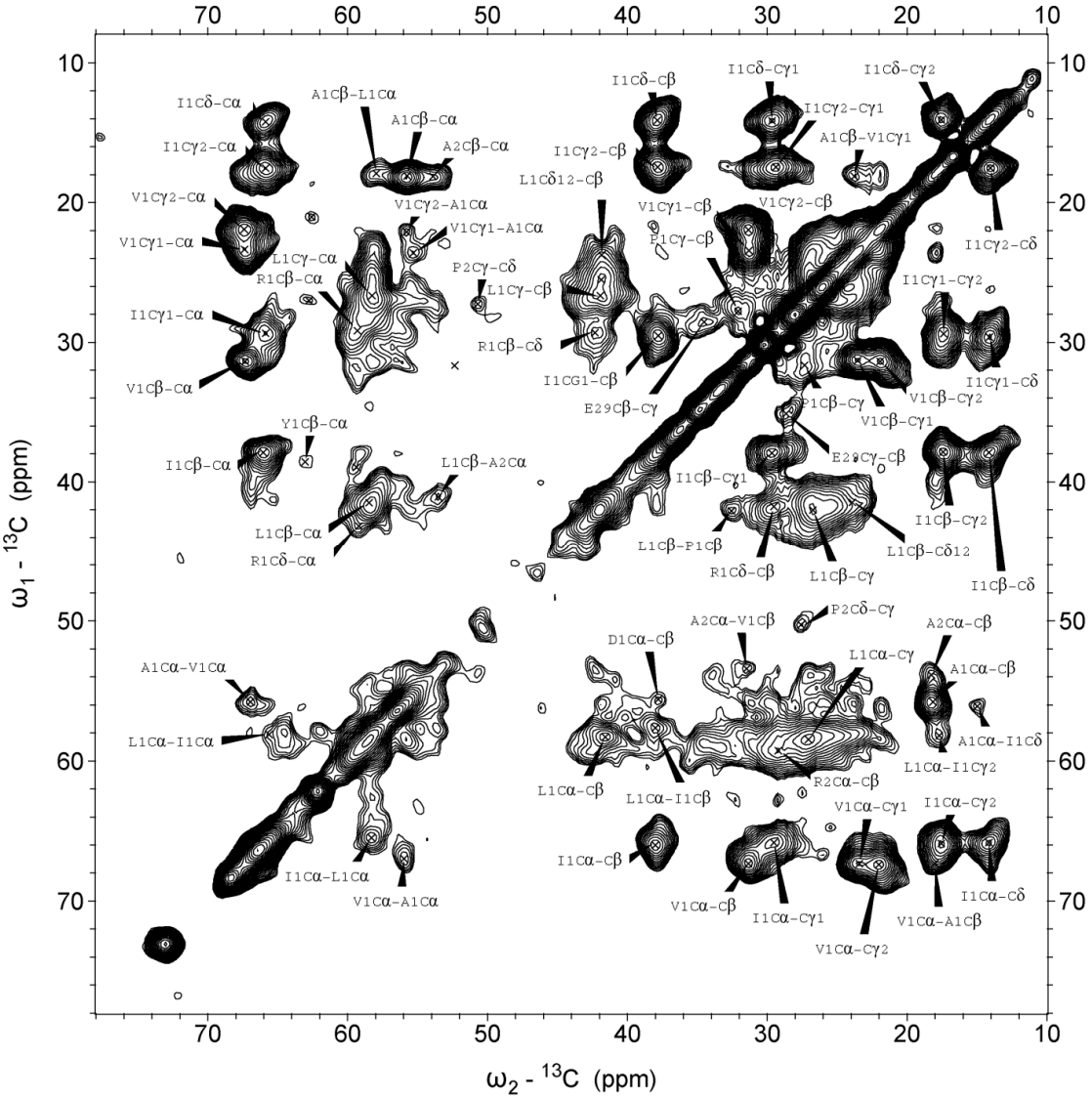

Fig. 3.11. A representative 2D ^{13}C -^{13}C correlation PDSD-RR spectrum of the uniformly labeled ^{13}C, ^{15}N full-length Vpu protein in POPC bilayers. The spectrum was acquired at 600 MHz ^{1}H frequency with a spinning speed of 9375 Hz,128 scans, 70 ms ^{13}C mixing time, 6.5 ms evolution time of ^{13}C. The experiment was conducted around 0°C (the sample temperature). Data were processed using Lorentzian-to-Gaussian apodization function with 100 Hz of Lorentzian line sharpening, 200 Hz of Gaussian line broadening prior to Fourier transform. For carbonyl region, see Fig. B3.

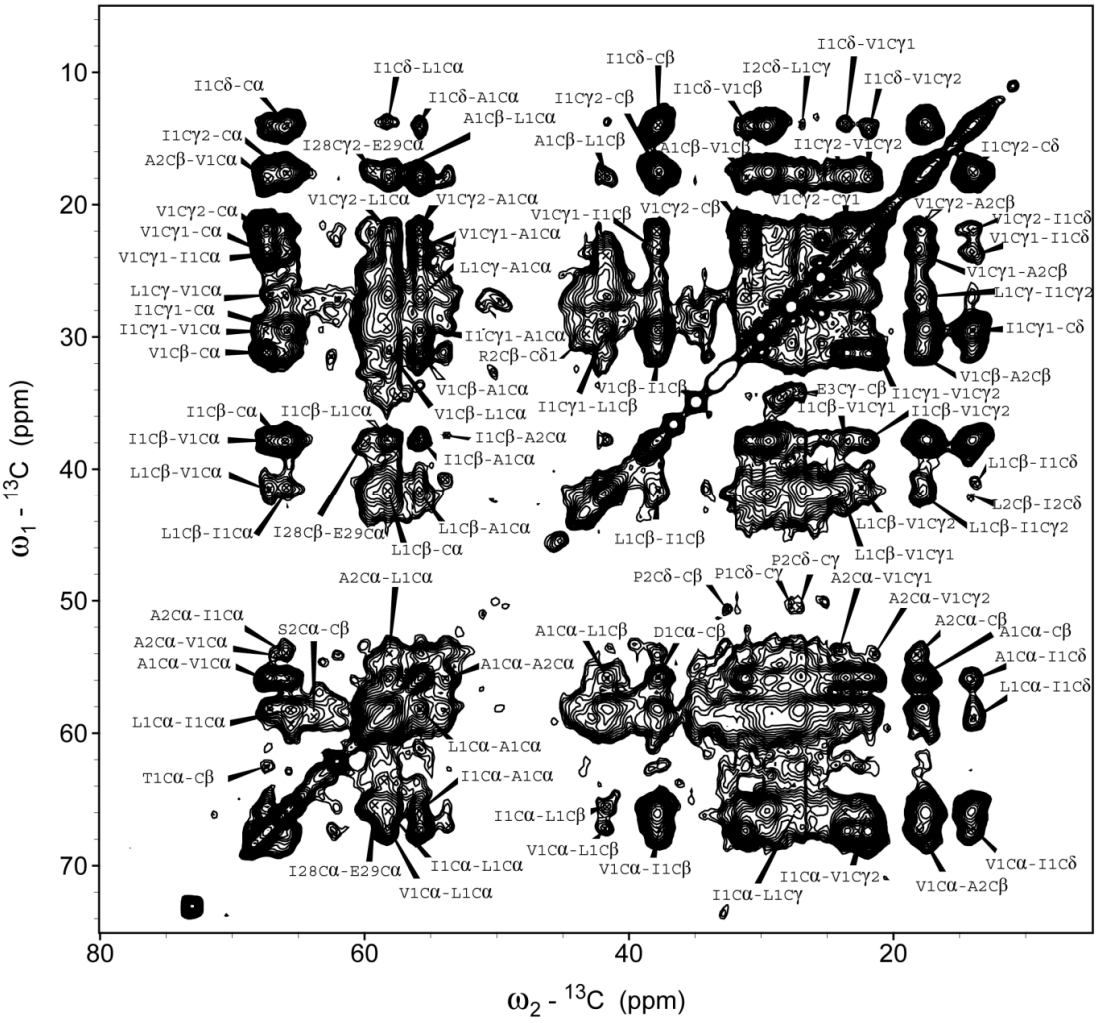

Fig. 3.12. A representative 2D ^{13}C -^{13}C correlation PDSD-RR spectrum of the uniformly labeled ^{13}C, ^{15}N full-length Vpu protein in POPC bilayers. The spectrum was acquired at 800 MHz ^{1}H frequency with a spinning speed of 12500 Hz, 160 scans. The ^{13}C mixing time is 300 ms. The evolution time of ^{13}C equals 4.5 ms. The experiment was conducted around 0°C (the sample temperature). Data were processed using Lorentzian-to-Gaussian apodization function with 100 Hz of Lorentzian line sharpening, 200 Hz of Gaussian line broadening prior to Fourier transform. For carbonyl region, see Fig. 3.25B.

Table 2. List of inter-residue cross peaks. The first row shows the residue pairs and the occurance of the pairs in the primary structure of Vpu.

A-A (1)	A-L (4)	A-I (4)	A-V (2)	L-V (3)	I-L (3)	I-V (3)
A1Cα-A2Cα	A1Cα-L1Cα	A1Cα-I1Cα	A1Cα-V1Cα	L1Cα-V1Cα	I1Cα-L1Cα	I1Cα-V1Cγ1
A1Cα-A2Cα	A1Cα-L1Cβ	A1Cα-I1Cδ	A1Cβ-V1Cβ	L1Cα-V1CG2	I1Cα-L1Cβ	I1Cα-V1Cγ2
A2Cα-A1Cα	A1Cβ-L1Cα	A2Cα-I1Cα	A1Cβ-V1Cγ1	L1Cβ-V1Cα	I1Cα-L1Cγ	I1Cβ-V1Cα
A2Cα-A1Cα	A1Cβ-L1Cβ	A2Cα-I1Cα	A2CA-V1Cα	L1Cβ-V1CG1	I1Cβ-L1Cα	I1Cβ-V1Cβ
	A2Cα-L1Cα	I1Cα-A1Cα	A2Cα-V1Cγ1	L1Cβ-V1CG2	I1Cβ-L1Cβ	I1Cβ-V1Cγ1
	L1Cα-A1Cα	I1Cα-A1Cα	A2Cα-V1Cγ2	L1Cγ-V1Cα	I1Cδ-L1Cα	I1Cβ-V1Cγ2
	L1Cα-A1Cβ	I1Cβ-A1Cα	A2Cβ-V1Cα	L1Cγ-V1Cβ	I1Cγ1-L1Cβ	I1Cδ-V1Cα
	L1Cα-A2Cα	I1Cβ-A1Cα	V1Cα-A1Cα	V1Cα-L1Cα	I1Cγ2-L1Cγ	I1Cγ-V1Cβ
	L1Cβ-A1Cα	I1Cβ-A2Cα	V1Cα-A2Cα	V1Cα-L1Cβ	I2Cδ1-L1Cγ	I1Cδ-V1Cγ1
	L1Cγ-A1Cα	I1Cβ-A2Cα	V1Cα-A2Cβ	V1CB-L1Cα	L1Cα-I1Cα	I1Cδ-V1Cγ2
		I1Cδ-A1Cα	V1Cβ-A1Cα	V1Cγ1-L1Cβ	L1Cα-I1Cδ	I1Cγ1-V1Cα
		I1Cδ-A1Cα	V1Cβ-A2Cα	V1Cγ2-L1Cα	L1Cβ-I1Cα	I1Cγ1-V1Cγ1
		I1Cγ1-A1Cα	V1Cβ-A2Cβ		L1Cβ-I1Cβ	I1Cγ1-V1Cγ2
		I1Cγ1-A1Cα	V1Cγ1-A1Cα		L1Cβ-I1Cδ	I1Cγ2-V1Cγ2
			V1Cγ1-A2Cα		L1Cβ-I1CG1	V1Cα-I1Cβ
			V1Cγ1-A2Cβ		L1Cγ-I1Cα	V1Cα-I1Cδ
			V1Cγ2-A1Cα		L1Cγ-I1Cγ2	V1Cβ-I1Cα
			V1Cγ2-A2Cβ		L1Cγ-I1Cδ	V1Cβ-I1Cβ
						V1Cγ1-I1Cα
						V1Cγ1-I1Cβ
						V1Cγ1-I1Cδ
						V1Cγ2-I1Cα
						V1Cγ2-I1Cβ
						V1Cγ2-I1Cδ

Table 3. Inter-residue cross peaks between the pair Ile28-Glu29 at long mixing time of the PDSD-RR experiment performed on Vpu in POPC bilayers (Fig. 3.2)

Inter-residue cross peaks	I28Cα-E29Cα	E29Cα - I28Cα	I28CB-E29Cα	I28Cγ2-E29Cα

The carbon atoms of the side-chains of amino acid types Ala, Val, Leu, Ile, Thr, and Pro were found again in the DQ/SQ-SPC5 spectrum (Fig. 3.13) that was recorded using a the double quantum SPC5 technique (section 1.2.4). This technique allows detecting one bond correlation between ^{13}C atoms and therefore it helps to confirm the presence of the amino acid residues in the reconstituted Vpu.

There are also unassigned signals due to the lack of specific chemical shifts (Fig. 3.13). However, when the ^{13}C shifts of the unassigned signals (ellipsoids 3 and 4) were compared with the ^{13}C shifts of Vpu(39-81) in micelles[10] (Fig. 2.6 –the DQ/SQ map), it indicates that the unassigned ^{13}C shifts of the current work are overlapped with the alpha and beta carbons of the residues Arg41, Glu48, Arg49, Gln61, Glu62, Glu63, Glu69, Arg70, His72, and Trp76 (Fig. B6.) These residues belong to the cytoplasmic part in the primary structure of the Vpu (Fig. 1.2.A).

When the temperature of the sample was reduced far below the freezing point (around -20°C), the signals within and nearby the ellipsoids 3 and 4 are increased significantly (Fig. 3.16). A similar phenomenon was observed for the signals in the spectral area between 60 ppm -80 ppm (along the ω_1 dimension) and 20 ppm -40 ppm (along the ω_2 dimension). Furthermore, the signals deriving from amino acid types Ser, Gly, and Asp but not Glu (Fig. 3.14) were also found to significantly increase when reducing the sample temperature. It is likely that the water surrounding or inside the part of the Vpu containing residues Ser, Gly, Asp, Arg41, Glu48, Arg49, Gln61, Glu62, Glu63, Glu69, Arg70, His72, Trp76 is frozen below the freezing temperature. The motion of this protein fragment is thereby inhibited leading to the significantly increase of the NMR signals.

In contrast, no pronounced change was observed for the cross peaks deriving from Ala1, Val1, Ile1, Leu1 residues when changing the temperature of the sample, except for cross peaks arising from the methyl carbons of the residues Leu, Ile, and Ala (i.e. (LCδ1, LCδ2, ICδ1, ICγ2, ACβ) in which the position of peaks is slightly shifted.

The signals within the ovals 1 and 2 (Fig. 3.13) are also cross peaks that might be assigned as Ala or Thr. Further studies employing other polarization transfer schemes rather than the PDSD-RR and the DQ-SPC5 are needed to clarify this assignment.

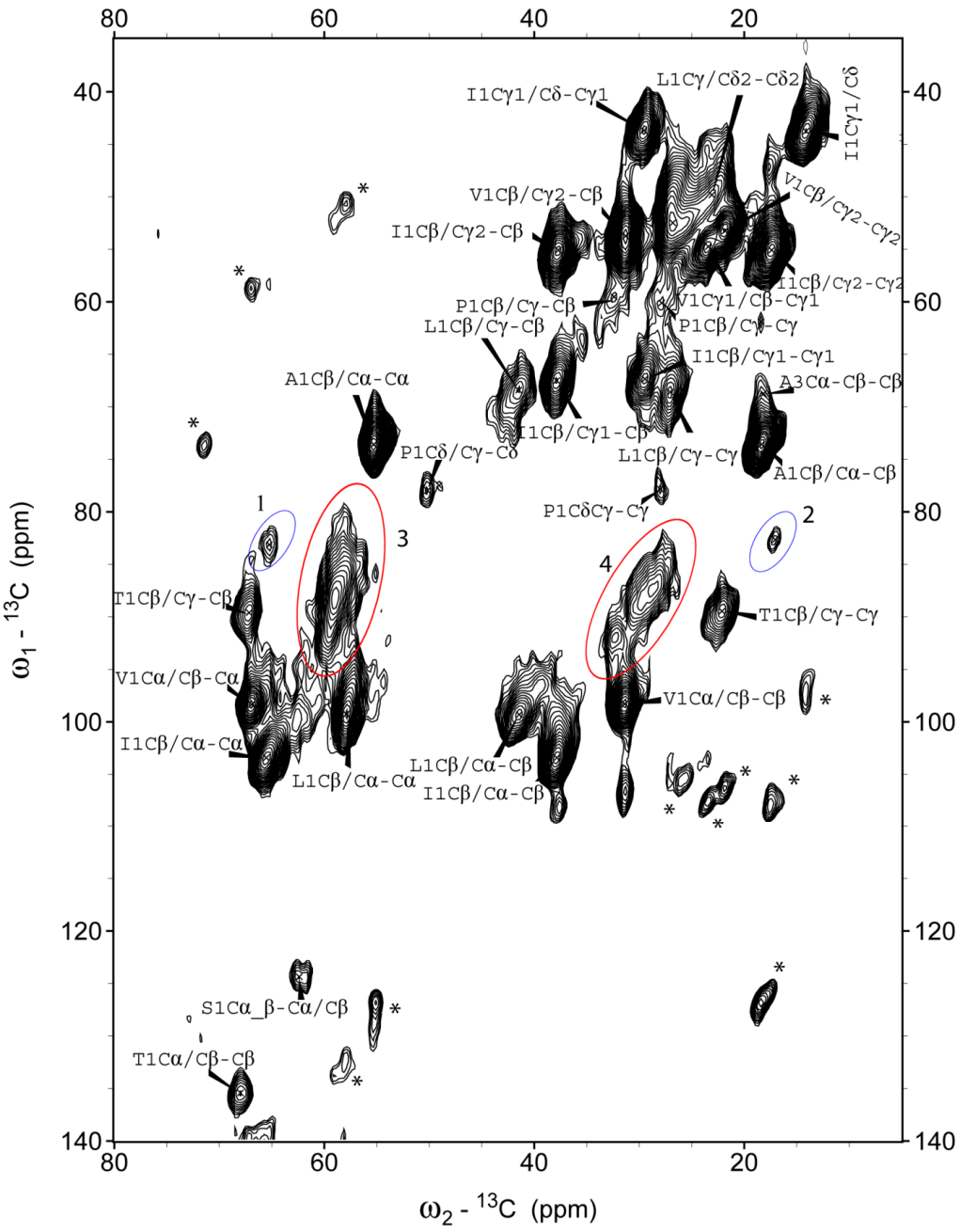

Fig. 3.13. Aliphatic region of the 2D ^{13}C -^{13}C correlation DQ/SQ-SPC5 spectrum of the uniformly labeled ^{13}C, ^{15}N full-length Vpu protein in POPC bilayers. The spectrum was acquired at 600 MHz ^{1}H frequency with a spinning speed of 8000Hz, 256 scans with the pulse sequence in Fig A5. The experiments were conducted around 0°C (the temperature of the sample). The data were processed using sine-bell apodization function prior to Fourier transform.

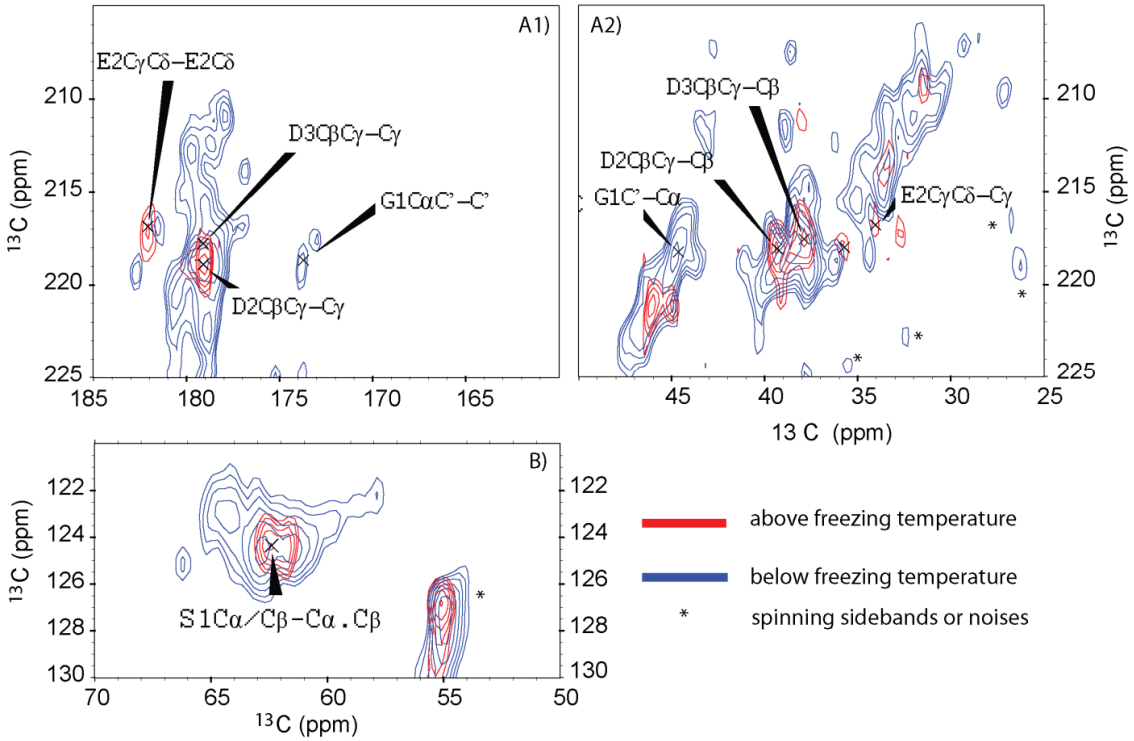

Fig. 3.14. Serine and Aspartic acid regions of 2D ^{13}C -^{13}C correlation DQ/SQ-SPC5 spectra of the uniformly labeled ^{13}C, ^{15}N full-length Vpu protein in POPC bilayers at different temperatures. The blue spectrum was collected far below the freezing point, the red spectrum was collected above the freezing point. The spectra were acquired at 600 MHz ^{1}H frequency with a spinning speed of 8000 Hz, 256 scans. The peaks next to asterisk symbol (*) are spinning sidebands or noise. Numbers 1, 2 after one letter code of amino acid show the number of the detected residues. The data were processed using sine-bell apodization function prior to Fourier transform.

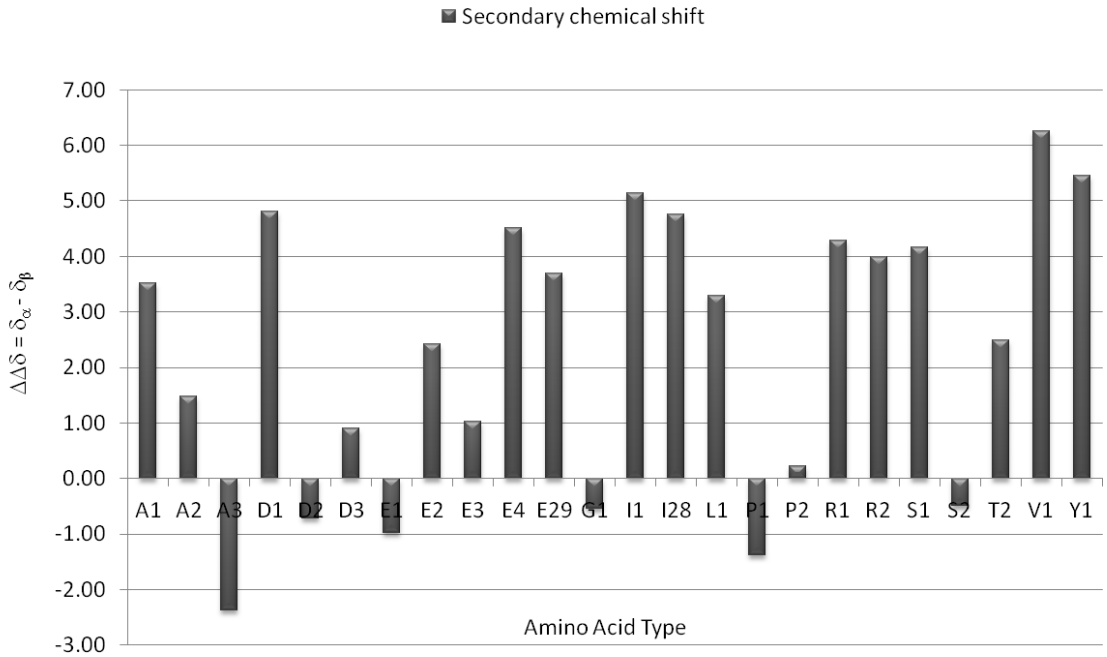

Fig. 3.15. Chemical shift index of the identified amino acid type of the uniformly labeled ^{13}C, ^{15}N full-length Vpu protein in POPC bilayers. The positive indices (greater than +1.5) indicate α helical structure while the negative indices (smaller than -1.5) present β-strand elements. The numbers in E29, I28 show the positions of these residues in the Vpu primary structure. Other number such as 1, 2, 3 and 4 present the number of same amino acid types which were identified in this work.

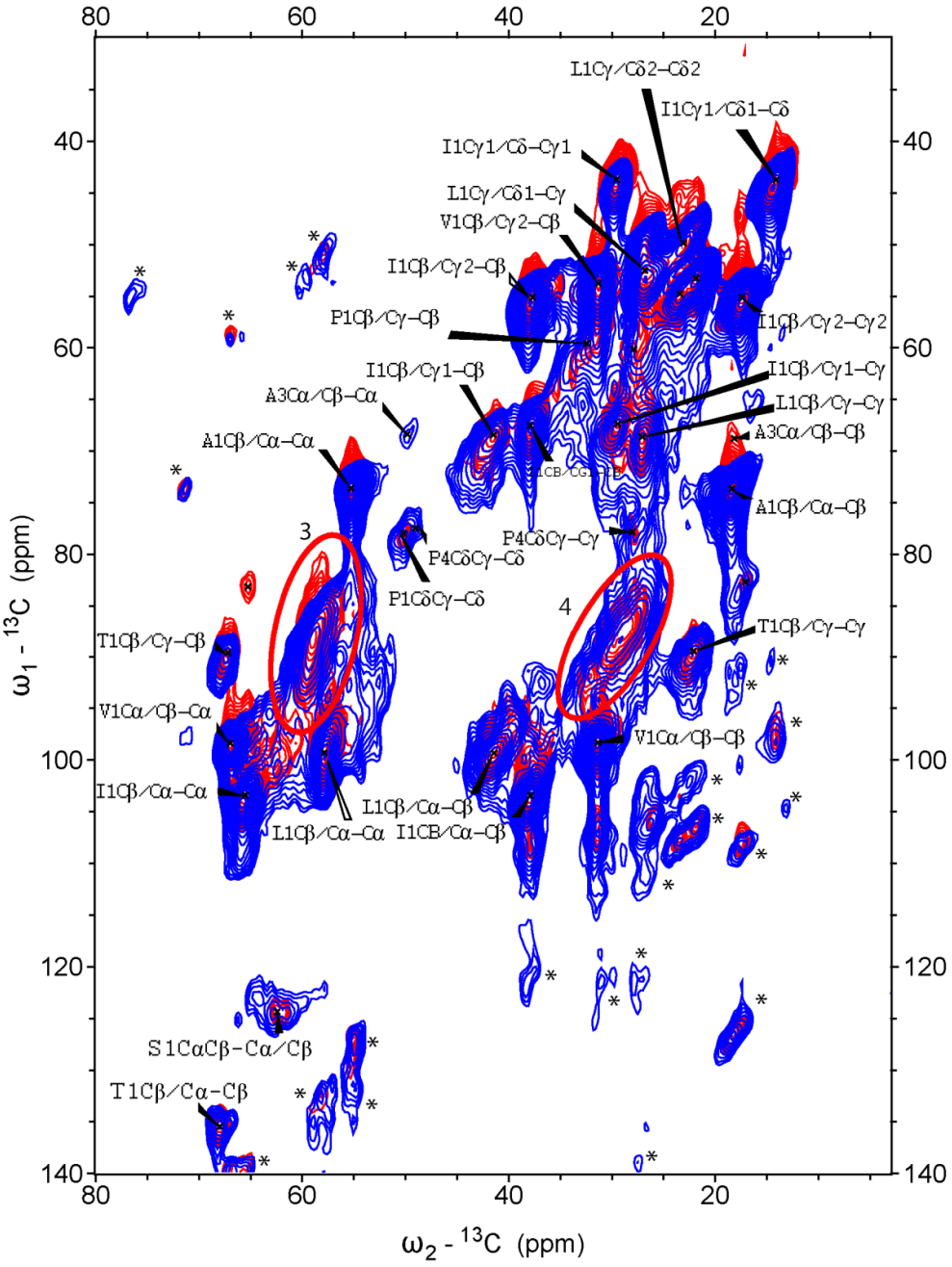

Fig. 3.16. Aliphatic region of 2D ^{13}C-^{13}C correlation DQ/SQ-SPC5 spectra of the uniformly labeled ^{13}C, ^{15}N full-length Vpu protein in POPC bilayers at different temperatures. The blue spectrum was recorded far below the freezing point; the red spectrum was collected above the freezing point. The spectra were acquired at 600 MHz ^{1}H frequency with a spinning speed of 8000 Hz, 256 scans. The peaks next to asterisk symbol (*) are spinning sidebands or noise. The data were processed using sine-bell apodization function prior to Fourier transform.

3.3.2. Resonance assignments of CD4(372-433) peptide in POPC bilayers

Similar to the Vpu in POPC bilayers, the assignment strategy (section 2.2.3) and 2D ^{13}C-^{13}C correlation set as PDSD-RR and DQ/SQ of spectra were utilized to assign the resonances of the CD4(372-433) peptide in POPC bilayers. The results are presented in Fig. 3.17-3.19. In addition to the PDSD-RR technique, the NCOCX technique[11,12] (the pulse sequence in Fig. A6) was also used to determine sequential links. The result is presented in Fig. 3.20.

Fig. 3.17 displays a 2D ^{13}C-^{13}C spin diffusion spectrum recorded with a mixing time of 50 ms. In this spectrum, both intra-residue cross peaks and inter-residue cross peaks of amino acids were observed. The intra-residue cross peaks were assigned to 8 amino acid types i.e. Ala, Val, Ile, Leu, Pro, Phe, Gly, and Ser, whereas the inter-residue cross peaks were found among 7/8 identified amino acid types (Table 4) including the following residue pairs: Ile-Phe, Leu-Val, Ile-Gly, Gly-Leu, Ala373-Leu374, Leu374-Ile375, Gly379-Val380, and Leu385-Phe386. With a longer mixing time of 200ms, the number of inter-reside cross peaks in each pair is increased, particularly in unique pairs as Leu374-Ile375 and Gly379-Val380. Furthermore, two additional pairs Val380-Ala381 and Ala381-Gly382 were detected at the longer mixing time of the PDSD-RR experiment (Fig. 3.18 and Table 4).

Table 4. List of inter-residue cross peaks. The first row in A) shows the residue pairs and the number of the repetitive pairs in the primary structure of Vpu. The first row in B) shows the unique pairs in the primary structure. The highlighted cross-peaks with ***the italic and bold format*** were found at both short (50 ms, Fig. 3.17) and long (200 ms, Fig. 3.18) mixing times. The non-highlighted peaks are found only at the longer mixing time.

A) Non site-specific inter–residue cross peaks					
I-F (2)	L-V (2)	I-G (2)	G-L(4)		
ICα-FCα	***LCα-VCα***	***GCα-ICα***	***GCα-LCα***		
FCα-ICα	LCα-VCα	***ICβ-GCα***	***GCα-LCβ***		
	LCβ-VCβ	GCα-ICβ	***GCα-LCγ***		
			LCα-GCα		
			LCβ-GCα		
			LCγ-GCα		
			LCδ2-GCα		
			GCα-LCδ2		
B) Site-specific inter–residue cross peaks					
A373-L374	L374-I375	G379-V380	V380-A381	A381-G382	L385-F386
ACα-LCα	ICα-LCα	GCα-VCα	ACβ-VCβ	ACα-GCα	***FCα-LCα***
LCα-ACα	ICα-LCβ	GCα-VCα	ACα-VCα	ACβ-GCα	***FCβ-LCα***
ACβ-LCα	ICα-LCδ	GCα-VCα	ACβ-VCδ2	GCα-ACβ	***LCα-FCα***
ACβ-LCβ	***ICβ-LCα***	VCα-GCα	VCα-ACα		***LCα-FCβ***
ACβ-LCγ	ICβ-LCβ	VCα-GC’	VCβ-ACα		LCβ-FCβ
LCα-ACβ	ICδ-LCγ	VCβ-GCα			
LCδ2-ACβ	ICγ2-LCδ2	VCβ-GCα			
	ICγ2-LCδ	***VCβ-GCα***			
	LCα-ICα				
	LCα-ICβ				
	LCβ-ICγ2				
	LCγ-ICδ				
	LCγ-ICγ2				

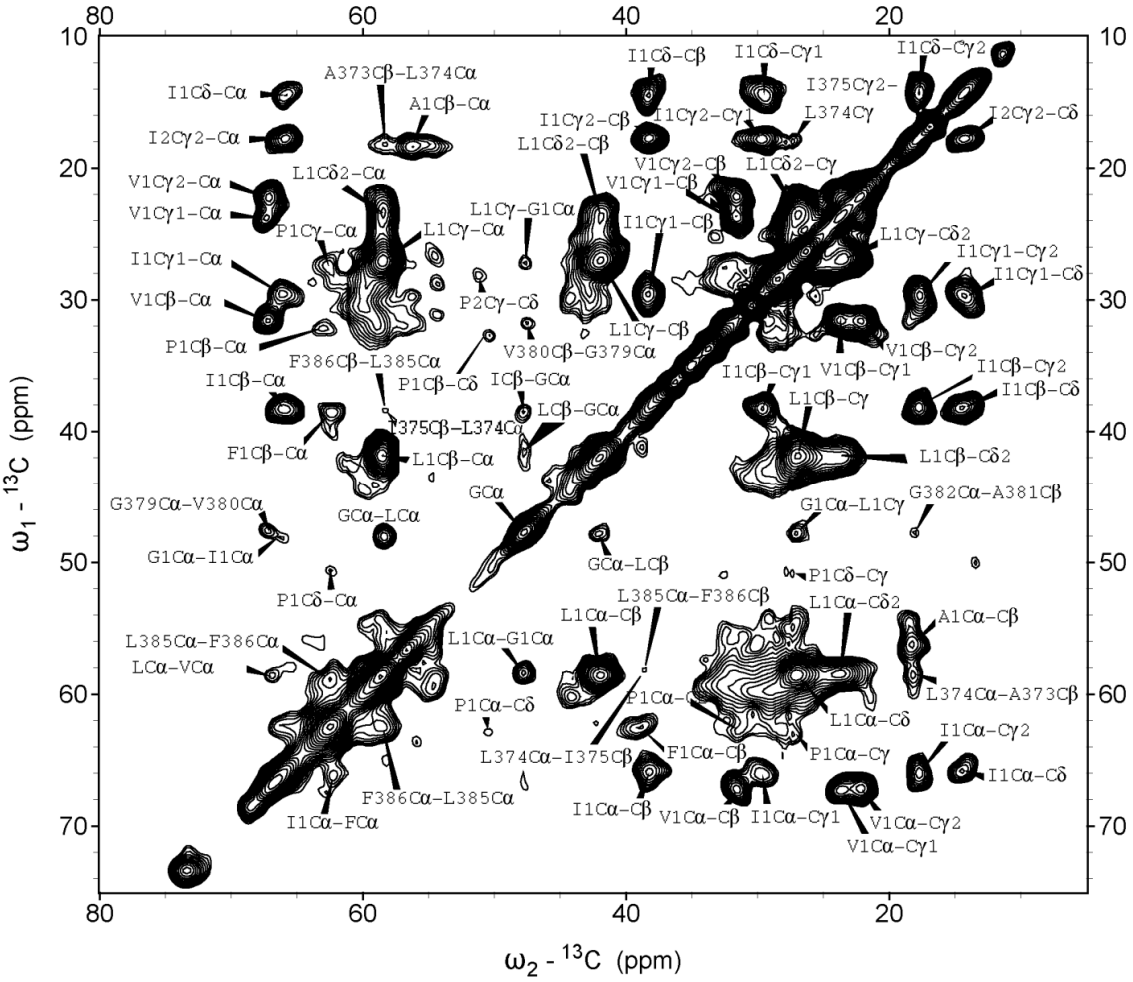

Fig. 3.17. A 2D ^{13}C -^{13}C correlation PDSD-RR spectrum of the uniformly labeled ^{13}C, ^{15}N CD4(372-433) peptide in POPC bilayers. The spectrum was acquired using the PDSD-RR technique at 600 MHz ^{1}H frequency with a spinning speed of 9375 Hz, 160 scans. The ^{13}C mixing time is 50 ms. (For carbonyl and aromatic carbon region, see Fig. B4). The experiment was conducted around 0°C (the temperature of the sample). The data were processed using Lorentzian-to-Gaussian apodization function with 100 Hz of Lorentzian line sharpening, 200 Hz of Gaussian line broadening prior to Fourier transform.

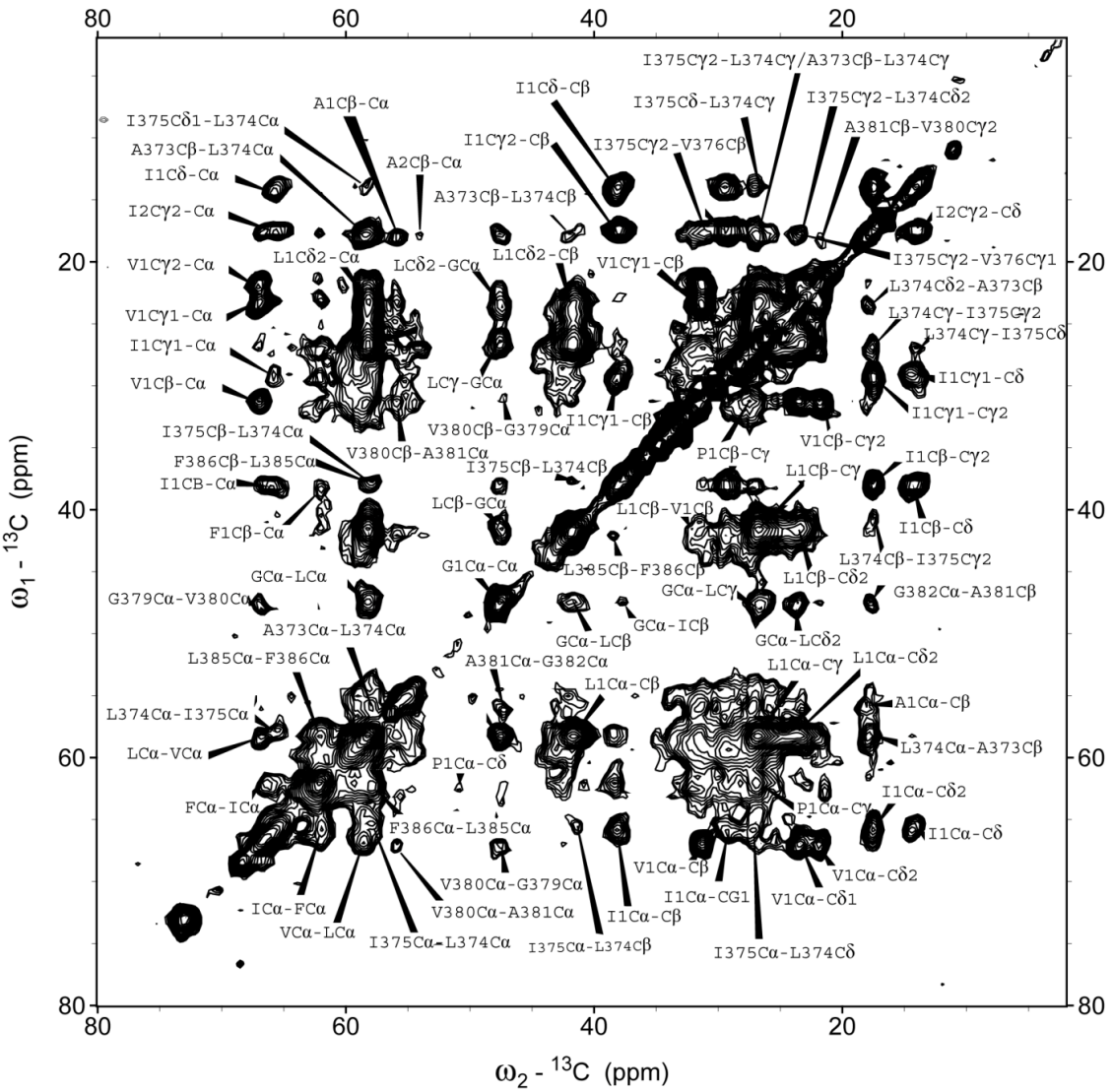

Fig. 3.18. A 2D ^{13}C -^{13}C correlation PDSD-RR spectrum of the uniformly labeled ^{13}C, ^{15}N CD4(372-433) peptide in POPC bilayers. The spectrum was acquired at 800 MHz ^{1}H frequency with a spinning speed of 12500 Hz, 288 scans. The ^{13}C mixing time is 200ms. The experiment was conducted around 0°C (the temperature of the sample). The data were processed using Lorentzian-to-Gaussian apodization function with 100 Hz of Lorentzian line sharpening, 200 Hz of Gaussian line broadening prior to Fourier transform. (For carbonyl and aromatic carbon regions see Fig. B5).

As mentioned earlier, in addition to the PDSD-RR, the sequential links were also determined with the aid of the NCOCX pulse sequence and the result is presented in Fig. 3.19. Linking between Ala381 and Gly382 residues is reproducible and additional sequential links were assigned specifically such as Gly378-Gly379, Ile387-Gly388 and Leu377-Gly378 (or Leu389-Gly390). However, the poor dispersion of ^{15}N shift does not help to distinguish between the pairs Leu377-Gly378 and Leu389-Gly390.

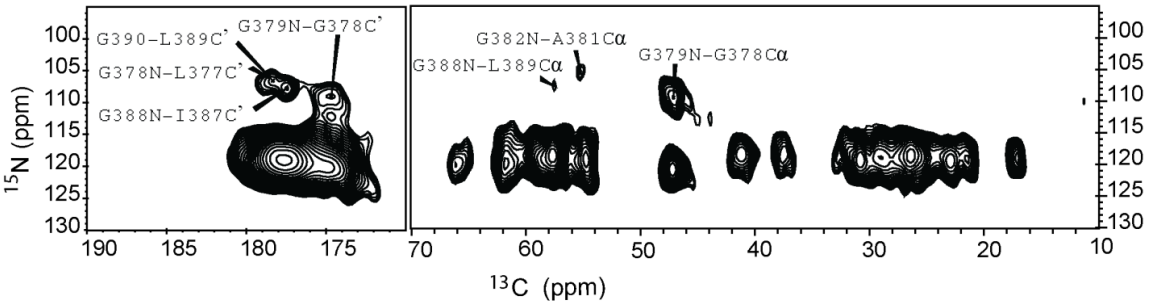

Fig. 3.19. A 2D NCOCX - ^{15}N-^{13}C correlation spectrum of the uniformly labeled ^{13}C, ^{15}N CD4(372-433) peptide in POPC bilayers. The spectrum had been acquired for 7 days, at MAS speed of 11000 Hz on a Varian spectrometer operating at a ^{1}H Larmor frequency of 600 MHz.

Taken together, the specific spin systems identified from the uniformly labeled CD4(372-433) in POPC bilayers are Ala373, Leu374, Ile375, Gly378, Gly379, Val380, Ala381, Gly382, Leu385, Phe386, Ile387, Gly388 and either Leu377 or Leu389, and Gly390. These residues all belong to the transmembrane part of CD4 and are underlined in Fig. 3.20. Among the identified residues, the secondary chemical shifts of Ala373, Leu374, Ile375, Gly378, Gly379, Val380, Ala381, Gly382, Leu385, and Phe386 are indicative of alpha helical structure as shown in Fig. 3.23. There is no significant difference between the secondary chemical shifts of these residues and those obtained from CD4(372-433) in micelles using liquid state NMR spectroscopy[8,9] (Fig. 3.23).

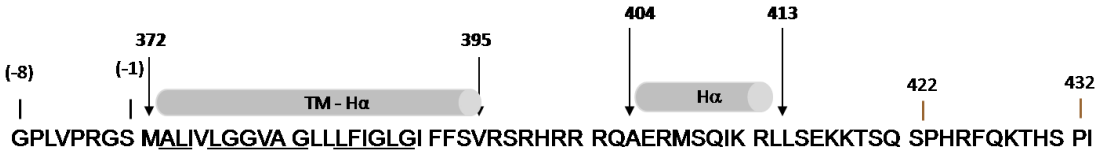

Fig. 3.20. The primary structure of the CD4(372-433) peptide. The information of the secondary structure is summary from the previous studies[8,13]. The underline amino acid residues are identied in this work. The residues from (-8) to (-1) are the left of PreScission cleavege (Section 2.1.1)

Similar to the case of the reconstituted Vpu, the majority of the identified amino acid types of the CD4(372-433) by means of the PDSD-RR technique belong to the transmembrane part, whereas other amino acid types that belong to the cytoplasmic part were found with the aid of DQ/SQ-SPC5 spectrum. Fig. 3.21 shows a 2D DQ/SQ-SPC5 spectrum collected from the reconstituted CD4(372-433) with a poor dispersion of ^{13}C shifts. The side-chain atoms of amino acid types Ala, Val, Ile, Leu, and Phe are

reproducible and additional signal deriving from Ser residue without specific shifts was detected. Furthermore, when the temperature of the sample was reduced below the freezing point, the signals within the ellipsoid regions are significantly enhanced (Fig. 3.22). This observation is different from what was observed for the signals outside the ellipsoids in which the slight changes of the signals in the blue spectrum is due to the number of scans. When unassigned signals within the ellipsoids in Fig. 3.22 were compared with the ^{13}C shifts obtained from the CD4(372-433) in micelles[9] (Fig. 2.5), the unassigned ^{13}C shifts in the current work were found to overlap with the ^{13}C shifts of the cytoplasmic residues as Arg396, Arg398, His399, Arg412, Lys411, Lys417, Gln409 (Fig. B7).

The residue types Ala, Val, Ile, Leu, Phe, Gly, and Arg, which were tentatively assigned basing on the PDSD-RR and the DQ/SQ spectra, are indicative of alpha helical structure while Pro residue has the random coil shift. The data are shown in Fig. 3.24.

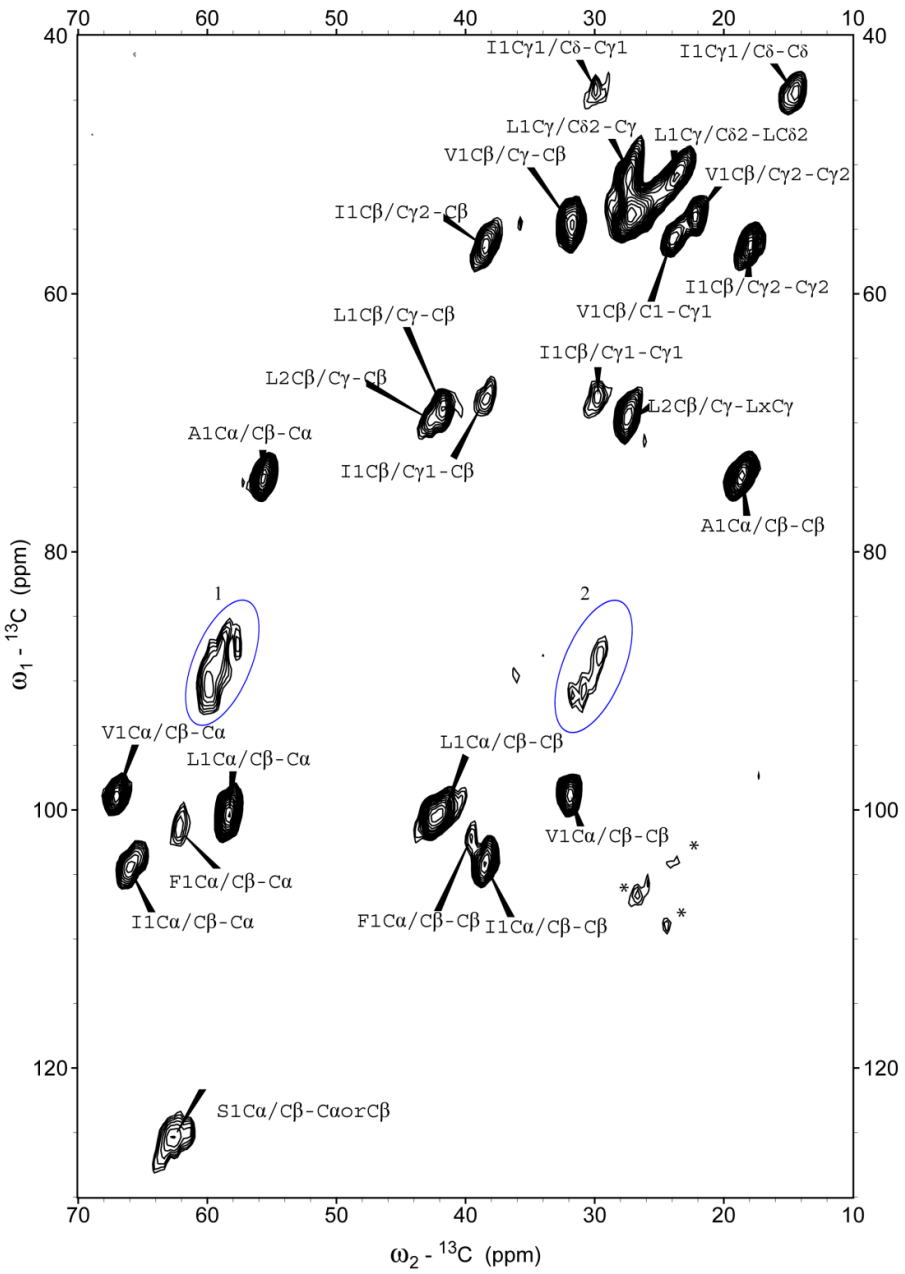

Fig. 3.21. Aliphatic region of a 2D ^{13}C-^{13}C correlation DQ-SPC5 spectrum of the uniformly labeled ^{13}C, ^{15}N CD4(372-433) peptide in POPC bilayers. The spectrum was acquired using double quantum filter SPC-5 at 600 MHz ^{1}H frequency with spinning speed of 8000 Hz and 192 scans. The data were processed using sine-bell apodization function prior to Fourier transform. The peaks next to asterisk symbol (*) are spinning sidebands or the noises.

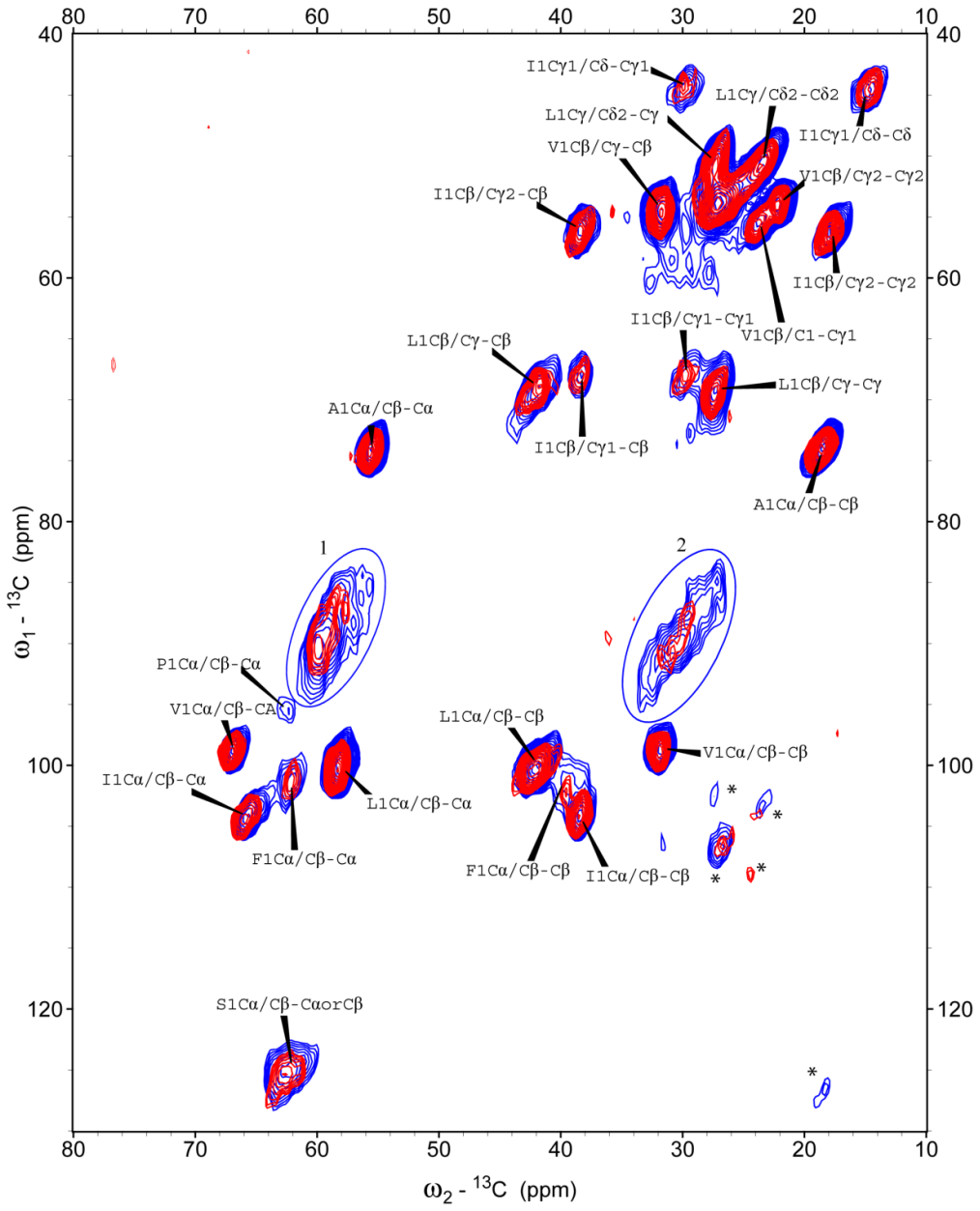

Fig. 3.22. Aliphatic region of a 2D ^{13}C -^{13}C correlation DQ/SQ-SPC5 spectra of the uniformly labeled ^{13}C, ^{15}N CD4(372-433) peptide reconstituted in POPC lipid bilayers at different sample temperatures. The blue spectrum was collected far below the freezing point with 480 scans; the red spectrum was collected around the freezing point with 192 scans. The spectra were acquired at 600 MHz ^{1}H frequency with a spinning speed of 8000 Hz. The data were processed using sine-bell apodization function prior to Fourier transform. The peaks next to asterisk symbol (*) are spinning sidebands or the noises. The blue line is the spectral diagonal line.

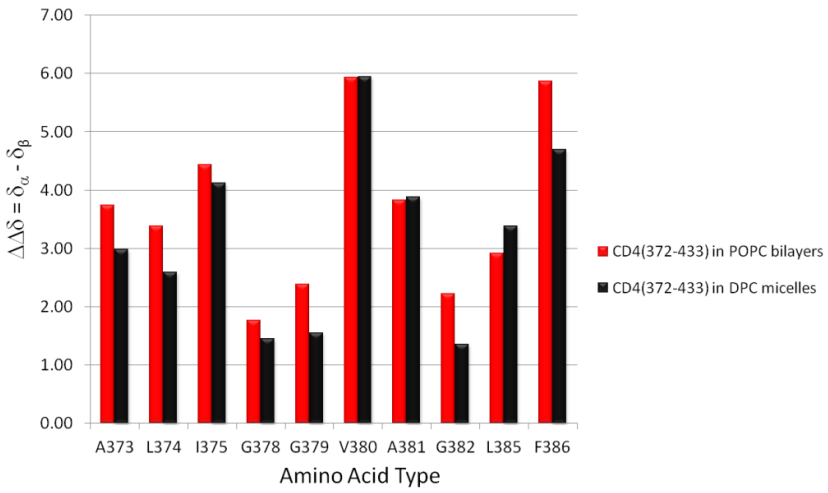

Fig. 3.23. Chemical shift index of the identified amino acids of the uniformly labeled ^{13}C, ^{15}N CD4(372-433) peptide. ΔΔδ means secondary chemical shift as described in section 2.2.3. The red columns show the secondary chemical shifts obtained from CD4(372-433) reconstituted in POPC lipid bilayers of the current work. Positive indices (greater than +1.5) indicate α helical structure. The numbers in Ala381, Phe386, Gly378, Gly379, Gly382, Ile375, Leu374, Leu385, Val380 show the positions of these residues in the CD4(372-433) primary structure. The black columns show the secondary chemical shifts obtained from CD4(372-433) reconstituted in micelles of the previous work[8,9].

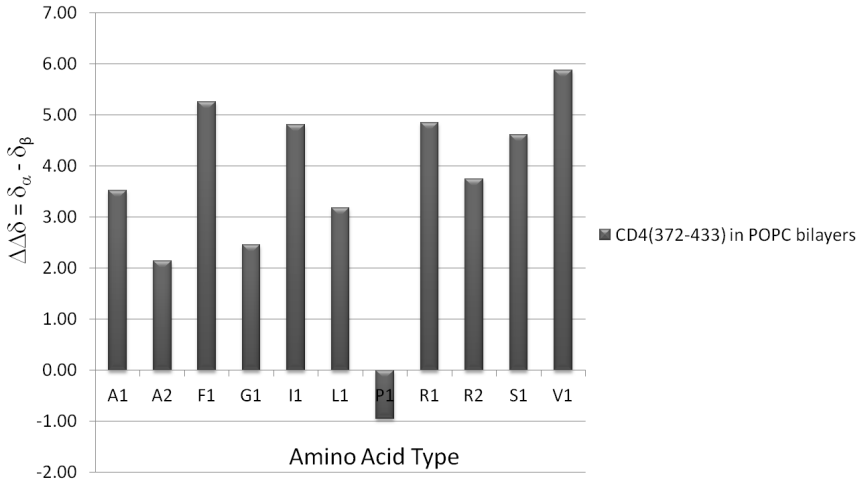

Fig. 3.24. Chemical shift index of the identified amino acid type of the uniformly labeled ^{13}C, ^{15}N CD4(372-433) peptide reconstituted into POPC lipid bilayers of the current work. ΔΔδ means secondary chemical shift as described in section 2.2.3. Positive indices (greater than +1.5) indicate α helical structure while negative indices (smaller than -1.5) present β-strand elements. The number such as 1, 2 present the number of same amino acid types which were assigned tentatively in this work.

All assigned signals of the reconstituted CD4(372-433) collected from PDSD-RR, NCOCX and DQ/SQ-SPC5 spectra are listed in Table 5.

Table 5. Resonance list of the identified amino acids of CD4(372-433) in POPC bilayers

Number of Resonance	Group	Atom	Nucleus	Shift (ppm)	Assignments	Standard Deviation
1	A1	Cα	13C	55.871	16	0.24
2	A1	Cβ	13C	18.238	14	0.151
3	F1	Cα	13C	62.191	42	0.206
4	F1	Cβ	13C	38.838	29	0.366
5	F1	Cδ	13C	132.45	4	0.317
6	F1	Cε	13C	130.978	9	0.3
7	F1	C’	13C	177.188	6	0.289
8	F1	Cζ	13C	129.383	7	0.418
9	G1	Cα	13C	47.809	75	0.165
10	G1	C’	13C	175.475	18	0.299
11	I1	Cα	13C	65.946	77	0.264
12	I1	Cβ	13C	38.159	77	0.254
13	I1	Cδ	13C	14.291	60	0.19
14	I1	Cγ1	13C	29.521	74	0.188
15	I1	Cγ2	13C	17.696	54	0.174
16	I1	C’	13C	177.824	5	0.203
17	L1	Cα	13C	58.364	86	0.162
18	L1	Cβ	13C	41.876	86	0.246
19	L1	Cδ1,2	13C	23.435	51	0.236
20	L1	Cγ	13C	26.967	88	0.233
21	L1	C’	13C	178.364	24	0.137
22	P1	Cα	13C	62.624	20	0.269
23	P1	Cβ	13C	32.099	17	0.41
24	P1	Cδ	13C	50.645	11	0.293
25	P1	Cγ	13C	27.441	22	0.302
26	R1	Cα	13C	59.88	5	0.273
27	R1	Cβ	13C	28.956	2	0.785
28	R1	Cδ	13C	43.402	6	0.511
29	R1	Cζ	13C	159.753	3	0.034
30	S1	Cα	13C	62.346	2	0.281

31	S1	Cβ	13C	62.816	2	0.315
32	V1	Cα	13C	67.132	79	0.171
33	V1	Cβ	13C	31.523	66	0.163
34	V1	Cγ1	13C	23.536	48	0.346
35	V1	Cγ2	13C	22.07	48	0.154
36	V1	C’	13C	177.865	13	0.294
37	A2	Cα	13C	54.389	2	0.349
38	A2	Cβ	13C	18.127	2	0.234
39	R2	Cα	13C	58.926	1	0
40	R2	Cβ	13C	29.099	1	0
41	R2	Cδ	13C	43.596	1	0
42	R2	Cζ	13C	159.164	3	0.037
43	A373	Cα	13C	55.874	2	0.1
44	A373	Cβ	13C	18.015	10	0.144
45	L374	Cα	13C	58.233	16	0.189
46	L374	Cβ	13C	41.535	4	0.423
47	L374	Cδ	13C	23.551	2	0.01
48	L374	Cγ	13C	27.051	6	0.16
49	I375	Cα	13C	65.55	4	0.207
50	I375	Cβ	13C	38.132	5	0.359
51	I375	Cδ	13C	13.98	3	0.018
52	I375	Cγ2	13C	17.67	4	0.147
53	G378	Cα	13C	47.112	1	0
54	G378	C’	13C	174.684	1	0
55	G379	Cα	13C	47.733	9	0.207
56	G379	C’	13C	175.299	1	0
57	G379	N	15N	109.193	2	0.207
58	V380	Cα	13C	67.095	15	0.144
59	V380	Cβ	13C	31.404	5	0.287
60	V380	Cγ1	13C	23.744	1	0
61	V380	Cγ2	13C	22.116	3	0.202
62	A381	Cα	13C	56.05	23	0.296
63	A381	Cβ	13C	18.105	15	0.209
64	V381	Cγ1	13C	23.744	1	0

65	G382	Cα	13C	47.575	12	0.133
66	G382	N	15N	105.349	1	0
67	L385	Cα	13C	58.337	13	0.28
68	L385	Cβ	13C	42.114	1	0
69	F386	Cα	13C	62.335	4	0.163
70	F386	Cβ	13C	38.36	10	0.208
71	I387	C'	13C	177.462	1	0
72	G388	N	15N	107.616	2	0.147
73	L389	Cα	13C	57.533	1	0

3.4. Interaction of CD4(372-433) and Vpu in POPC bilayers

After the topologies of CD4(372-433) and Vpu in POPC bilayers were tested separately, unlabeled CD4(372-433) peptide and ^{13}C-, ^{15}N- labeled full-length Vpu protein were co-reconstituted into POPC bilayers using the same lyophilization method as described in section 2.1.2. The NMR signals deriving from the reconstituted Vpu in absence (Fig. 3.25A) and presence (Fig. 3.25.B) of CD4(372-433) were analyzed to see if there are spectral peaks that indicate interaction between CD4(372-433) and full-length Vpu in phospholipid bilayers. However, due to the ^{13}C, ^{15}N uniformly labeled scheme that gives rise to crowded peaks in the PDSD-RR spectra of Vpu samples and the dominant NMR signals of the transmembrane part of Vpu, no significant difference was observed in the aliphatic carbon regions of the PDSD-RR spectra (Fig. 3.25).

There are significant differences in the carbonyl regions of Fig. 3.25, which is the appearance of the delta carbons from glutamic amino acids (Fig. 3.25.B, rectangle 1). However, the data from current work is not statistically enough to claim whether the delta carbon (GluCδ) signals are involved in the interaction between Vpu and CD4(372-433) in POPC bilayers. Besides, the rehydration level that was used in the lyophilization method to prepare proteoliposome as presented in section 2.1.2 might also effect to the mobility of the cytoplasmic part and therefore to the appearance of GluCδ signals. The GluCδ signals appear at the rehydration level of 18% (Fig.3.25.B, rectangle 1) but disappear at the rehydration level of 0% (Fig. 3.26, rectangle 1). It

seems there is a correlation between the appearance of GluCδ signals and the rehydration level. However, the correlation between the appearance of GluCδ signals and the rehydration level of 18% was tested once in this work. The data is not statistically enough to confirm if the appearance of GluCδ signals only depends on the rehydration level. Furthermore, the interaction between the Vpu cytoplasmic part and POPC bilayers was not yet tested in this work.

Taken together, effects of rehydration levels and interaction of Vpu cytoplasmic part to POPC bilayers on the Vpu cytoplasmic part also need to be taken into account together in studies of interaction between CD4 and Vpu.

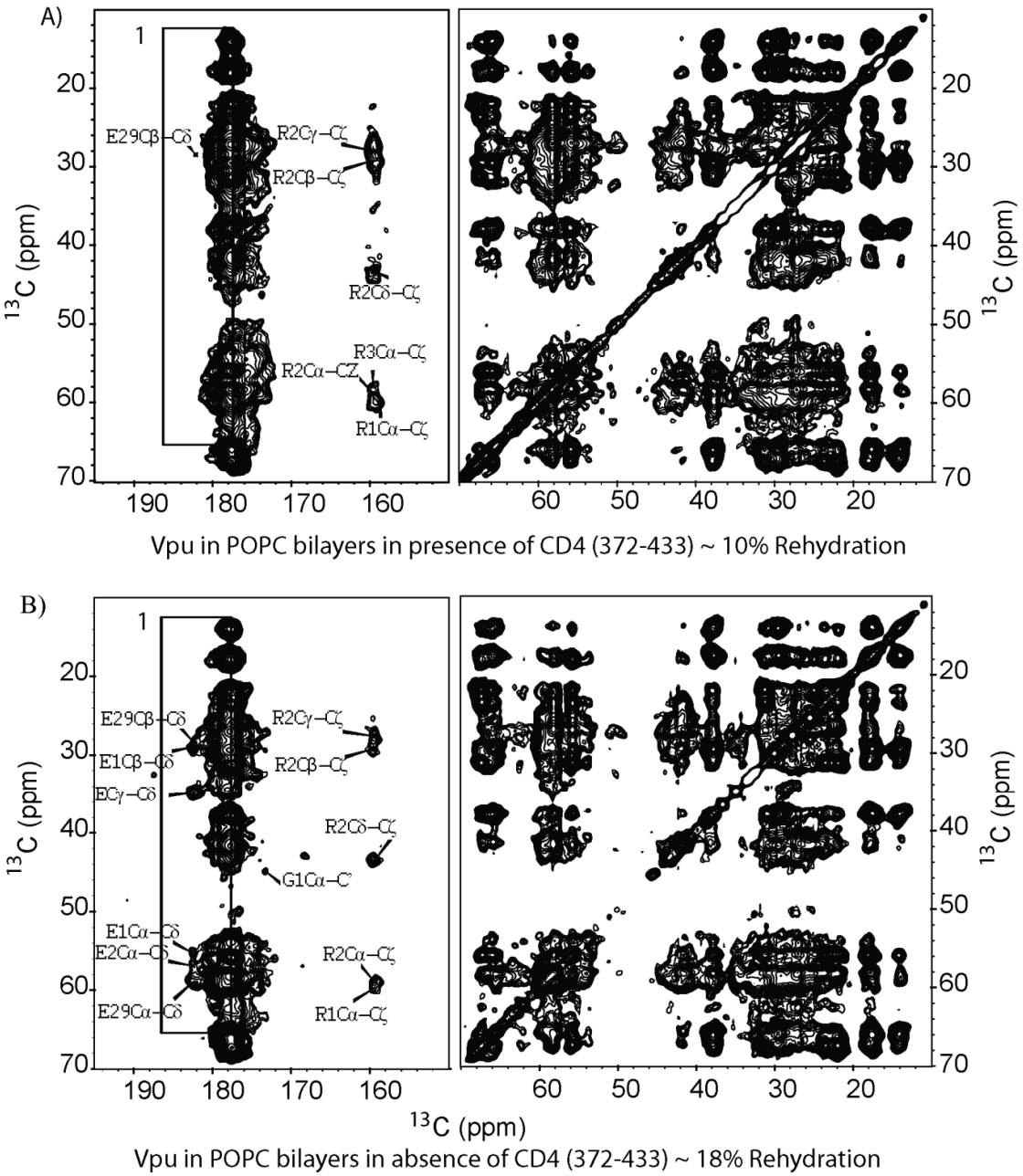

Fig. 3.25. 2D ^{13}C -^{13}C correlation PDSD-RR spectra of the uniformly labeled ^{13}C, ^{15}N full-length Vpu protein in POPC lipid bilayers. A) The Vpu sample was reconstituted into the bilayers in presence of CD4(372-433) with the rehydration degree of 10%. B) The Vpu sample was reconstituted into the bilayers in absence of CD4(372-433) with the rehydration degree of 18%. Each spectrum with 3 mg of the Vpu protein was acquired at 800 MHz ^{1}H Larmor frequency with a spinning speed of 12500 Hz, 160 scans and 300 ms of mixing time. The experiment was conducted around 0°C (the temperature of the sample). The data were processed using Lorentzian-to-Gaussian apodization function with 100 Hz of Lorentzian line sharpening, 200 Hz of Gaussian line broadening prior to Fourier transform.

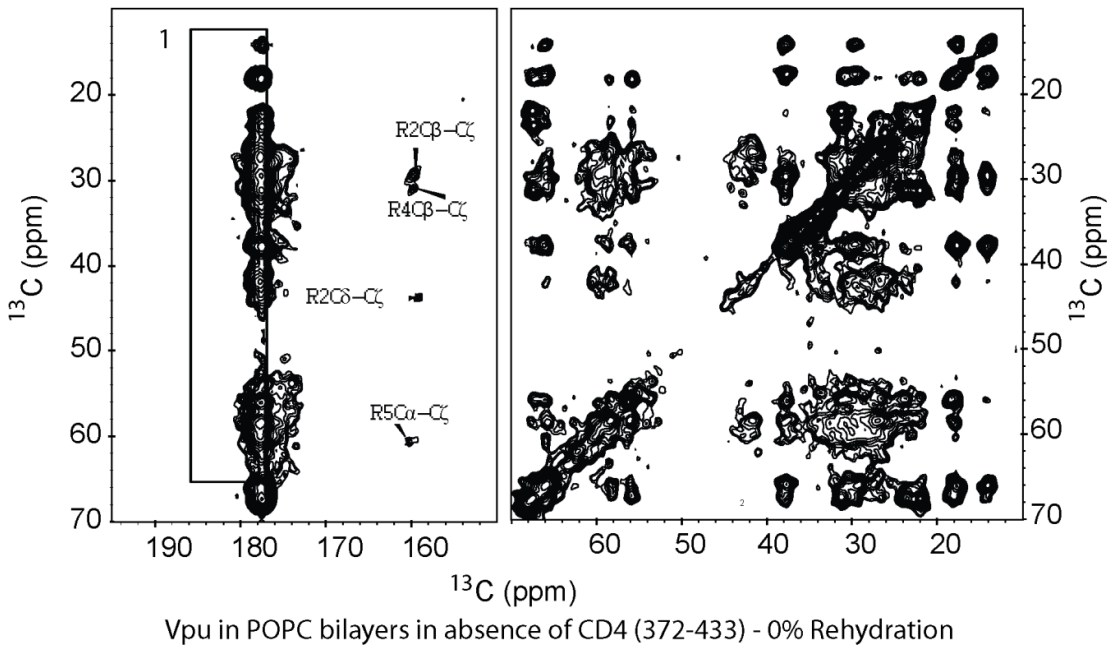

Fig. 3.26. 2D ^{13}C -^{13}C correlation PDSD-RR spectra of the uniformly labeled ^{13}C, ^{15}N full-length Vpu protein in POPC bilayers with 3 mg of the Vpu protein. The spectrum was acquired at 800 MHz ^{1}H Larmor frequency with a spinning speed of 12500 Hz, 160 scans and 300 ms of mixing time. The experiment was conducted around 0°C (the temperature of the sample). The data were processed using Lorentzian-to-Gaussian apodization function with 100 Hz of Lorentzian line sharpening, 200 Hz of Gaussian line broadening prior to Fourier transform.

References

1. Pines, A., Gibby, M.G. & Waugh, J.S. Proton-Enhanced Nmr of Dilute Spins in Solids. *Journal of Chemical Physics* **59**, 569-590 (1973).
2. Hartmann, S.R. & Hahn, E.L. Nuclear Double Resonance in Rotating Frame. *Physical Review* **128**, 2042-& (1962).
3. Morris, G.A. & Freeman, R. Enhancement of Nuclear Magnetic-Resonance Signals by Polarization Transfer. *Journal of the American Chemical Society* **101**, 760-762 (1979).
4. Burum, D.P. & Ernst, R.R. Net Polarization Transfer Via a J-Ordered State for Signal Enhancement of Low-Sensitivity Nuclei. *Journal of Magnetic Resonance* **39**, 163-168 (1980).
5. Grice, A.L., Kerr, I.D. & Sansom, M.S.P. Ion channels formed by HIV-1 Vpu: A modelling and simulation study. *Febs Letters* **405**, 299-304 (1997).
6. Moore, P.B., Zhong, Q.F., Husslein, T. & Klein, M.L. Simulation of the HIV-1 Vpu transmembrane domain as a pentameric bundle. *Febs Letters* **431**, 143-148 (1998).
7. Chengmayer, C., Quiroga, M., Tung, J.W., Dina, D. & Levy, J.A. Viral determinants of human-immunodeficiency-virus type-1 T-cell or macrophage tropism, cytopathogenicity, and CD4 antigen modulation. *Journal of Virology* **64**, 4390-4398 (1990).
8. Wittlich, M., Koenig, B.W., Hoffinann, S. & Willbold, D. Structural characterization of the transmembrane and cytoplasmic domains of human CD4. *Biochimica Et Biophysica Acta-Biomembranes* **1768**, 2949-2960 (2007).
9. Wittlich, M., Thiagarajan, P., Koenig, B.W., Hartmann, R. & Willbold, D. NMR structure of the transmembrane and cytoplasmic domains of human CD4 in micelles. *Biochim Biophys Acta* **1798**, 122-7 (2010).
10. Wittlich, M., Koenig, B.W., Stoldt, M., Schmidt, H. & Willbold, D. NMR structural characterization of HIV-1 virus protein U cytoplasmic domain in the presence of dodecylphosphatidylcholine micelles. *Febs Journal* **276**, 6560-6575 (2009).
11. Baldus, M., Petkova, A.T., Herzfeld, J. & Griffin, R.G. Cross polarization in the tilted frame: assignment and spectral simplification in heteronuclear spin systems. *Molecular Physics* **95**, 1197-1207 (1998).
12. vanRossum, B.J., Forster, H. & deGroot, H.J.M. High-field and high-speed CP-MAS C-13 NMR heteronuclear dipolar-correlation spectroscopy of solids with frequency-switched Lee-Goldburg homonuclear decoupling. *Journal of Magnetic Resonance* **124**, 516-519 (1997).
13. Wittlich, M., Wiesehan, K., Koenig, B.W. & Willbold, D. Expression, purification, and membrane reconstitution of a CD4 fragment comprising the transmembrane and cytoplasmic domains of the receptor. *Protein Expression and Purification* **55**, 198-207 (2007).

Chapter 4. Discussion and Conclusions

The mobility, topology and conformation of full-length Vpu and CD4(372-433) in POPC lipid bilayers were explored with the aid of solid-state NMR spectroscopy. The findings suggest that: (i) the cytoplasmic parts of Vpu and CD4(372-433) in POPC lipid bilayers are mobile and the Vpu cytoplasmic part is located in the proximity of the water region; (ii) the transmembrane parts of the reconstituted proteins are inserted in POPC lipid bilayers in which the reconstituted Vpu forms a pore-like structure with water accessibility; (iii) Vpu and CD4(372-433) in POPC bilayers adopt a well-folded conformation in which the transmembrane part of the CD4(372-433) and the identified amino acids Val, Ala, Ile which are major component of the transmembrane part of Vpu have an alpha helical structure; (iv) the cytoplasmic part of Vpu is indicative of conformational disorder.

4.1. Mobility of the reconstituted proteins and the effects of reconstitution methods

The missing signals deriving from the amino acids Thr, Ser, Asp, Lys, Gln, and Glu (Fig. 3.1.C and Fig. 3.2) are indicative of mobility in the cytoplasmic part of the reconstituted Vpu. This mobility was observed again via the enhancement of the NMR signals deriving from GCα, DCγ, SCα, SCβ (Fig.3.14) and the amorphous regions (the ovals 3 and 4 in Fig. 3.16) when cooling the sample below the freezing point. The mobility was also seen via the enhancement of the non- specific ^{13}C shifts deriving from the cytoplasmic part of CD4(372-433) in POPC bilayers when cooling the sample in the DQ/SQ experiment (Fig. 3.22).

The finding of the mobility on the atomic level in the cytoplasmic part of Vpu in POPC bilayers contributes additional information to the understanding of the dynamics of this protein in the lipid environment. There is evidence of a modification of the activity of proteins[1-3] in the bilayers and the dynamics complex assembly[4] by the lipid environment. Thus, understanding the mobility of Vpu in POPC bilayers in the current work is very useful for future studies, specifically the studies of interaction between Vpu and its partners.

In addition to the observation of mobility, the appearance of NMR signals in spectra was shown to be strongly affected by the preparation of the reconstituted proteins. In one preparation of CD4(372-433) that was prepared by centrifugation instead of lyophilization followed by rehydration, many protein signals are missing (Fig. 3.3, red). This finding may be caused by a loss of sample or an increased mobility due to a higher hydration level of the sample, which may lead to an increased mobility of the protein.

Thus, these results are the helpful guidance for future investigations when choosing the pulse schemes and preparing lipid models using POPC lipids to study CD4, Vpu, and other integral membrane proteins.

4.2. Vpu in POPC bilayers with and without presence of CD4(372-433)

The analysis of NMR signals deriving from Vpu in POPC bilayers with and without presence of CD4(372-433) were performed to get insight into the binding interface of Vpu-CD4(372-433) interaction on Vpu amino acid sequence. However, NMR peaks in the ^{13}C-^{13}C correlation spectra recorded from the Vpu proteoliposomes were overlapped and most of the peaks in the spectra recorded above the freezing point can be assigned to the transmembrane domain of Vpu. This obscures the search for NMR signals involved in Vpu-CD4(372-433) interaction. No significant difference was found in the aliphatic carbon regions of Vpu samples with and without presence of CD4(372-433) (Fig. 3.25).

The crowded spectra with the dominant signals deriving from the Vpu transmembrane domain would be reduced by replacing the labeling scheme for Vpu and CD4(372-433). For example, instead of using uniformly ^{13}C, ^{15}N glucose as in this work, 1-^{13}C glucose and 2-^{13}C glucose may be used to label Vpu and CD4(372-433), respectively. This labeling scheme may help not only to reduce the overlapping signals from the Vpu TM domain but also to increase the ability to identify binding interfaces of Vpu-CD4(372-433) interaction in both Vpu and CD4(372-433) amino acid sequences.

The significant difference found between spectra of Vpu reconstituted in presence of CD4(372-433) and the Vpu reconstituted in absence of CD4(372-433) is the

missing of GluCδ in the reconstituted Vpu in presence of CD4(372-433). However, this observation may attributed to a difference in the hydration levels of the samples or the interaction of the Vpu cytoplasmic domain with POPC lipid.

As mentioned before, full-length Vpu(1-81) is known to have two amphipathic alpha helical fragments in the cytoplasmic domain[5,6]. The first amphipathic alpha helical fragment includes residues from 39 to 50, whereas the second consists of residues from 60 to 70 (Fig. 1.2.A). Except for Glu29, other Glu residues are mainly located in the loop that contains the phosphorylation sites (Ser53 and Ser57) and in the second amphipathic alpha helical fragment such as Glu48, Glu51, Glu56, Glu58, Glu62, Glu63 and Glu69. Thus, the changes of GluCδ observed in this work suggest some structural changes of the cytoplasmic part of Vpu in POPC bilayers. The changes might be caused by the binding between Vpu and CD4(372-433) as mentioned in previous studies. It was indicated that the folding of the cytoplasmic part of Vpu depends on the membrane-like environment[10,11] and that the folding of Vpu cytoplasmic part might be important for interaction between Vpu and CD4[7]. A synthetic Vpu peptide comprising the cytoplasmic domain from residues 32 to 81[8] forms an alpha helical structure in the aqueous solution only when trifluorethanol that mimics a membrane-like environment is present[8,9]. This synthetic peptide was not found to bind to CD4 in an in vitro assay, while other Vpu cytoplasmic domain ($Vpu_{2/6}$) that forms amphipathic alpha-helical structure could still bind to CD4[7].

Together with these previous findings, the above questions rising from the findings of the GluCδ signals in this work recommends further experiments which focus on the structural changes of the Vpu cytoplasmic domain in POPC bilayers and the ability of Vpu to bind to CD4.

4.3. Topology of Vpu and CD4(372-433) in POPC lipid bilayers

The topology of the reconstituted Vpu and CD4(372-433) were determined and analyzed as shown in Section 3.2.1 and Section 3.2.2, respectively. In both cases, residues Val and Ile, which are mainly located in the transmembrane domains of Vpu and CD4, were found predominantly in the lipid side-chain planes of the 3D data set. Furthermore, the ^{13}C signals from Gly residues, which are located mainly in the CD4

transmembrane part (Fig.1.1.C), were found primarily receiving the ^{1}H magnetization from the lipid side-chain source (Fig. 3.9). Taken together, the transmembrane parts of the reconstituted proteins Vpu and CD4 are inserted into the lipid side-chain region.

The residues Glu and Lys, which are located only in the cytoplasmic part of the Vpu primary structure (Fig.1.2.A), were found in the water plane but not in the lipid side-chain plane (Fig. 3.8). This suggests that the cytoplasmic part of the reconstituted Vpu is in close contact with the water interface.

The comparison of the number of the ^{13}C cross-peaks in the lipid side-chain planes (Fig.3.8.C&D) with the number of the peaks in the water interface (Fig.3.8.A) reveals that the Vpu protein part that is inserted in the lipid bilayers has a higher degree of rigidity than the Vpu protein part in the proximity of the water interface. In addition, the observation of the very similar configuration of residue type Val in both of the water and lipid planes (Fig. 3.8.A,C,&D) indicates that these signals may originate from the identical set of amino acids. Similar phenomena were found for amino acid types Ala and Ile. Because most of the residues Val, Ala, Ile are belong to the transmembrane part in the Vpu primary structure, it is likely that these Val, Ala, and Ile reside in the Vpu TM part of the reconstituted Vpu.

If the TM helices of a membrane-reconstituted protein are in close proximity to the inner part of the lipid as well as to the water, this finding can best be explained by a formation of a water-permeable pore of VpU.

Taken together, these findings of the Vpu TM part in POPC bilayers suggest the existence of a pore-like structure which is water permeable.

As introduced in section 1.1.2, the transmembrane part of Vpu is responsible for the budding of new virions from infected cells. When analyzing this biological function of Vpu, several previous studies and reviews postulated that Vpu could function as an ion channel[10-12]. This postulate was then demonstrated by experimental evidences and the conclusion is that Vpu forms an ion channel in lipid bilayers[13,14,15,16]. The formation of the ion channel is attributed by association of alpha helical transmembrane segments into homo-oligomeric bundles in which ions pass through the central pore of the helix bundle[6,17,18,19].

Thus, the finding of the pore-like structure with the water accessibility in the current work provides additionally experimental evidence for the existence of the channel in transmembrane part of Vpu in the lipid bilayers.

In case of CD4, the surrounding of the cytoplasmic part by water is not as clear as in the case of the Vpu even certain Leu signals were found in the water plane. It is possible that the mobility of the cytoplasmic part (Fig. 3.22 and Fig. B7) results in the missing of this part in the 3D water-edited experiment (Fig. 3.10.A).

The Leu residues of the reconstituted CD4 were also found to have similar conformation in both of the lipid side-chain and the water planes. However, there is no pore-like structure formed in this case because the signals from residue types Val and Ile, which are main component of the transmembrane part of CD4 primary structure, were not found above the noise level in the water plane. This evidence also supports the finding of the pore-like structure in the reconstituted Vpu.

4.4. Resonance assignments of the reconstituted proteins

In both cases of the reconstituted Vpu and CD4(372-433), prominent intra-residue and inter-residue cross-peaks were found and assigned to the amino acids in the transmembrane domains of the primary structures. The analysis of secondary chemical shift shows that the detected residues indicate alpha helical structure (Fig. 3.15, 3.23, 3.24). In the case of CD4(372-433), the amino acid site-specific assignment was achievable for most of the residues in the transembrane part, whereas the assignment of the reconstituted Vpu is only amino acid type-specific. This finding thus shows the well-folded conformation in both of the reconstituted Vpu and CD4(372-433). The well-folded conformation is also accountable for the higher degree of rigidity in the Vpu transmembrane part compared with its cytoplasmic part in the results of the water-edited experiments (section 3.2.1).

The finding of the alpha helical structure in the identified amino acids deriving from the transmembrane part of the reconstituted Vpu is consistent with previous studies on Vpu(1-40)[20] and Vpu(2-30+)[21]. These previous studies confirms that the transmembrane part of Vpu possess alpha-helical structure. Similar agreement was

also found for the CD4(372-433): the alpha helical structure was reported for a CD4(372-433) in aqueous solution[22] and micelles[23].

The cytoplasmic part of Vpu contains the identified amino acids with different secondary structures (Fig. 3.15). This shows a conformational disorder in the cytoplasmic part of the reconstituted Vpu. In contrast, the identified amino acids of the cytoplasmic part of CD4 only show alpha helical structures for residues Arg and Ser (Fig 3.24). This information is insufficient to claim that the cytoplasmic part CD4 is completely disordered. In addition, the major parts of the cytoplasmic parts in both reconstituted proteins were not able to be assigned due to the missing signals that were caused by the mobility in these parts.

The assignment in the current work was performed on the uniformly labeled ^{13}C, ^{15}N proteins. The results clearly show that with this labeling scheme, it is impossible to get NMR constraints for determining 3D structures. It is possible that the strong mobility in the cytoplasmic parts and the oligomerization of Vpu in the transmembrane part cause the difficulties in the assignment. For the future work, other pulse schemes rather than the PDSD-RR and the DQ-SPC5 (for example PARIS-xy[24], DARR[25] with higher spinning speeds- more than 20kHz), lower temperature (-40°, -50°C) and different composition of lipid environment (rather than using only POPC) should be used to handle the mobility and obtain additional information of the structure of the cytoplasmic parts.

References

1. van der Does, C., Swaving, J., van Klompenburg, W. & Driessen, A.J.M. Non-bilayer lipids stimulate the activity of the reconstituted bacterial protein translocase. *Journal of Biological Chemistry* **275**, 2472-2478 (2000).
2. Bogdanov, M. & Dowhan, W. Phospholipid-assisted protein folding: phosphatidylethanolamine is required at a late step of the conformational maturation of the polytopic membrane protein lactose permease. *Embo Journal* **17**, 5255-5264 (1998).
3. de Leeuw, E., Kaat, K.T., Moser, C., Menestrina, G., Demel, R., de Kruijff, B., Oudega, B., Luirink, J. & Sinning, I. Anionic phospholipids are involved in membrane association of FtsY and stimulate its GTPase activity. *Embo Journal* **19**, 531-541 (2000).
4. Helms, V. Attraction within the membrane - Forces behind transmembrane protein folding and supramolecular complex assembly. *Embo Reports* **3**, 1133-1138 (2002).
5. Willbold, D., Hoffmann, S. & Rosch, P. Secondary structure and tertiary fold of the human immunodeficiency virus protein U (Vpu) cytoplasmic domain in solution. *European Journal of Biochemistry* **245**, 581-588 (1997).
6. Wittlich, M., Koenig, B.W., Stoldt, M., Schmidt, H. & Willbold, D. NMR structural characterization of HIV-1 virus protein U cytoplasmic domain in the presence of dodecylphosphatidylcholine micelles. *Febs Journal* **276**, 6560-6575 (2009).
7. Bour, S., Schubert, U. & Strebel, K. The human-immunodeficiency-virus type-1 Vpu protein specifically binds to the cytoplasmic domain of CD4 - implications for the mechanism of degradation. *Journal of Virology* **69**, 1510-1520 (1995).
8. Henklein, P., Schubert, U., Kunert, O., Klabunde, S., Wray, V., Kloppel, K.D., Kiess, M., Portsmann, T. & Schomburg, D. Synthesis and characterization of the hydrophilic C-terminal domain of the human immunodeficiency virus type 1-encoded virus protein U (Vpu). *Pept Res* **6**, 79-87 (1993).
9. Wray, V., Kinder, R., Federau, T., Henklein, P., Bechinger, B. & Schubert, U. Solution structure and orientation of the transmembrane anchor domain of the HTV-1-encoded virus protein U by high-resolution and solid-state NMR spectroscopy. *Biochemistry* **38**, 5272-5282 (1999).
10. Willey, R.L., Maldarelli, F., Martin, M.A. & Strebel, K. Human immunodeficiency virus type-1 Vpu protein regulates the formation of intracellular gp160-CD4 complexes. *Journal of Virology* **66**, 226-234 (1992).
11. Schubert, U., Henklein, P., Boldyreff, B., Wingender, E., Strebel, K. & Porstmann, T. The human immunodeficiency virus type 1 encoded Vpu protein is phosphorylated by casein kinase-2 (CK-2) at positions Ser52 and Ser56 within a predicted alpha-helix-turn-alpha-helix-motif. *J Mol Biol* **236**, 16-25 (1994).
12. Trono, D. HIV accessory proteins: leading roles for the supporting cast. *Cell* **82**, 189-92 (1995).

13. Ewart, G.D., Sutherland, T., Gage, P.W. & Cox, G.B. The Vpu protein of human immunodeficiency virus type 1 forms cation-selective ion channels. *Journal of Virology* **70**, 7108-7115 (1996).
14. Schubert, U., FerrerMontiel, A.V., OblattMontal, M., Henklein, P., Strebel, K. & Montal, M. Identification of an ion channel activity of the Vpu transmembrane domain and its involvement in the regulation of virus release from HIV-1-infected cells. *Febs Letters* **398**, 12-18 (1996).
15. Marassi, F.M., Ma, C., Gratkowski, H., Straus, S.K., Strebel, K., Oblatt-Montal, M., Montal, M. & Opella, S.J. Correlation of the structural and functional domains in the membrane protein Vpu from HIV-1. *Proceedings of the National Academy of Sciences of the United States of America* **96**, 14336-14341 (1999).
16. Ma, C., Marassi, F.M., Jones, D.H., Straus, S.K., Bour, S., Strebel, K., Schubert, U., Oblatt-Montal, M., Montal, M. & Opella, S.J. Expression, purification, and activities of full-length and truncated versions of the integral membrane protein Vpu from HIV-1. *Protein Science* **11**, 546-557 (2002).
17. Moore, P.B., Zhong, Q.F., Husslein, T. & Klein, M.L. Simulation of the HIV-1 Vpu transmembrane domain as a pentameric bundle. *Febs Letters* **431**, 143-148 (1998).
18. Grice, A.L., Kerr, I.D. & Sansom, M.S.P. Ion channels formed by HIV-1 Vpu: A modelling and simulation study. *Febs Letters* **405**, 299-304 (1997).
19. Cordes, F.S., Tustian, A.D., Sansom, M.S.P., Watts, A. & Fischer, W.B. Bundles consisting of extended transmembrane segments of Vpu from HIV-1: Computer simulations and conductance measurements. *Biochemistry* **41**, 7359-7365 (2002).
20. Sharpe, S., Yau, W.M. & Tycko, R. Structure and dynamics of the HIV-1 Vpu transmembrane domain revealed by solid-state NMR with magic-angle spinning. *Biochemistry* **45**, 918-933 (2006).
21. Park, S.H., Mrse, A.A., Nevzorov, A.A., Mesleh, M.F., Oblatt-Montal, M., Montal, M. & Opella, S.J. Three-dimensional structure of the channel-forming trans-membrane domain of virus protein "u" (Vpu) from HIV-1. *Journal of Molecular Biology* **333**, 409-424 (2003).
22. Wittlich, M., Koenig, B.W., Hoffinann, S. & Willbold, D. Structural characterization of the transmembrane and cytoplasmic domains of human CD4. *Biochimica Et Biophysica Acta-Biomembranes* **1768**, 2949-2960 (2007).
23. Wittlich, M., Thiagarajan, P., Koenig, B.W., Hartmann, R. & Willbold, D. NMR structure of the transmembrane and cytoplasmic domains of human CD4 in micelles. *Biochim Biophys Acta* **1798**, 122-7 (2010).
24. Weingarth, M., Bodenhausen, G. & Tekely, P. Broadband magnetization transfer using moderate radio-frequency fields for NMR with very high static fields and spinning speeds. *Chemical Physics Letters* **488**, 10-16 (2010).
25. Takegoshi, K., Nakamura, S. & Terao, T. C-13-H-1 dipolar-assisted rotational resonance in magic-angle spinning NMR. *Chemical Physics Letters* **344**, 631-637 (2001).

Appendix A

Pulse Sequences

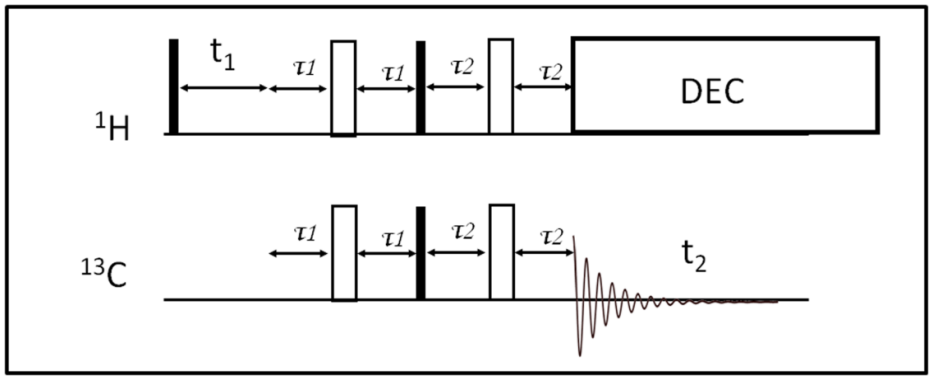

Fig. A1. Pulse sequence of INEPT experiment without proton spin diffusion block. The filled and empty rectangular boxes present 90° and 180° pulses, respectively. During the delays τ1, the anti-phase magnetization is generated under the effect of *J* coupling. In the end of this duration, the anti-phase magnetization from proton was transferred carbon via two 90° pulses. During the delays τ2 the anti-phase magnetization of ^{13}C spins evolves into an in-phase state that is observable and detected on the carbon channel. DEC is the decoupling which is used to remove the heteronuclear dipolar-dipolar coupling between proton and carbon. t_1 is the evolution time and t_2 is acquisition time.

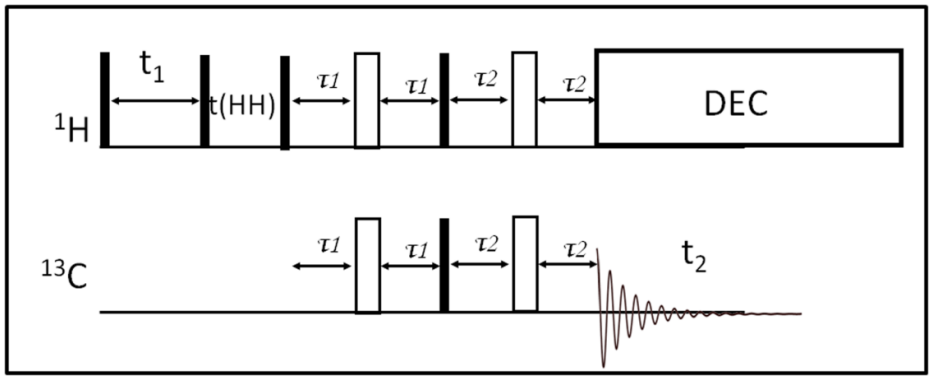

Fig. A2. Pulse sequence of INEPT experiment with proton spin diffusion block t(HH). The filled and empty rectangular boxes present 90°, 180° pulses, respectively. During the delays τ1, the anti-phase magnetization is generated under the effect of *J* coupling. In the end of this duration, the anti-phase magnetization from proton was transferred carbon via two 90° pulses. During the delays τ2, the anti-phase magnetization of ^{13}C spins evolves into an in-phase state which is observable and detected on the carbon channel. DEC is the decoupling which is used to remove the heteronuclear dipolar-dipolar coupling between proton and carbon. t_1 is the evolution time and t_2 is acquisition time.

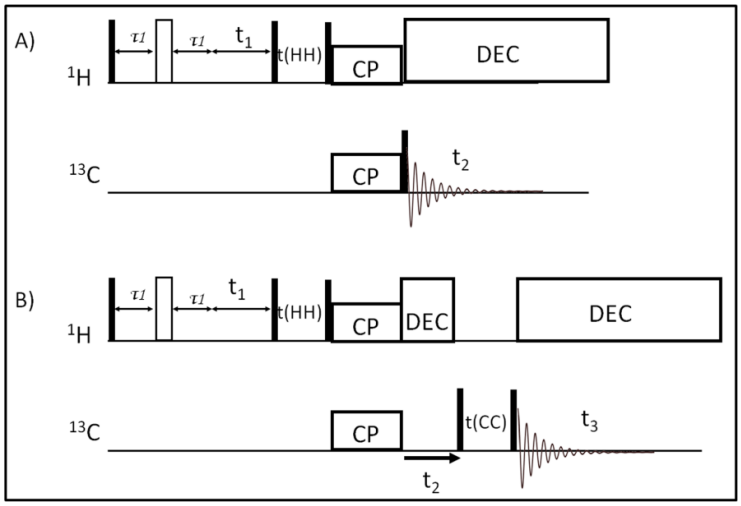

Fig. A3. The pulse schemes of water-edited solid-state NMR spectroscopy. The filled and empty rectangular boxes present 90°, 180° pulses, respectively. τ1 is the delay. t(HH) is proton spin diffusion period. CP is the cross polarization technique (section 1.2.2). A) Pulse sequence is used to record 2D ^{1}H -^{13}C correlation spectra. t_1 and t_2 show evolution and acquisition times. B) Pulse sequence is used to record 3D ^{1}H -^{13}C -^{13}C spectra. t(CC) is the carbon-carbon mixing period. t_1 and t_2 show evolution times of ^{1}H and ^{13}C, respectively. t_3 show the acquisition time.

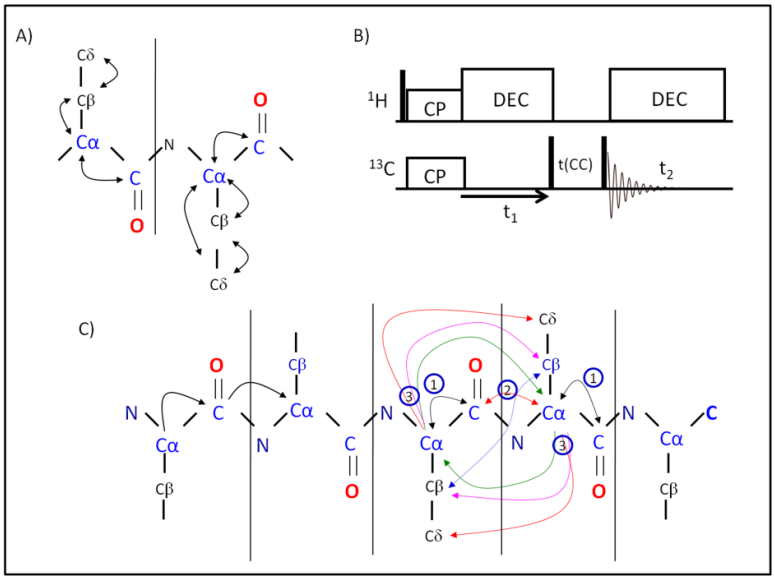

Fig. A4. A) The magnetization transfer pathway at short carbon-carbon mixing times (t(CC) in range of 10 ms -50 ms), which gives rise to intra-residue cross peaks in MAS solid-state NMR spectra. B) Pulse sequence of PDSD-RR technique. CP means cross polarization (section 1.2.2). The black bars indicate the 90° pulses. DEC is SPINAL decoupling technique (as introduced in section 1.2.3 and section 2.2.1). t(CC) is the carbon-carbon mixing time. C) Pathway 1: polarization transfer among C'-Cα of the same amino acid. Pathway 2: the weak inter-residue coupling mediates the polarization transfer between C'-Cα of consecutive amino acids. Pathway 3 happens at long mixing time (in range of 50 ms -300 ms or more) and gives rise to the inter-residue cross peaks in NMR spectra. The magnetization transfer pathways were depicted in absence of ^{1}H spins.

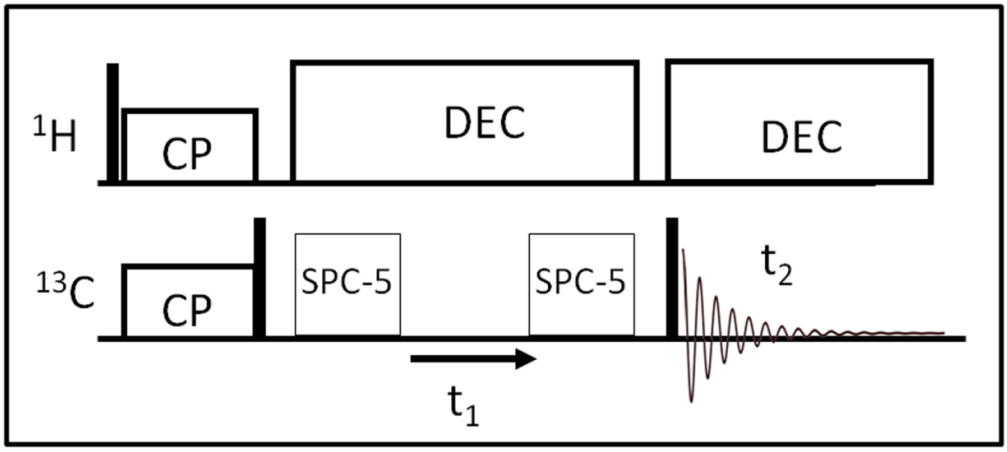

Fig. A5. Pulse sequence of double quantum SPC5 experiment. The black bars indicate the 90° pulses. SPC-5 means the double quantum filter SPC5 technique. t_1 and t_2 shows the evolution and acquisition times, respectively. After Fouriour transformation, data collected during t1 are presented in DQ dimension of DQ/SQ spectrum.

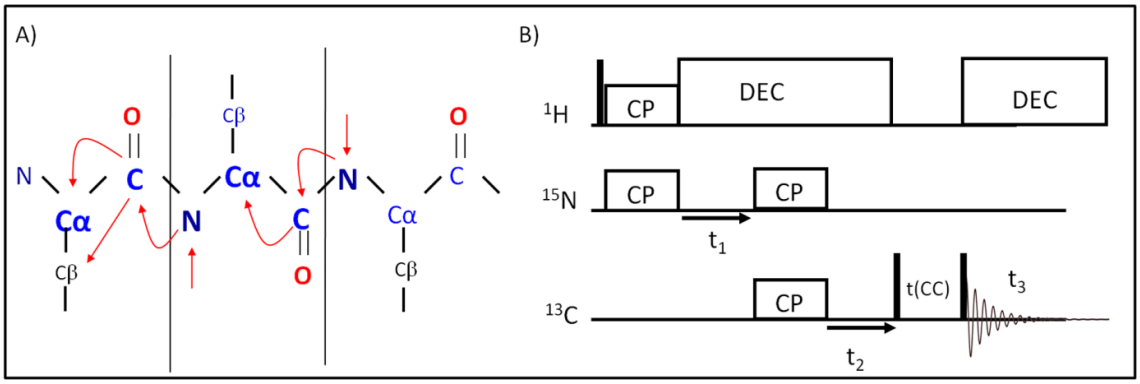

Fig. A6. Pulse sequence of sequential link NCOCX experiment. A) Polarization transfer pathway with CC mixing time t(CC) in the pulse scheme (B) shorter than 70ms. The black bars indicate the 90° pulses. CP means the cross-polarization technique. DEC means the decoupling. t_1, t_2 and t_3 show evolution and acquisition times. t2 = 0 in a 2 dimensional experiment.

Appendix B

Additional figures from the experimental results

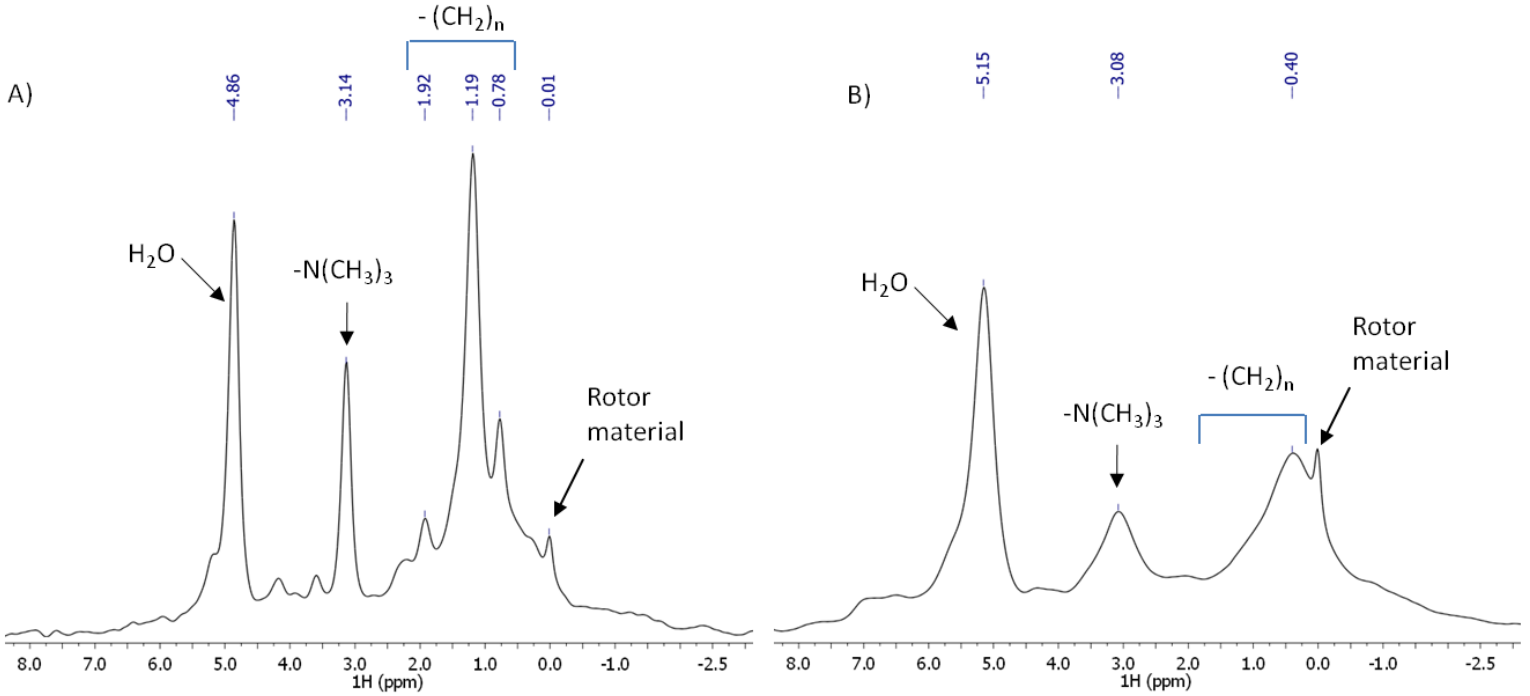

Fig. B1. Lipid signals at above (A) and below (B) the gel to liquid phase transition. (at the temperatures from -3°C to -15°C).–N–$(CH_2)_3$ shows shifts of ^{1}H atoms in the methyl group at the head of POPC. –(CH_2)n– presents shifts of ^{1}H which reside in the side-chain of POPC.

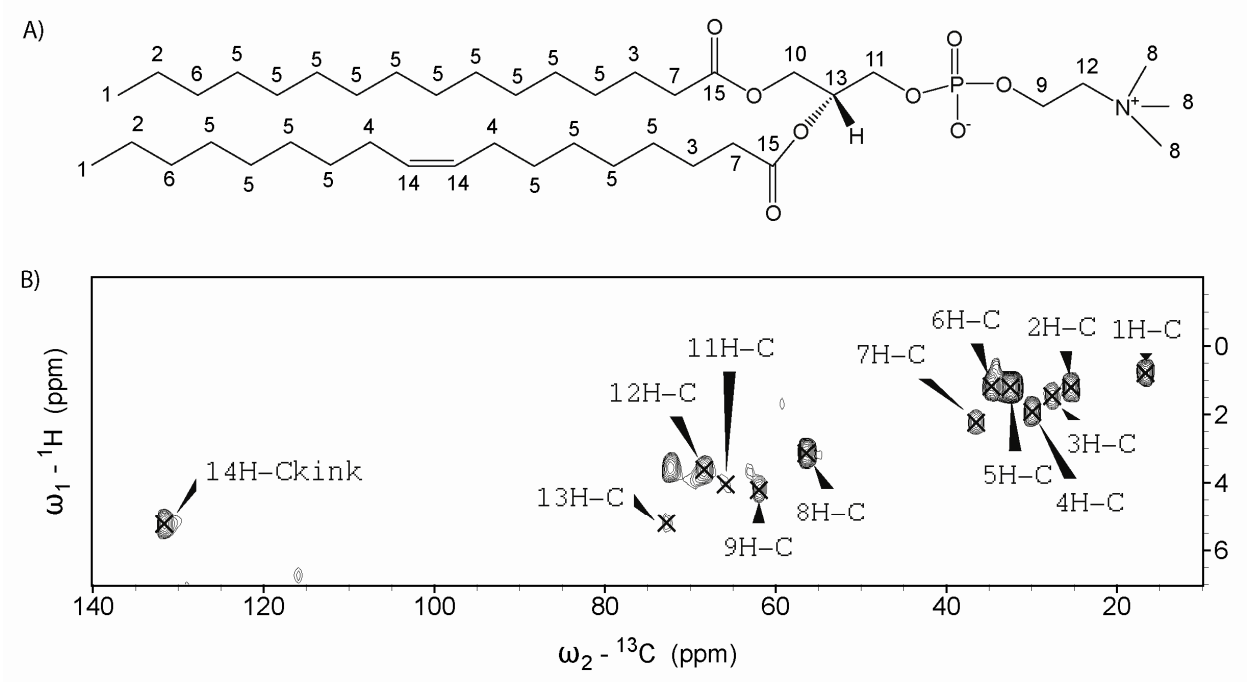

Fig. B2. Structure of POPC lipid from Atvanti Polar Lipids, Inc (A) and and INEPT 2D 1H-13C correlation spectrum of the POPC lipid. The spectrum was acquired at 600 MHz ^{1}H frequency with spinning speed of 9375 Hz, 128 scans. The experiment was conducted above the gel to liquid phase transition temperature of the POPC lipid. The pulse scheme is presented in Fig. A4.

Table B1: Chemical shifts of POPC lipid (POPC structure in Fig. B3)

Assignment	1H-C	2H-C	3H-C	4H-C	5H-C	6H-C	7H-C	8H-C	9H-C	11H-C	12H-H	13H-C	14H-C
^{1}H (ppm)	0.79	1.21	1.46	1.92	1.21	1.18	2.23	3.14	4.20	4.05	3.62	5.20	5.23
^{13}C (ppm)	16.65	25.39	27.60	29.93	32.49	34.68	36.51	56.39	61.93	65.84	68.38	72.75	131.63

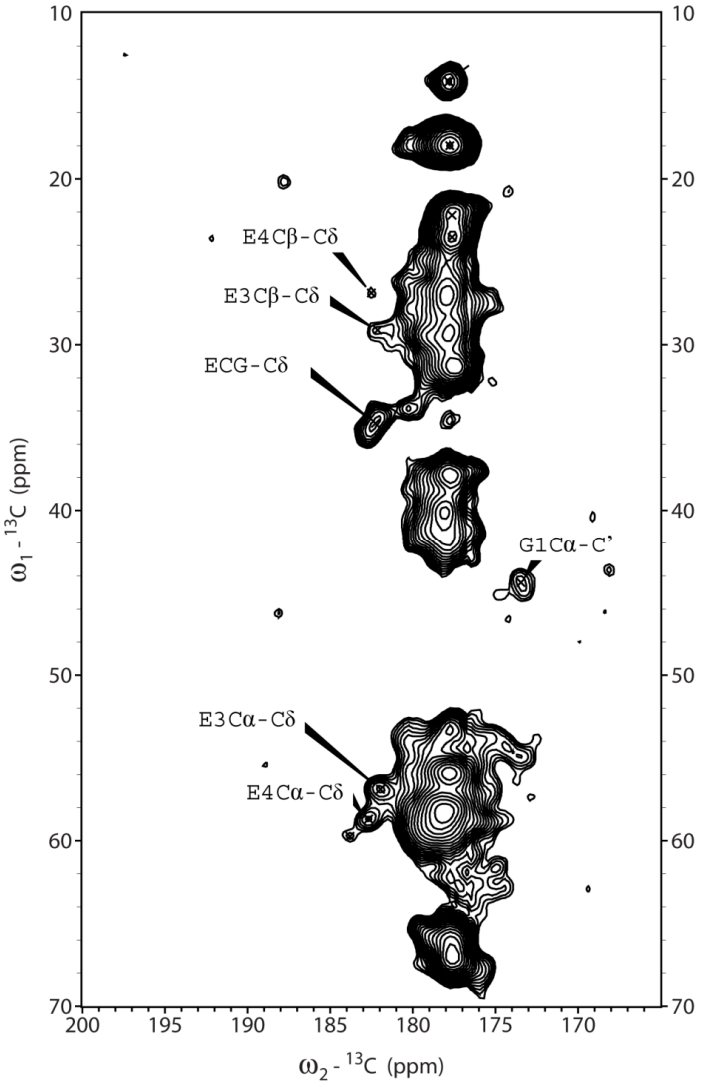

Fig. B3. Carbonyl region of 2D ^{13}C -^{13}C correlation PDSD-RR spectrum of the uniformly labeled ^{13}C, ^{15}N full-length Vpu protein in POPC bilayers. The spectrum was acquired at 800 MHz ^{1}H frequency with a spinning speed of 12500 Hz, 160 scans. The ^{13}C mixing time is 300 ms. The evolution time of ^{13}C equals 4.5 ms. The experiment was conducted around 0°C (the sample temperature). Data were processed using Lorentzian-to-Gaussian apodization function with 100 Hz of Lorentzian line sharpening, 200 Hz of Gaussian line broadening prior to Fourier transform.

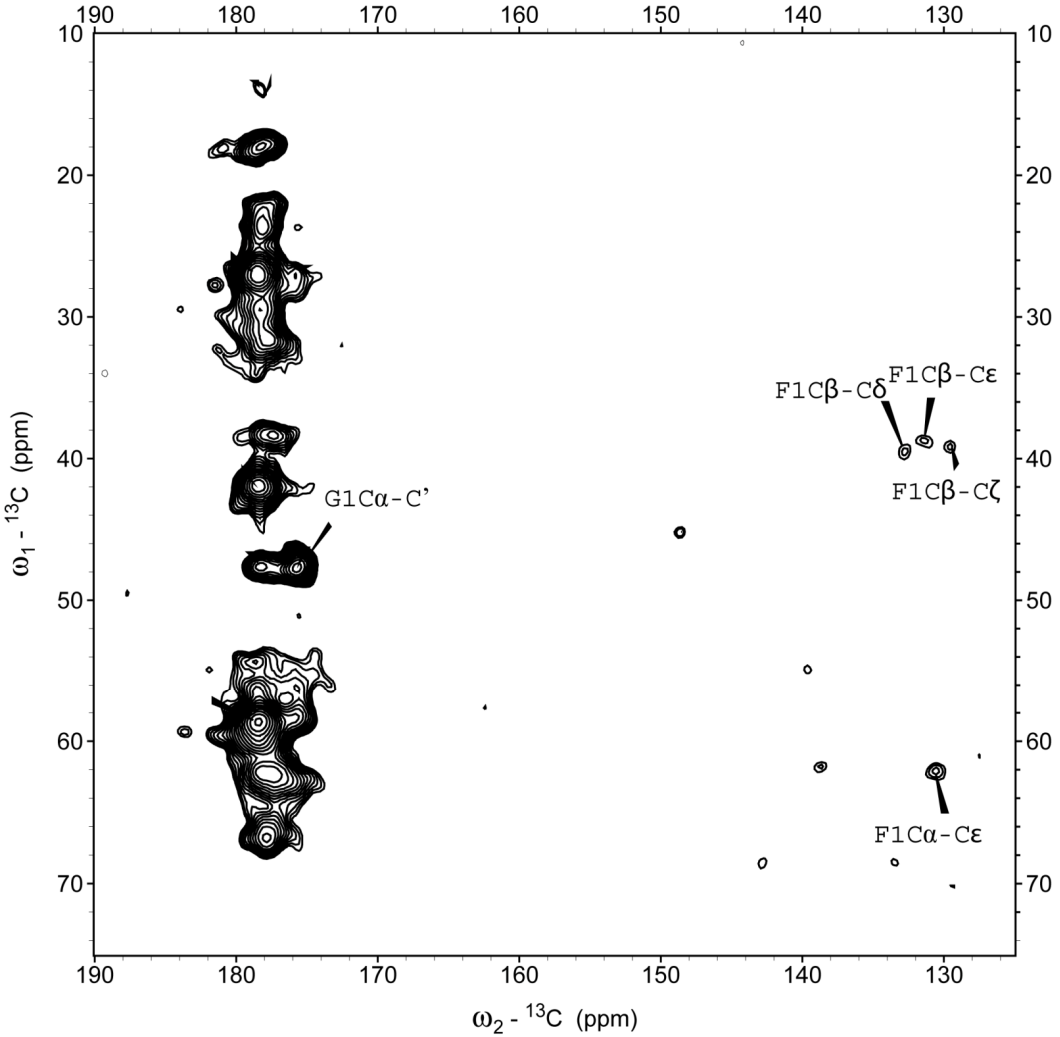

Fig. B4. Carbonyl and aromatic carbon regions of 2D ^{13}C-^{13}C correlation PDSD-RR spectrum of the uniformly labeled CD4(372-433) in POPC bilayers. The spectrum was acquired at 600 MHz ^{1}H frequency with spinning speed of 9375 Hz, 160 scans. The ^{13}C mixing time is 50 ms.

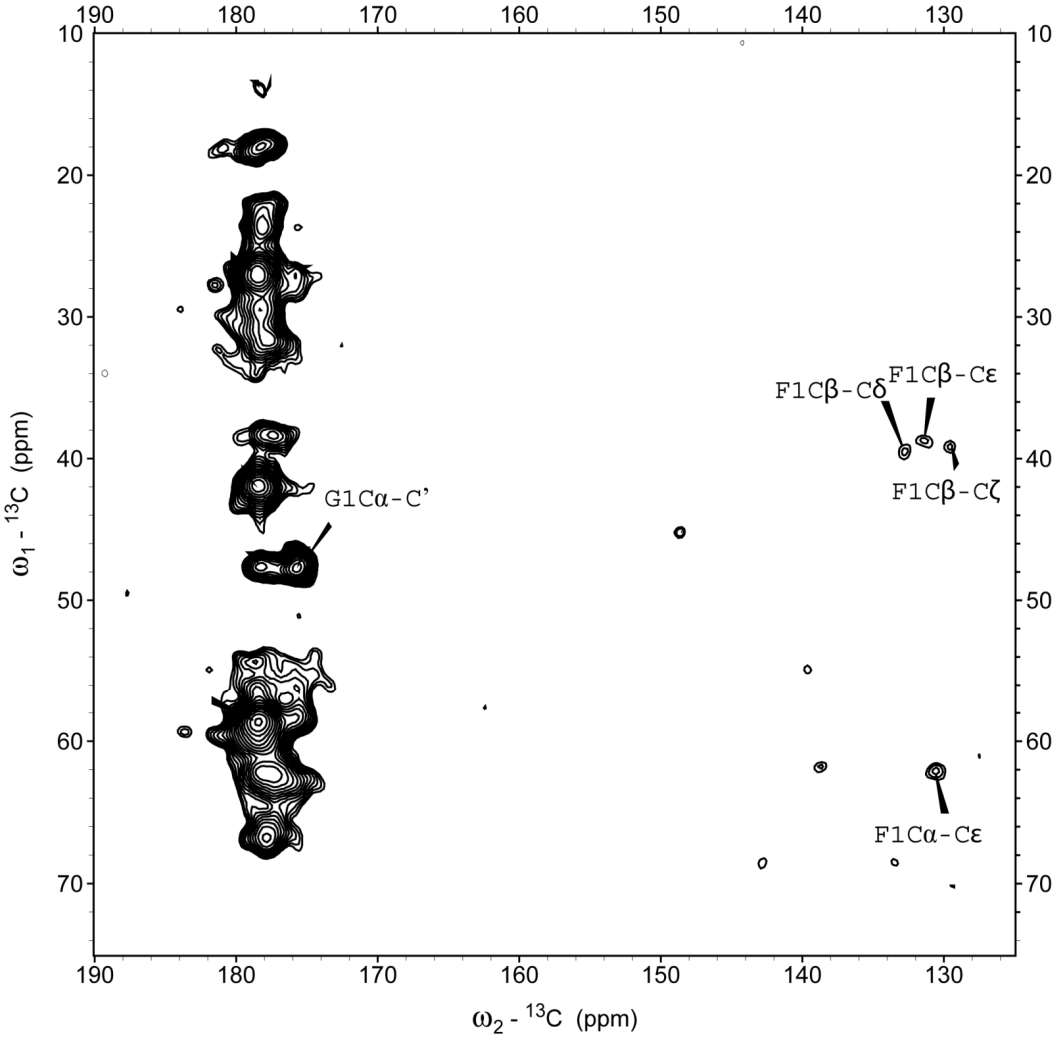

Fig. B5. A CO region of 2D ^{13}C-^{13}C correlation PDSD-RR spectrum of the uniformly labeled ^{13}C, ^{15}N CD4(372-433) peptide in POPC bilayers. The spectrum was acquired at 800 MHz ^{1}H frequency with spinning speed of 12500 Hz, 288 scans. The ^{13}C is 200 ms.

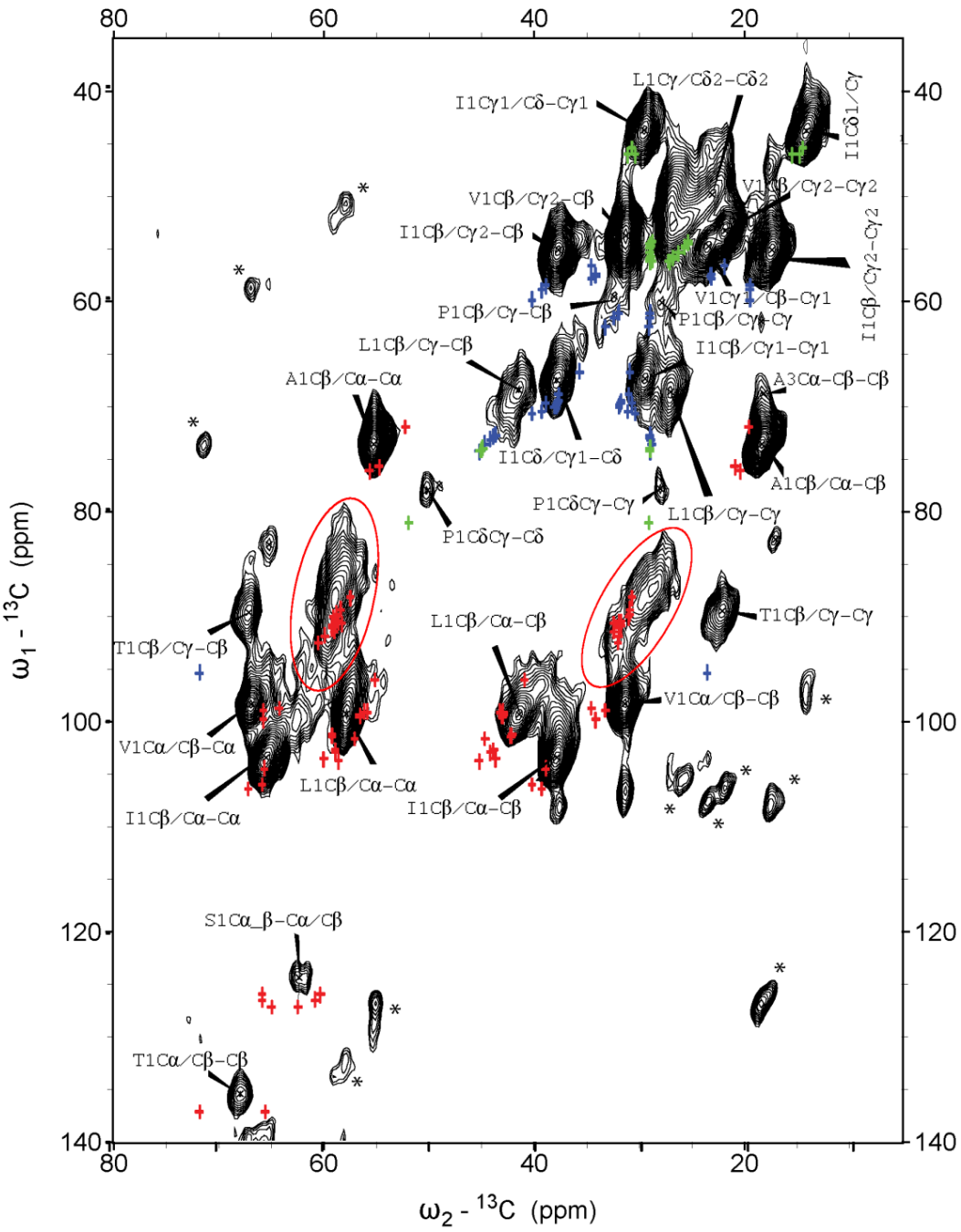

Fig. B6. A comparison of the carbon shifts of Vpu in POPC bilayers with carbon shifts of Vpu (39-81) in micelle. The back contour signals are from DQ/SQ spectrum shown in Fig. 3.13). The plus symbols are the carbon shifts deriving from the liquid state NMR experiments using Vpu (39-81) peptide sample reconstituted into DPC as described in Fig. 2.6

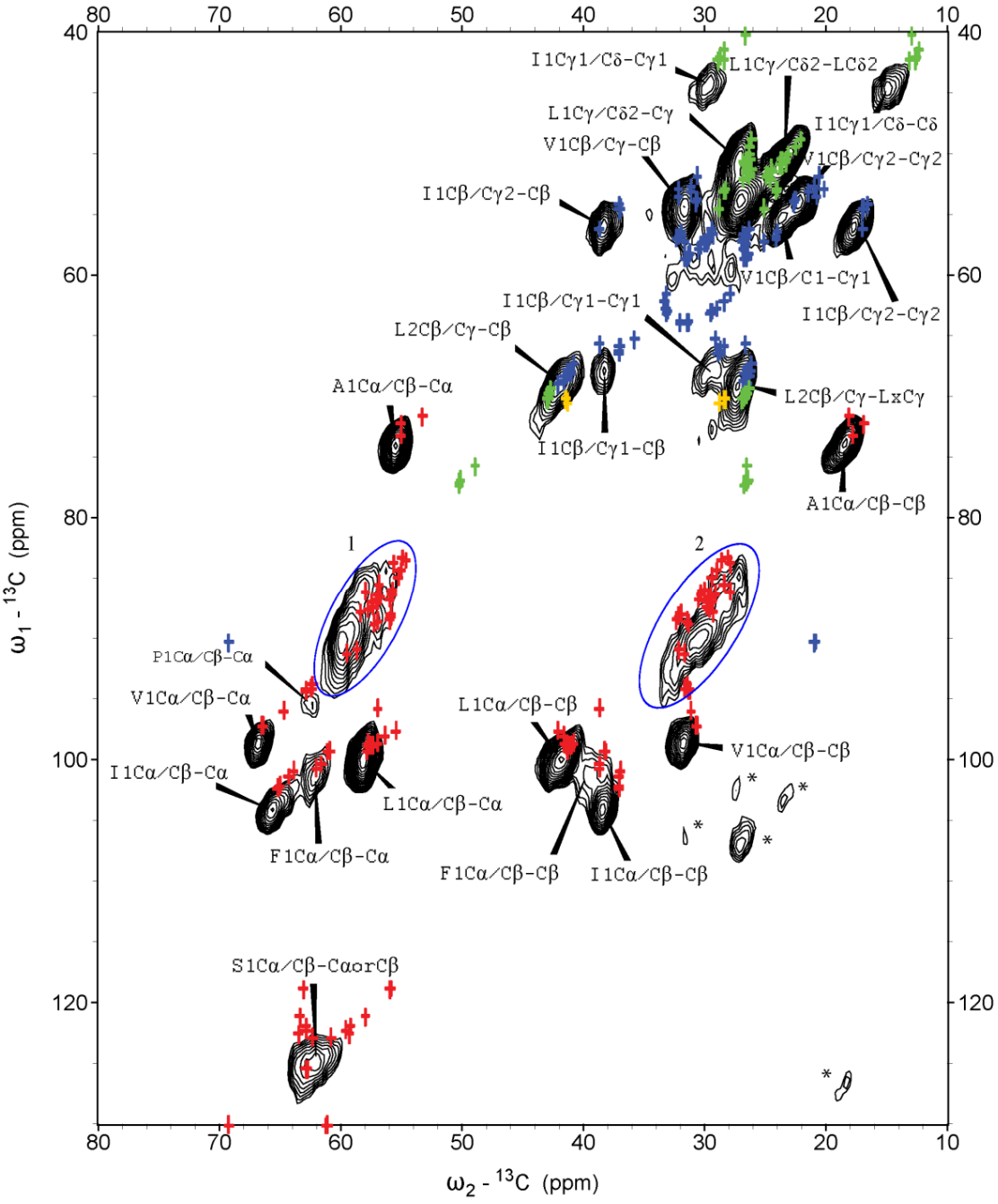

Fig. B7. A comparison of the carbon chemical shifts of CD4 (372-433) into POPC bilayers with CD4 (372-433) into micelle. The back contour line signals are signals from the DQ/SQ-SPC5 spectrum as previously shown in Fig. 3.22. The plus symbols are the carbon shifts deriving from the liquid state NMR experiments with the CD4 (372-433) peptite reconstituted into DPC micelles as described in Fig. 2.5.

Declaration

I hereby declare that this dissertation was produced autonomously and independently and without using any unauthorized help. This dissertation has not been handed in another institution or university. I do not have unsuccessful attempts of obtaining a doctoral degree.

Jülich, 24.01.2012

Hoa Quynh Do